WIND EFFECTS ON AIR CURTAIN AERODYNAMICS PERFORMANCE

Senwen Yang

A Thesis

in

the Department

of

Building, Civil and Environmental Engineering

Presented in Partial Fulfillment of the Requirements

for the Degree of

Master of Applied Science (Building Engineering) at

Concordia University

Montreal, Quebec, Canada

July 2018

CONCORDIA UNIVERSITY

School of Graduate Studies

This is to certify that the thesis prepared

By: Senwen Yang

Entitled: Wind Effects on Air Curtain Aerodynamics Performance

and submitted in partial fulfillment of the requirements for the degree of

Master of Applied Science (Building Engineering)

complies with the regulations of the University and meets the accepted standards with respect to originality and quality.

Signed by the final Examining Committee:

Dr. S. Li	Chair
Dr. L. Kadem	Examiner
Dr. H. Ge	Examiner
Dr. L. Wang	Co-Supervisor
Dr. T. Stathopoulos	Co-Supervisor

Approved by: _____

Chair of Department or Graduate Program Director

_____

Dean of Faculty

Date: _____ 2018

ABSTRACT

Wind Effects on Air Curtain Aerodynamics Performance

Senwen Yang

Air curtains are widely used in various building types to reduce infiltration and associated energy losses through building entrances. Quantifying the infiltration rate through a building entrance is directly related to the evaluation of the energy performance of air curtains. Consequently, many previous studies identify and measure the impacts of various factors on performance, including door operation, usage frequency and air supply angle and velocity. However, to date limited studies have focused on the effect of wind on air curtain performance, even though wind is commonly considered to play an important role. The purpose of this research is to identify wind effects on the performance of air curtains through an experimental study, taking into account parameters including wind speed and angle, air curtain supply flow speed and supply flow angle, and the pressure difference acting across an air curtain. The relation between air infiltration and the pressure difference across an air curtain with and without wind is analyzed. Experiments are conducted in a large chamber equipped with an air curtain and a corresponding sub-scaled model in the wind tunnel. The results from differing wind speeds and air curtain supplies from both experiments are subsequently compared, and the wind effects in both cases are found to be consistent. This study finds the following: when the air curtain jet is able to reach the floor, thus providing a good sealing of the door, it can effectively resist the wind; a strong wind blowing directly towards the air curtain reduces its performance; and the performance is related to both wind speed and wind incident angle.

ACKNOWLEDGEMENT

I would like to express my thanks and gratitude to my supervisors, Dr. Liangzhu (Leon) Wang and Dr. Theodore Stathopoulos. Their supervision and advice have been important throughout completing this research and thesis. I would like to appreciate their continuous guidance, suggestions and support for my study.

Furthermore, I would like to express my appreciation to all of my colleagues in the group, Dr. Dahai Qi, Dr. Wael Fayrouz, Cheng Zhang and Hatem Alrawashdeh, who have given much support and advice. In particular:

Dr. Dahai Qi helped to develop the air curtain scale method and instruct the author start the experiment.; Cheng Zhang assisted to with particle image velocimetry measurement data processing; Hatem Alrawashdeh helped to install the experiment the model and instruct to operate the devices in the Wind Tunnel; Dr. Wael Fairouz EzzEldin helped to install the particle image velocimetry devices, including the laser, camera, and traverse.

It has also been a joyful experience to work with and learn from them.

I also want to acknowledge the financial and technical support from the Air Management and Control Association (AMCA) and the valuable comments and advice from Mr. David Johnson at Berner International, Mr. Frank Cuaderno at Mars Air Systems, Mr. Brian Jones at Powered Aire, and Ms. Amanda Hickman at the Hickman Group.

Finally, I would like to acknowledge the great support and encouragement of my family, without which it would have been impossible for me to have access to this study and complete the research.

I also want to thank my friends both in North America and China, as it has been very important to have their encouragement and support while continuing my study.

TABLE OF CONTENTS

LIST OF FIGURES

LIST OF TABLES

NOMENCLATURE

A	Area, m^2
A_d	Cross-sectional area of the duct connector, m^2
b_0	Width of the air curtain nozzle, m
C_A	Airflow coefficient
C_d	Discharge coefficient
C_{Dave}	Average discharge coefficient for each door operation section
$D_{D,ave}$	Discharge modifier (air curtains)
H	Door height, m
Q	Volume flow rate, m^3/s
Q_e	flow rate of the exhaust CPU fans, m^3/s
Q_j	Air curtain jet flow rate, m^3/s
Re	Reynolds number
T_h	Usage per hour (doors), 1/h
u_0	Air curtain discharge speed, m/s
U_{max}	expected maximum flow speed in the field, m/s
V_{ave}	Average speed in the connection duct, m/s
V_g	Velocity at gradient height, m/s
$V_{(z)}$	Velocity at a certain height, m/s
Z	Height of a certain point, m
Z_G	Gradient height of different wind profiles, m

GREEK LETTERS

α	power law exponent for the specific terrain and exposure
α_0	the discharge angle (supply angle) of the air curtain unit, degree
β	Wind direction, degree
ΔP (or ΔP_a)	Pressure difference across the air curtain door due to the air curtain, Pa
Δp_f	Pressure difference caused by friction
Δt	the time delay between laser pulses, μs
θ	Air curtain jet discharge angle, degree
ρ	Air density, kg/m^3

ACRONYMS

Air curtain door	Double swing doors opening installed with air curtain unit
AMCA	Air Movement and Control Association (International)
ASHRAE	American Society of Heating, Refrigerating and Air-Conditioning Engineers
CFD	Computational Fluid Dynamics
CUBE	Concordia University Built Environment lab
HVAC	Heating, ventilation, and air conditioning
PIV	Particle Image Velocimetry
PSV	Particle Streak Velocimetry
PTV	Particle Tracking Velocimetry

1. INTRODUCTION

1.1 Background

Air infiltration, which is defined as unconditioned outdoor air passing through building openings like doors, windows and leakages on building envelopes, contributes to a large proportion of building heating and/or cooling loads. Air exfiltration, the opposite phenomenon whereby indoor air flows into the environment, is often considered not to contribute to energy losses directly in buildings with well-designed air handling systems but may sometimes do so indirectly by increasing the amount of infiltration. In this study, the word "infiltration" is used to represent both by default, unless stated otherwise. The amount of air infiltration and exfiltration depends on the pressure difference across a building opening, for example an entrance door, as a result of wind effects, stack effect, or the building HVAC (Heating, Ventilation, and Air Conditioning) system operating conditions (ASHRAE 2007). An air curtain is considered an effective measure for reducing infiltration and exfiltration, by supplying a high-speed stream that can separate the conditioned zone from the unconditioned area in order to control the penetration of airflow in both directions. At a building entrance, it can also help to prevent external pollutants, dust and insects from entering through the doorway. Accordingly, air curtains have been widely used in various types of buildings.

Many studies have been conducted to quantify the infiltration rate through building entrances and the related energy performance of air curtains. For instance, one experimental study examined the air curtain characteristics of several types of air curtain stream supplies, and Particle Image Velocimetry (PIV) measurements were used to capture flow patterns in different performance conditions (Goubran et al. 2016). A study of air curtain energy performance was also conducted

by Wang (2013) and compared the infiltration rates of building entrances equipped with air curtains with those equipped with vestibules for climate zones 3–8. Annual energy simulations in different climates using EnergyPlus and CONTAM were also completed by Goubran et al. (2015; 2017). However, very few studies of wind effects on air curtain performance can be found in the literature, although the wind effect is commonly considered to be potentially significant. One of the previous studies (Goubran et al. 2016) investigated the wind effect on air curtains through experiments. A duct blaster was used to produce an airflow stream to roughly mimic a wind speed of 10 m/s (22 mph) for an air curtain supply with a slot width of 6.35 cm, a supply speed of 13.75 m/s and an outwards angle of 20°. The preliminary study indicated that the tested air curtain was capable of resisting certain wind speeds, although it may not maintain performance under strong wind. The tests used the duct blaster fan to create the "wind", which was preliminary and rather rough.

To extend the preliminary study and confirm its findings, in the current study a large-scale wind generator was built to create the required wind field in front of a large-scale chamber with a full-size air curtain. However, due to limited space in the lab the wind generator was placed close to the chamber, generating concern that the resultant wind may not represent an actual wind field. More specifically: 1) real wind has an atmospheric boundary layer profile, whereas wind from the wind generator has a mostly uniform velocity distribution; 2) the wind generator can only provide an airflow speed up to 4 m/s, representing a light breeze situation, but it is important to study the influence of higher wind speeds, e.g. 10 m/s, on air curtain performance. 3) The wind generator flow outlet is installed close to the air curtain chamber, due to limited space, so the wind pressure measured near the outlet is affected by the turbulent of generator and disturbance of air curtain chamber.

Therefore, to complement the large-scale wind generator tests, sub-scaled tests in Concordia's Building Aerodynamics and Boundary Layer Wind Tunnel were also conducted. The following sections introduce the background methodology and theory of air curtains, followed by the experimental setups of both the large-scale and sub-scaled experiments, and finally present the results and discussion of the experimental data.

1.2 Experimental Tasks and Objectives

1.2.1 Experimental Study in Large-scale Chamber

The large-scale chamber tests were conducted at the Concordia University Building Environment (CUBE) lab and were divided into the following steps.

- **Experimental Setup**

For this study, the wind generator (as shown in section 3.1.1) was provided by one of the sponsors and a flow straightener was added to achieve a uniform and unidirectional flow. Due to the size of the wind generator, the current test chamber setup was also adjusted with help from the subcontractor for wind speed and pressure measurements.

- **Data Collection and Analysis**

Data collection and analysis included accurate quantifications of wind speed and pressures, flow visualizations with the use of an artificial fog machine, and measurement of flow rates across the door with an air curtain.

1.2.2 Scaled Model Study in Wind Tunnel

- **Design, Fabrication and Experimental Setup of the Scaled Model**

For the wind tunnel test, the sub-scaled model of the large-scale chamber consists of three components: the scaled chamber, fan connections, and computer central process unit (CPU) cooling fans with fan controller. As shown in Fig. 1-1, the scaled chamber is a 1:10 version of the large-scale test chamber at the CUBE lab. To confirm the similarity of the two models, preliminary tests without wind were conducted to ensure the correct scaling (the results are shown in section 2.3). Several CPU fans were either paralleled or serially connected and then controlled by variable-speed controllers to achieve the desired pressure differences and airflow rates through the door, which are comparable to those of the duct blaster fan in the large-scale tests. The air curtain jet flow was achieved through the outlet of the plenum (Fig. 1-1), pressurized by air from a compressed air cylinder controlled by a digital flow controller. The detailed dimension information for scaled model will be described in the section 3.2.2.

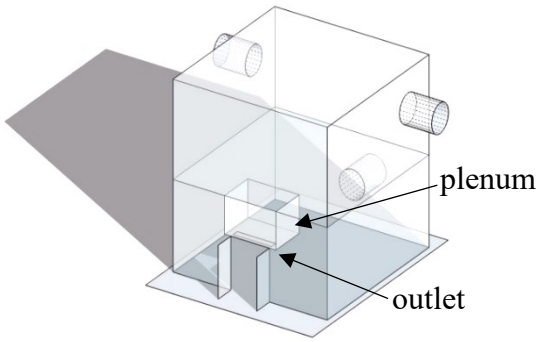

Figure 1-1. Scaled model of the CUBE test chamber for the wind tunnel test.

- **Experimental Data Collection and Analysis**

Experimental tests were conducted in the wind tunnel with different wind speeds and angles, and different air curtain speeds and supply angles. Flow visualizations performed by the PIV technique

were also employed in the tests. The wind tunnel data were then compared with the large-scale tests, which helped to verify the large-scale wind generator tests.

2. LITERATURE REVIEW

2.1 Infiltration through Building Entrance

A simplified method to calculate the flow through large openings comes from the continuity equation and the Bernoulli equation on both sides of the opening. The physical model is based on the incompressible inviscid steady flow generated by the pressure difference across the openings (Van der Mass, 1992). Assuming that air density is constant and applying the Bernoulli equation for two points:

$$p_2 - p_1 + \frac{1}{2}\rho({u_2}^2 - {u_1}^2) + \rho g(z_2 - z_1) + \Delta p_f = 0 \quad (1)$$

In addition, the airflow rate through an opening is often expressed as a function of the pressure drop across the opening:

$$Q = C_d A\sqrt{\frac{2\Delta P}{\rho}} \quad (2)$$

In many studies that consider the flow through large building openings, especially when dealing with isothermal flow cases, the discharge coefficient is used to describe the flow through those different pressure conditions.

Flow through large building openings has been described with the discharge coefficient C_d in many previous studies (Yuill, 1996; Yuill et al., 2000), especially when the flow is regarded as an isothermal flow, whereby temperature differences are neglected, and no heat transfer takes place in in the flow. Furthermore, infiltration in large openings can be considered as a flow from the orifice in entrance types like a single door or vestibule.

For certain sizes of door openings and configurations, this relation between the penetration flow and the pressure difference (Eq. 2) across the opening can be obtained as by Yuill (1996). In this

experimental study, the discharge coefficients, C_d, were utilized to account for resistances, primarily for evaluating the performance of vestibules (i.e. the vestibule door in Fig. 1-1) compared to that of doors without a vestibule (i.e. a single door).

The experimental setup designed by Yuill (1996) was based on a chamber with the dimensions 2.44 m × 2.44 m × 1.3 m (W × L × H), which was a 1:3 scale (down) of a real building. The doorway opening for this chamber had the dimensions 0.61 m × 0.71 m (width × height). A blower-door exhaust fan was placed across the door to generate a pressure difference between the inside and outside of the chamber, and a multi-configuration attachment was built to work as a vestibule in front of the doorway. The structure drawing and dimensions are shown in Figure 2-1. When the vestibule was removed, the only door entrance was considered as a "single door" condition. In the "single door" condition, two door swings are designed to installed on both sides of door opening (perpendicular to the wall).

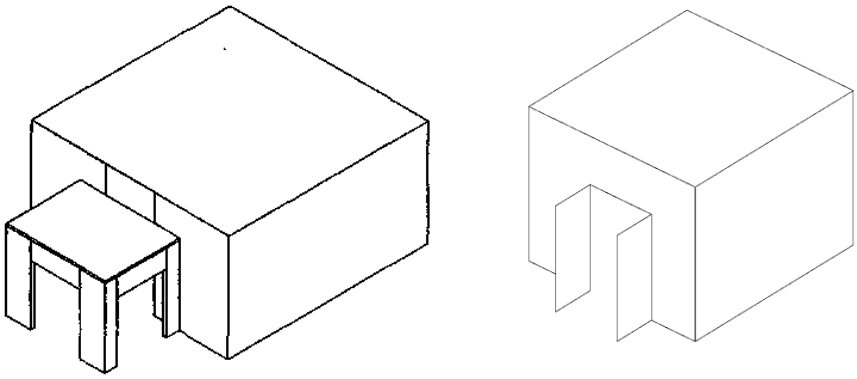

Figure 2-1. Building entrance model with vestibule (Yuill, 1996) and single door.

Subsequently, the pressure difference was measured across the opening of different types of building entrance (single door or vestibule). Based on the results from these measurements, the discharge coefficient, C_d, can be calculated or correlated through the relation between pressure

difference and air infiltration in the equation. For different swing door opening angles, the discharge coefficient C_d could differ.

2.2 Air Curtains

In 1968, one of the earliest studies on air curtains was completed by Hayes (1968) in his PhD thesis. In the study, a theoretical model represents the vertical airflow or air jet that provides an air curtain screen for both isothermal and non-isothermal conditions. The model setup is shown in Figure 2-2.

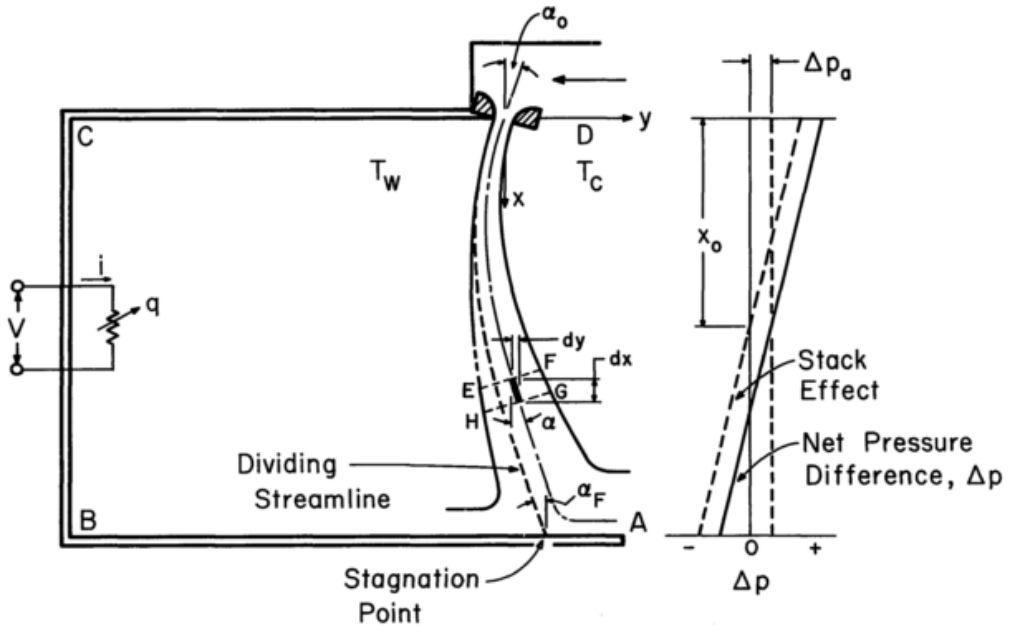

Figure 2-2. 2D air curtain theoretical model (Hayes, 1968).

In that study, a crucial theoretical model was deduced to describe the operating conditions of air curtains set at the opening of a closed chamber. The air curtain, installed immediately above the chamber opening, mainly takes flow from outside and supplies a screen jet flow vertically downwards, and initially the airflow is distributed evenly outside the door. This distribution causes

more flow to enter the room, resulting in a pressure increase inside the room. The jet curve then begins to bend and the deflection angle starts to change. Thus, more flow is divided into the outside section. When the amount of air entrained into the room reaches the value of the amount of air injected into the air, implying that the airflow into and out of the room is balanced, the theoretical model is in equilibrium and the condition becomes steady. The specific flow angle towards the floor in the equilibrium state is defined as the angle of deflection, represented by α_F, while the pressure across the opening at equilibrium is defined as ΔP_a. It is worth noting that this study assumes that the air curtain flow (injection) width exactly equals the size of the door opening and has a completely uniform flow state, and that the time required to reach equilibrium is very short (Hayes, 1968). For this model, a theoretical equation was developed to describe the relation between air curtain supply and pressure difference.

$$\frac{\Delta P_a}{\rho u_o^2} = \frac{b_0}{H}\left[2.4\sqrt{\frac{b_0}{H}\left(1 - 2.56\,\frac{b_0}{H}\right) - \sin\alpha_0}\right] \quad (3)$$

where,

ΔP_a is the pressure difference across the door ($\Delta P_a = P_{out} - P_{in}$),

b_0 is the width of the air curtain nozzle (air outlet width), m,

H is the door height, m,

α_0 is the discharge angle (supply angle) of the air curtain unit,

u_0 is the discharge speed, m/s,

ρ is the air density.

It is vital to note that in all of the analysis conducted in the abovementioned study, only the static inside pressure created by the air curtain is taken into consideration, while other factors (such as outside wind, temperature difference or building stack effects), which may have an impact on the

pressure difference across the doorway, were not taken into consideration. In fact, the pressure difference only represents the pressure changes accompanying infiltration flow when the air curtain is in a steady condition.

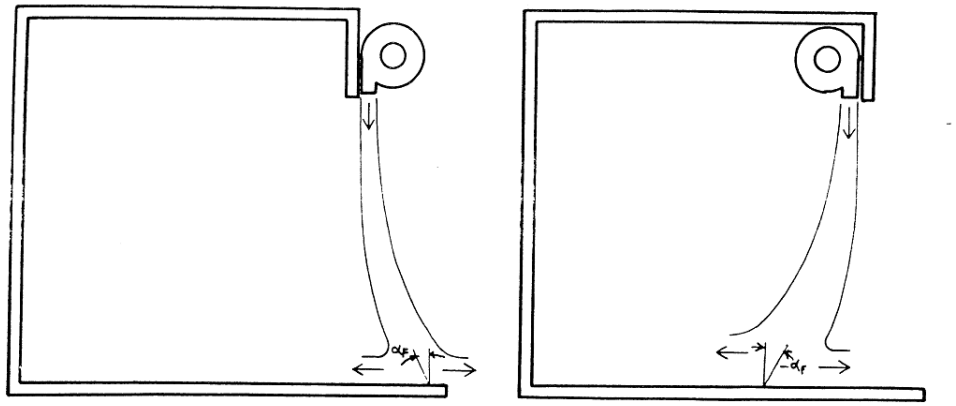

Figure 2-3. Inside-installed and outside-installed air curtains (Hayes, and Stoecker, 1969).

According to extensive studies conducted by Hayes, the most important factors affecting air curtain performance in the designing of air curtains are curtain supply type (discharge angle α_0 and supply velocity u) and air curtain slot dimension ratio b_0/H. From the theoretical model developed by Hayes, it is clear that a higher supply velocity or supply angle will lead to higher performance or sealing effects (higher ΔP_a). Meanwhile, a higher slot dimension ratio will also improve performance, and indicates increased ease of reaching the floor (Hayes and Stoecker, 1969).

A number of other researches focus on the efficiency of air curtains, and various methods have been developed to quantify performance and efficiency. In this regard, the efficiency factor, defined as η, is widely used (Belleghem et al., 2012;).

$$\eta_{\text{air}} = 1 - \frac{Q}{Q_{open}} \tag{4}$$

where

η_{air} is the efficiency factor of the air curtain in reducing the infiltration through the door,

Q is the infiltration volume flow rate through the door with the air curtain in operation, and

Q_{open} is the infiltration through the door with no air curtain.

It is important to note that the higher the value of η_{air}, the better the unit performs.

However, since that time no studies were conducted to relate the above theoretical models to air curtain infiltration and energy performance until the present study that investigated factors associated with air curtain infiltration and energy performance. These included door operation, usage frequency, air supply and velocity, and infiltration under different air curtain operating conditions (Wang and Zhong, 2014). There was also a Concordia university study examining the effects of infiltration through air curtain doors when used (Qi et al. 2016). In these studies, the operation of an air curtain was divided into three scenarios, as shown in Figure 2-5.

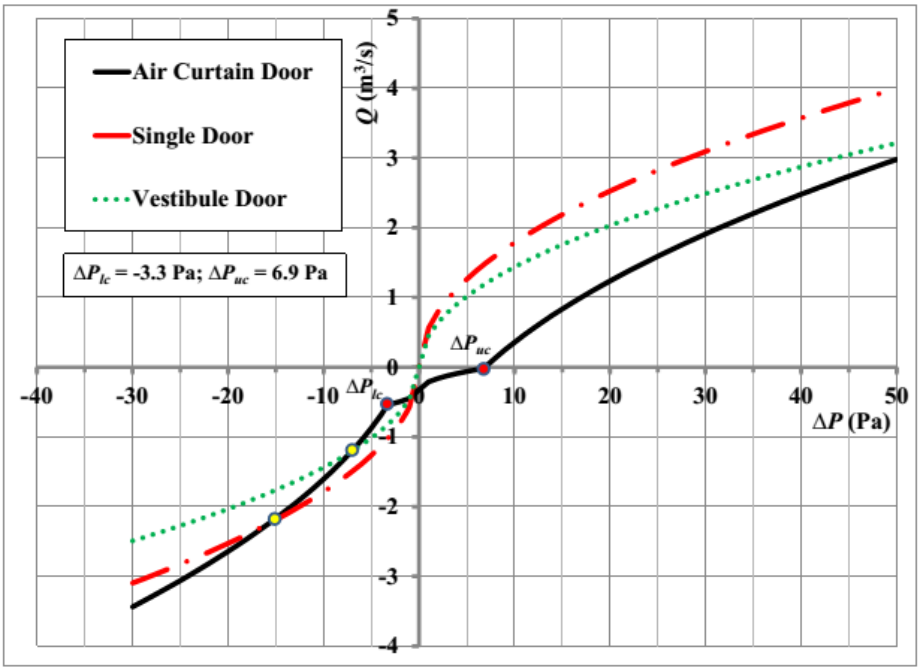

Figure 2-4. Infiltration and ex-filtration characteristics of air curtain doors in comparison to single and vestibule doors (supply 15 m/s at 20° outwards) (Wang, 2013).

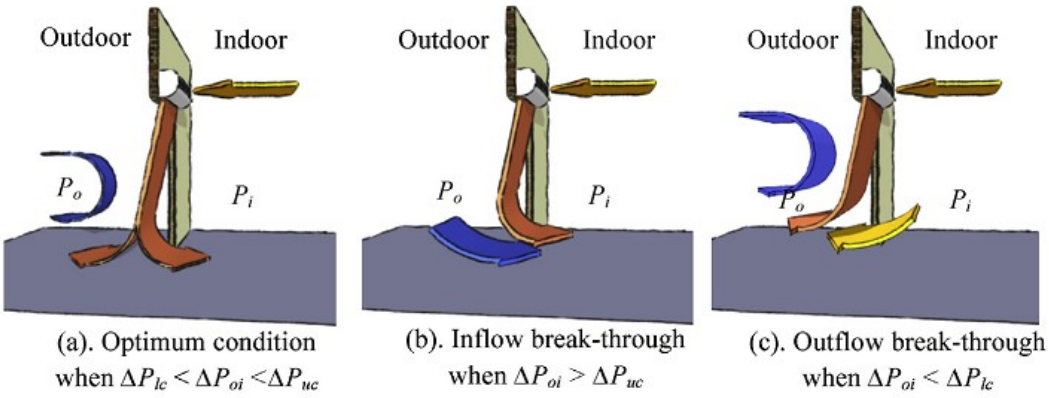

Figure 2-5. The three typical operation conditions of air curtains (Wang and Zhong, 2014).

(lc = lower critical condition; oi = outdoor and indoor difference; uc = upper critical condition; o = outside; i = inside)

- Optimum condition: air curtain flow reaches the floor and reach the floor;
- Inflow breakthrough: air curtain flow is curved inwards and does not reach the floor;
- Outflow breakthrough: air curtain flow is curved outwards and does not reach the floor.

The air curtain infiltration performance was evaluated by the proposed function of the infiltration (Q) and pressure difference across the air curtain door $\Delta P_{oi} = P_o - P_i$ (Wang, 2013). Note that by default $\Delta P = \Delta P_{oi}$ in this report, unless specified otherwise.

$$Q = (-1)^i \, C_{D,ave} \; A \, T_h \sqrt{\frac{2|\Delta P_{oi}|}{\rho}} + \; D_{D,ave} \, T_h \sqrt{\frac{2}{\rho}} \tag{5}$$

i = 0 when $\Delta P_{oi} > 0$ and I = 1 when $\Delta P_{oi} < 0$,

where

$$D_{D,ave} = \frac{D_{D,a}a + D_{D,b}b + D_{D,c}c + D_{D,d}d}{a+b+c+d} \tag{6}$$

In a simplified term:

$$Q = C\sqrt{\Delta P} + D \tag{7}$$

While the relation can be described by the following equation:

$$\frac{Q_{angle}}{A\sqrt{\frac{2}{\rho}}} = (-1)^i C_{D,angle}\sqrt{|\Delta P_{oi}|} + D_{D,angle} \tag{8}$$

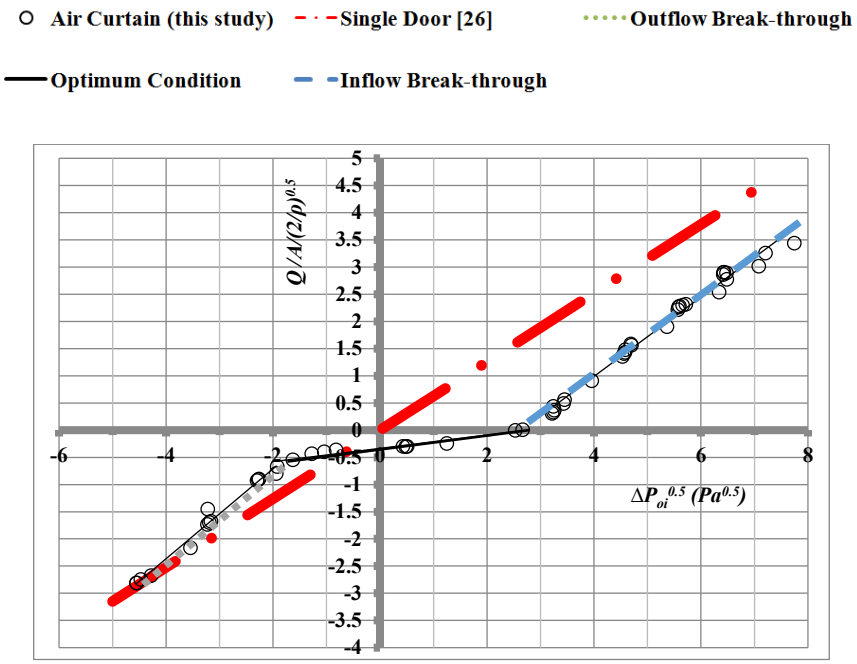

Figure 2-6. Correlation of air curtain door infiltration at a door opening angle of 90° (Wang and Zhong, 2014).

In 2016, an experimental study was conducted to investigate the characteristics of air curtain by Goubran (2016) in Concordia University Building Environment lab. In Goubran's study, experimental results and Computational Fluid Dynamics simulation results are compared to validate the characteristic performance. Two air curtain supplies are considered in his study:

13,75m/s, 0° (vertical), 9.1m/s, 20° outward. The performance of these two types of air curtain supply are also compared to that of single door as well as vestibule in previous studies.

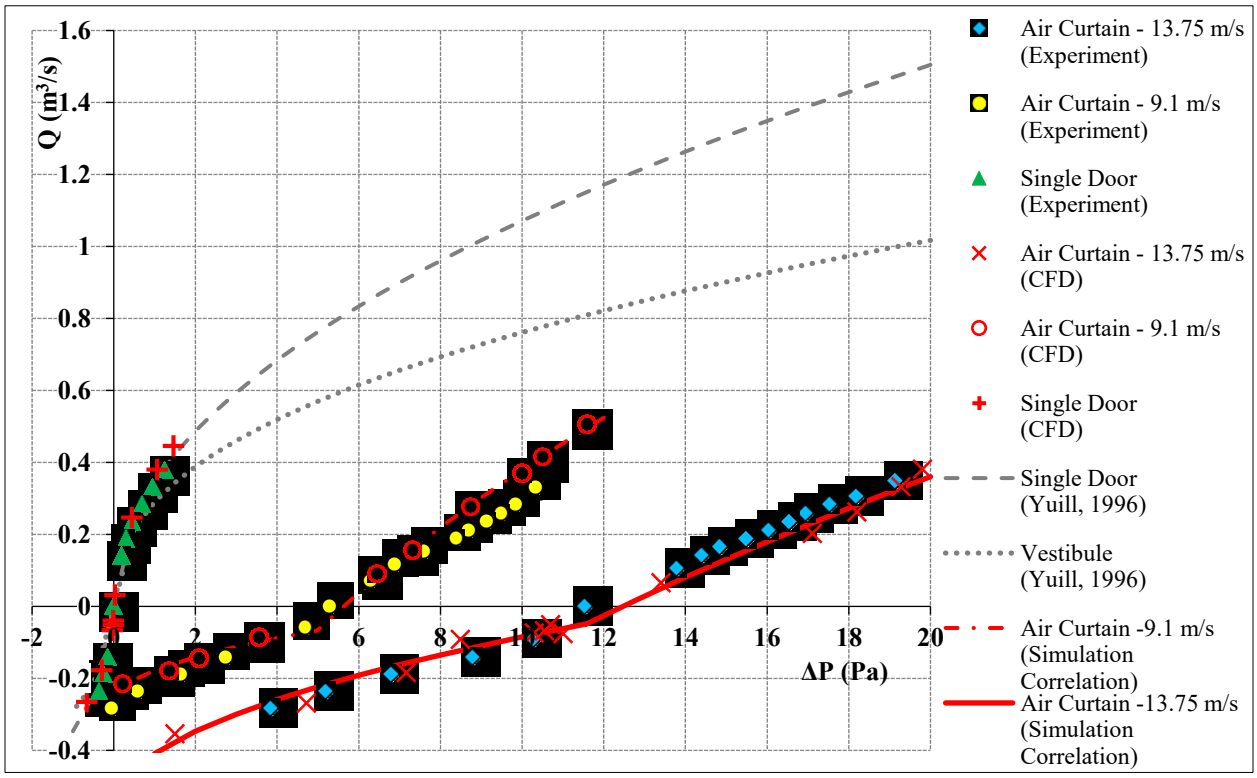

Figure 2-7. Experimental results and CFD simulations results for air curtains performance with jet supply 9.1 /s, 20° outward and 13.75m/s, 20° outward (Goubran, 2016).

2.3 Wind Engineering

2.3.1 Basics of wind engineering

Air movement in the atmosphere is mostly driven by the pressure difference between different locations on the surface of earth. Meanwhile, this pressure difference is mainly affected by a temperature gradient, which can be caused by radiation differences resulting from different latitudes. Additionally, other factors such as geographic variety, seasonal changes and even the

recirculation of ocean currents can cause different temperature distributions on the surface. Thus, wind movement is a globally common phenomenon, and can travel into cities and move around buildings. As a result, wind can be a critical factor for building environment studies.

The boundary layer is defined by the previous researchers as when the latter of the flow field is distributed into two sections: on one side the flow can be regarded as frictionless flow, and on the other side the flow field appears with the transition layer when close to solid walls, and the flow speed changes gradually near the wall (Prandtl, 1905).

When the surface of earth is regarded as a frictional solid wall, the air movement or wind travel above it can be considered as a boundary layer flow. According to the previous definition, the boundary layer is a layer of airflow that is affected by ground friction from terrain roughness and from the obstruction effect of terrain on the earth's surface. When the height is close to the earth's surface in the boundary layer, this leads to a decrease in wind speed and an increase in turbulence.

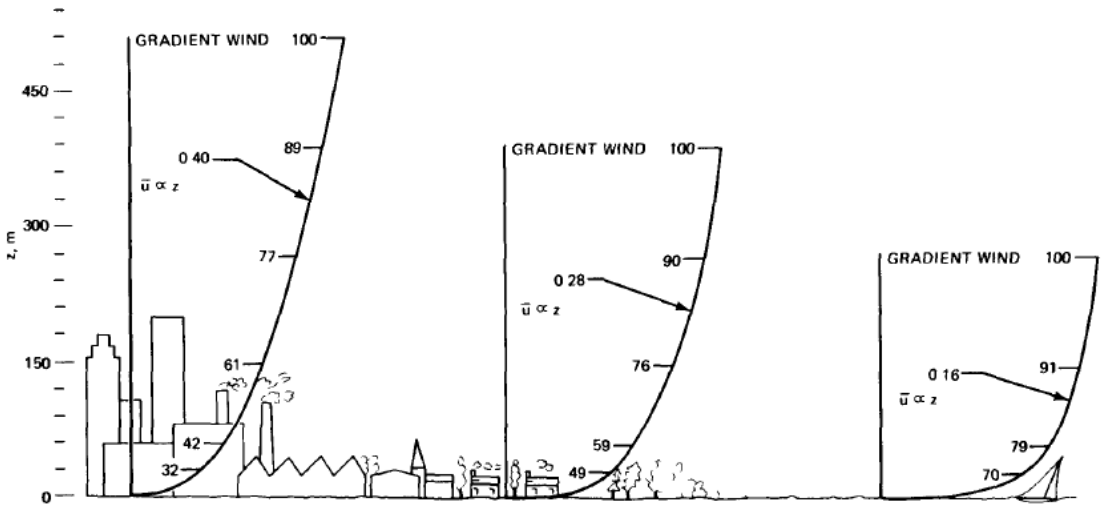

Figure 2-8. Empirical power laws over different terrains (Davenport, 1965).

Power laws for wind profiles have been determined and widely used in previous studies to describe the turbulent boundary velocity. The mean velocity distribution for the overall boundary layer can be defined in the following empirical equation.

$$\frac{V(z)}{V_G} = \left(\frac{Z}{Z_G}\right)^{\alpha} \quad (9)$$

where:

Z refers to the height of a certain point,

Z_G refers to the gradient height of different wind profiles,

V_g represents the velocity at gradient height, which does not change above the gradient height,

$V_{(z)}$ represents mean velocity at a certain height,

α is the power law exponent for the specific terrain and exposure.

The main parameters determining the exposure and roughness are the gradient height V_g and power law exponent α. Many researchers have conducted measurements to find the exponent and gradient height for different exposures (Oliver, 1971; Geurts and Bentum, 2007).

Table 1 Characteristic parameters in power law wind profile defined in wind loading code EN 1991-1-4 (Geurts and Bentum, 2007).

Exposure category and description	Power law exponent (α)	Roughness length (Z_o), m	Gradient height (Z_G), m
1: Open sea, ice, tundra, desert	0.11	0.001	250
2: Open country with low scrub or scattered trees	0.15	0.03	300
3: Suburban areas, small towns and wooded areas	0.25	0.3	400
4: Numerous tall buildings, city centers and developed industrial areas	0.36	3	500

2.3.2 **Boundary Layer Wind Tunnel**

Wind tunnel experimental studies have been widely developed and adopted to explore the impact of wind on building structures. The earliest wind tunnel experiments were conducted in uniform aeronautical wind tunnels, which is closely related to aerospace and aeronautical studies. After Jensen (1958) found that the results of a current-scaled test model were not able to represent a building under real boundary layer wind with profiles, increasing numbers of researchers began to design and fabricate the atmospheric boundary wind tunnel to make the scale building model fit the wind profile (Vickery, 1974; Holmes, 1977; Cooker, 1975; Stathopoulos, 1984). This was followed by the trend of conducting wind effect studies in boundary layer wind tunnels.

Following many studies carried out in boundary layer wind tunnels, the similarity of the Reynolds number has been found to be an issue in the wind tunnel scaling model test. The Reynolds number is largely reduced in the wind tunnel if the wind velocity is maintained at the same value as the

atmospheric boundary layer wind. Because of the reduction of model dimensions, the characteristic lengths of the building structure and obstruction are reduced by scaling, which leads to the decrease of the Reynolds number by three orders of magnitude compared to the real atmosphere. An ideal approach achieves the Reynolds similarity is to increase the wind speed based on the time of scaling. However, this is difficult to realize because of the limitation of maximum flow supply and can only be done with some small-scale wind experiments.

One wind tunnel study revealed that for model buildings, models with sharp edges can compensate for flow similarity (Simiu and Scanlan, 1996). For sharp edges set in the boundary layer flow, the air separates at the interaction site. Meanwhile, in the experiments of this study the Reynolds number was found to be independent, which implies that the Reynolds number has less impact at the sharp edges. Due to sharp corners causing flow separation, it can be recognized that experiments with flow in a wind tunnel are able to represent and simulate wind in the atmosphere.

2.4 **Wind Effects on Air Curtains**

For a building immersed in a wind field, the wind outside the building will have an impact on the entrance with an air curtain. Due to pressure differences changing under different wind conditions, the air curtain performance differs. However, the existing body of research investigating wind effects on air curtains is limited.

One of the most relevant studies examines air curtains under train-driven wind in a subway tunnel (Juraeva et al., 2016) as outlined in Fig. 1-3. Three types of air curtain supplies were investigated: 7.5 m/s, 15 m/s and 25 m/s. The results indicated that no particle infiltration occurred from the tunnel in all three cases without “wind”. In other words, the particle was totally blocked by the air curtain. When a wind of 3.8 m/s was applied, the researchers found that the wind led to particle penetration through the air curtain (see Juraeva et al. (2016) for more details).

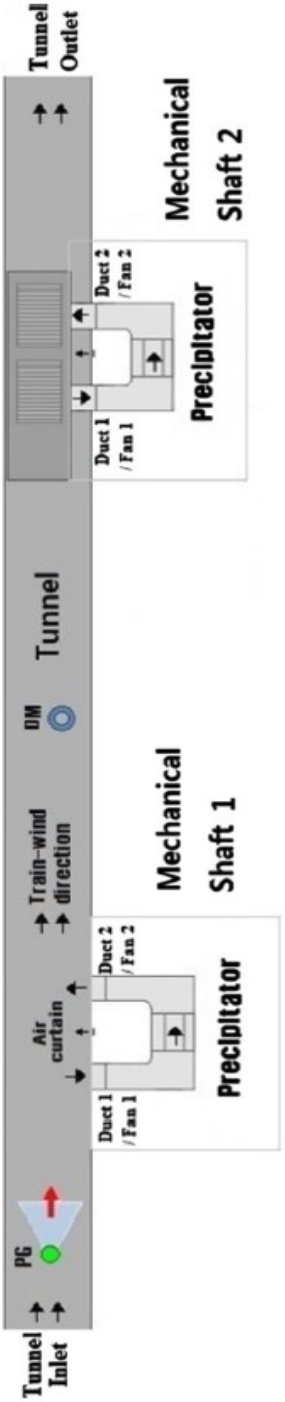

Figure 2-9. A schematic view of the model subway tunnel (Juraeva et al., 2016).

2.5 **Particle Image Velocimetry (PIV)**

Velocimetry involves measuring the velocity of a fluid field in order to understand fluid dynamics phenomena and acquire flow field information. Velocimetry is categorized into two sections according to the scale of measurement: point-wise and global-wise measurements (Sun and Zhang, 2007). Point-wise techniques conduct measurements through a single point, and the results are transferred from other types of signals or principles, such as pressure differentials or dynamic pressure (pitot tube), Doppler shift principles (laser Doppler) or heat transfer flux (hot-wire anemometry). Meanwhile, global-wise techniques are developed from optical principles, and also require computers for data processing and analysis. This includes PIV, which is widely adopted in many fields, particle tracking velocimetry (PTV) and particle streak velocimetry (PSV) (Cao et al., 2014; Adrian, 2005).

PIV is a widely used measurement technique to capture information and perform visualization for fluid velocity fields in many research areas (shown in Figure 2-10). It is able to provide quantitative velocity information, including speed and direction within the captured field of view. The most common PIV system comprises a multi-pulse laser, a CCD (Charge-Coupled Device) camera and a synchronizer to coordinate the laser, one or more cameras, and a computer with specified software to control the system and to acquire and analyze experimental data (Cao et al., 2014). In a 2D PIV system, one camera is used to capture the velocity field in one plane, and therefore may lose information relating to velocity vectors perpendicular to the laser plane. Meanwhile, a 3D-3C PIV system is developed to use two cameras to capture three-dimensional information in the observed plane. Additional types of systems use more than two cameras to generate the volumetric velocity field (Li et al., 2010).

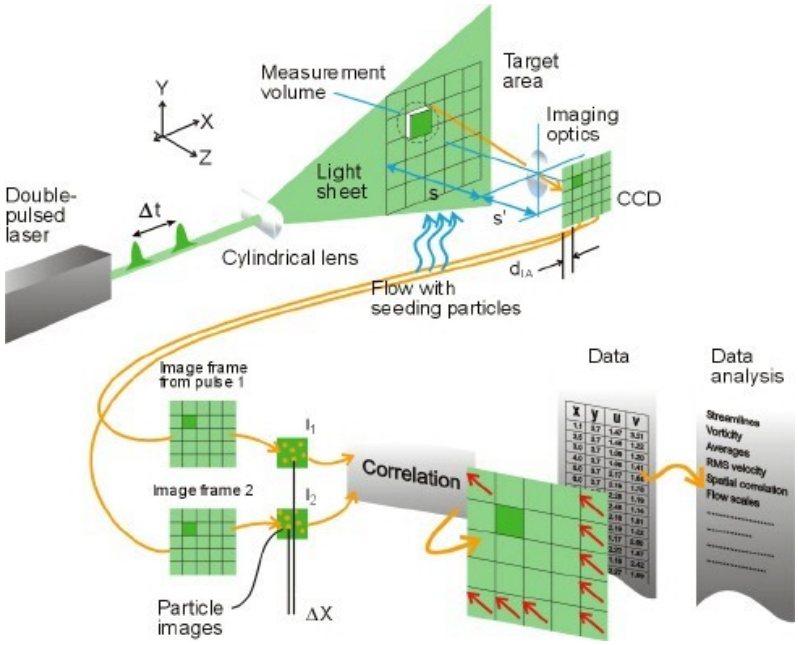

Figure 2-10. 2D PIV system components and the data processing stream ("Laser Optical CCD and sCMOS Cameras | Dantec Dynamics," n.d.).

For PIV system control, time delay (the time difference between two laser frames), represented by Δt, is one of the most significant input settings to acquire the reliable data based on flow domain and flow velocity. The time delay is designed to track the seed moving distance in a certain short time, and it helps to calculate the velocity information. The time delay setting is recommended to make the seed move a certain distance in the field of view. For most cases, the moving distance is set as 1/4 of the interrogation area (the single grid in the field of view). Theoretically, the method used to define Δt is shown below.

$$\Delta t = \frac{L}{4U_{max}} \quad (10)$$

where

L is the length of grid (interrogation area), m,

U_{max} is the expected maximum flow speed in the field, m/s, and

Δt is the time delay between laser pulses, s.

Meanwhile, an alternative method to define the time delay has been widely adopted in previous studies (Cao et al., 2014; Hart, 2000).

$$U_{max} \times \Delta t\ (\mu s) = 250 \qquad (11)$$

where

U_{max} is the maximum speed of flow to be captured, and

Δt is the time delay between laser pulses, μs.

Another factor essential to the quality of PIV tests is the seed type, which has been linked to the accuracy of results. Various types of seeding particles have been adopted in previous studies to visualization the gas flow based on the size of interrogation area, and the characteristics of those seed have been listed in Table 2. Melling (1997) conducted a study on scattering characteristic for different types of seeding particles. The study concluded that to improve the quality of measurements, seeding particles should be introduced and mixed into the flow in sufficient and stable concentrations with a uniform distribution. The seeding method should be selected carefully based on the experimental setup. For instance, the advantage of global seeding, whereby particles are introduced into the flow well upstream of the region of measurement, is that the seed fills the whole flow region, so that velocities over the whole flow field can be represented. This approach can only be implemented if the maximum achievable seeding concentration exceeds requirements. However, for most large wind tunnels, seeding the entire flow is not feasible because of the limited supply of seeding generators. In this case, the concentration of seed in the flow may not fulfill the requirements for signal capture.

Table 2 Seeding particles in gas flows (Melling, 1997).

Material	dp	Laser	Pulse energy	Light sheet		Reference
				W(mm)	T(mm)	
TiO_2	<1	Nd:YAG	10mJ,20ns	15	0.3	Reuss et al (1989)
TiO_2, ZrO_2	0.7-1	Nd:YAG	110mJ,12ns			Paone et al (1996)
Al_2O_3 (m=1.76, ρ= 3970 kg m^{-3})	0.3	Nd:YAG	400mJ		0.2	Muniz et al (1996)
	3	Nd:YAG	9mJ, 6ns	150	1	Anderson et al (1996)
	0.8	Ruby	20ns			Krothapalli (1996)
Polycrystalline	30	Nd: YAG	135mJ, 6ns			Grant et al (1994)
Glass	30	Ruby	5J			Schmidt and Löffer (1993)
Oil smoke	1	Ruby	100mJ			Stewart et al (1996)
Com oil	1-2	Nd: YAG	120mJ		0.4	Jakobsen et al (1994)
Oil	1-2	Nd: YAG	70mJ, 16ns		0.5	Westerweel et al (1993)
Olive oil	1.06	Nd: YAG				Höcker and Kompenhans (1991)
						Fischer (1994)
						Raffel et al (1996)

Finally, the data processing approach also has a significant impact on the reliability of results. The adaptive correlation and filter method (Dantec Dynamics & Nova Instruments, 2012) is the most commonly used data processing method, and has been recognized as the most reliable and advanced correlation method (Dantec Dynamics & Nova Instruments, 2012; G. Cao, et al., 2010).

2.6 **Conclusion**

Referring to the tasks and objectives described in section 1.2, a detailed literature review was conducted to establish the methodology including the experimental method and analytical approach for this study.

Many studies have been conducted to study the infiltration characteristics for different building entrances (section 2.1), including the single door and the vestibule (Yuill, 1996), in which the infiltration through the entrance was defined based on the discharge coefficient of the opening.

An extensive literature review relating to air curtain characteristics and performance was conducted. A widely used theoretical air curtain model was developed by Hayes and Stoecker (1969), and demonstrated the relation between air curtain supply and pressure difference across the doorway under steady condition when air infiltration or exfiltration penetrate the entrance. Characteristics of air curtain are found though CFD simulation by Wang (2013), and air curtain operation conditions are divided into three main zones. Experimental validation for air curtain charateristics was conducted by Goubran (2016).

However, to date, very few studies have been conducted to focus on wind effects on air curtains, while wind is a common factor which could have impact on air curtain aerodynamics performance. Based on the literature and objectives, the contribution of this thesis cound be determined as follows:

- Investigation of wind effects on air curtain aerodynamics performance through large-scale air curtain chamber tests and sub-scale wind tunnel tests
- Comparison of air curtain test results of large-scale tests with sub-scale tests.
- Validation of air curtain operation conditions in sub-scale tests through PIV measurements with and without wind.

3. METHODOLOGY

This section introduces the methodology, experimental results, data analysis and discussion for the air curtain tests. The large-scale tests were conducted in the CUBE laboratory, and the sub-scaled tests were conducted in the Building Aerodynamic and Boundary Layer Wind Tunnel laboratory.

3.1 Large-scale Air Curtain Study

The purpose of the large-scale tests is to investigate the wind effect on air curtain with several types of air curtain supplies and different wind speeds.

3.1.1 Experimental Design and Setup

As shown in Fig. 3-1, the experimental setup includes two main components: the transparent cubic chamber (2.44 m^3) with a duct blaster fan, an air curtain unit above the door entrance, and the wind generator with a square supply, 1.14 m × 1.14 m (Width × Height). The whole CUBE chamber is separated into two vertical sections, the upper section of which was isolated and not used in the current study. The chamber dimension is the same as that of the previous studies by Yuill (1996) and Goubran (2016). The air curtain supply unit is the same unit as in the study by Goubran et al. (2016) with the slot width of 6.35 cm. The estimated Reynolds number is 69,232 for 9.1 m/s supply and 104,610 for 13.75 m/s air curtain supply.

The chamber is with a double swing door: 0.61 m × 0.71 m (Width × Height). Inside the chamber, four pressure tubes were connected to a digital pressure gauge to measure the averaged internal pressure. For external pressure measurement, the pressure tube was installed in front of the door to measure the wind stagnation pressure. The duct blaster fan was also equipped with a flow gauge to measure the fan flow rate.

Figure 3-1. Concordia University Building Environment (CUBE) lab.

As shown in Fig. 3-2, the wind generator is comprised of two motors and four fans at the top. The "L-shape" duct delivers air from the top inlet to the square outlet equipped with a flow straightener. The honeycomb flow straightener at the outlet was used to improve the flow uniformity at different flow speeds. With the motors working up to 42 Hz, the wind generator can supply a maximum "wind" speed of 3.95 m/s. The vane switches on the sides of the duct can be adjusted for flow uniformity at the cross-section. Two digital monitors and displays are equipped to control the machine power supply and to adjust the rotation rate of the motors. Each of the motors is connected to the two fans which can be controlled separately. In this study, 0 Hz (no wind), and different power settings, 30 Hz, 35 Hz, 42 Hz, have been selected for the corresponding average supply

wind speeds: 0 m/s, 3.01 m/s, 3.51 m/s and 3.95 m/s, respectively. For simplicity, the average wind speeds were rounded to be 0 m/s, 3 m/s, 3.5 m/s and 4.0 m/s here.

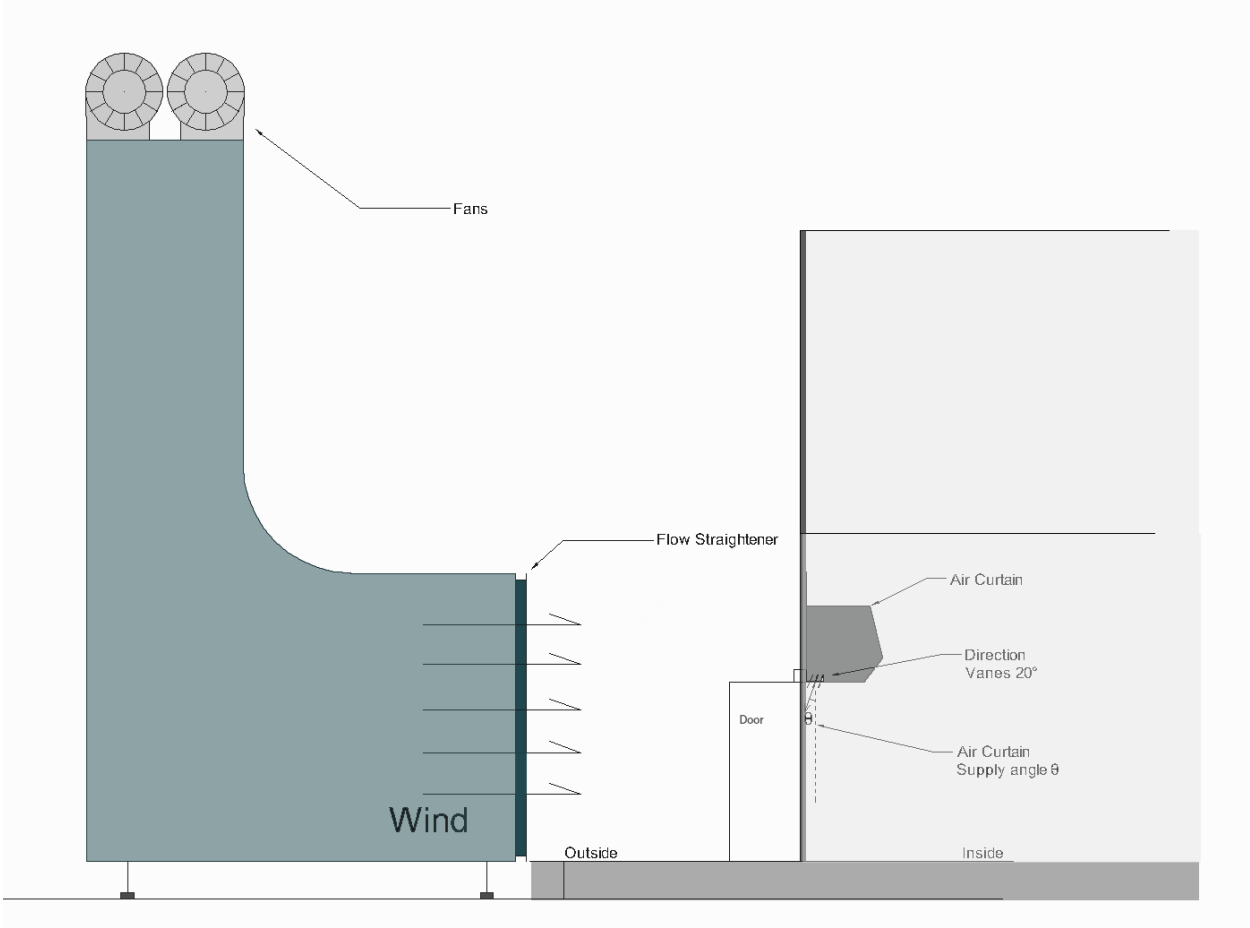

Figure 3-2. Schematic of wind generator and air curtain door.

To calibrate the wind generator device on site, the velocity distribution was measured to test the uniformity of the wind supply. If necessary, the flow uniformity can be adjusted by the internal vanes (Figs. 3-3 and 3-4). For the calibration of wind velocity distribution, the outlet cross-section is divided into 36 sections to measure the average wind speed by a hot-wire anemometer. The calibration results after installation is compared to the test results provided by the wind generator

manufacture (presented as Manufacture Test). The measured velocity distributions and uniformity are shown in Fig. 3-5 and Table 3.

Figure 3-3. Wind generator.

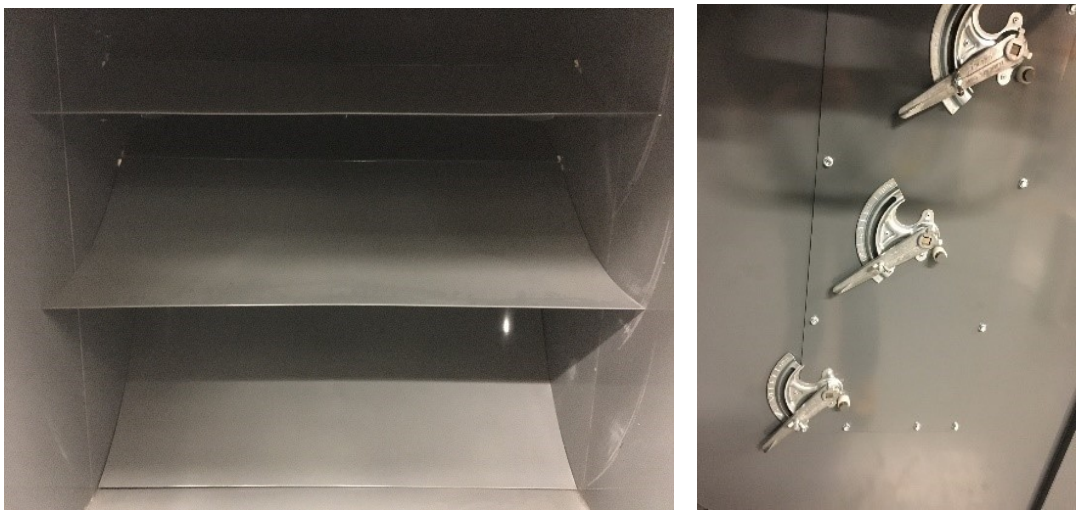

Figure 3-4. Internal vanes and external switches of the wind generator.

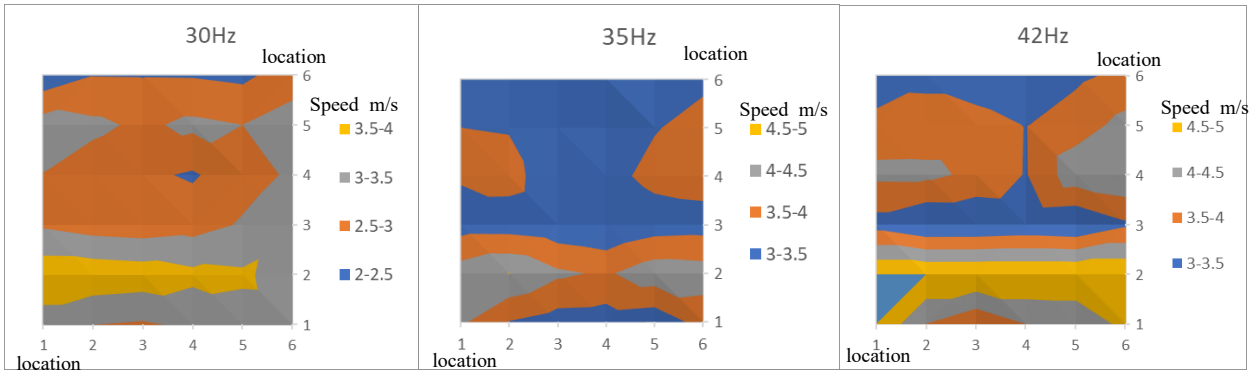

Figure 3-5. Measured velocity (m/s) distribution for the wind generator.

Table 3. Wind generator calibration information.

	Motor Settings (Hz)	Mean Wind Speed (m/s)	Relative Standard Deviation (%)
Present Study	30	3.01	10.8
Present Study	35	3.51	9.0
Present Study	42	3.95	13.4
Manufacture Test	42	3.94	14.3

For the air curtain, two average supply speeds were investigated: 9.1 m/s and 13.75 m/s. By adjusting the air curtain outlet damper, 0° and 20° jet supply angles were selected for the current study. The duct blaster fan at the back of the chamber is used to create the desirable pressure differences across the air curtain door of the chamber, and the corresponding flow rate is measured by the DG-700-gauge model (DG-700 Pressure and Flow Gauge-The Energy Conservatory) at the outlet of the fan. The fan has the maximum capability of 800 CFM (0.4 m^3/s) for exhausting (i.e. creating infiltration through the door), and 600 CFM (0.3 m^3/s) for supplying air to the chamber (i.e. exfiltration through the door). The chamber internal pressure was the measured average pressures at the four locations inside the chamber, and the external pressure was measured at a

location in front of the door at the height of 50 cm above the ground. The pressure tube was set against the incoming wind direction to measure the stagnation pressure of the wind.

The large-scale tests include two series of measurements: 1). **Air Curtain Overall Performance Tests**, which focus on the air curtain overall performance under wind (i.e. variable infiltration rates under a same wind speed); 2). **Comparative Tests for Wind Effects,** focusing on the study of variable wind effects on the same infiltration rates (i.e. varying different wind speeds while keeping the settings of air curtain and duct blaster flows constant). Specifically, in the Air Curtain Overall Performance Tests, the wind generator was maintained for a certain wind speed; the pressure differences and infiltration rates of the chamber were then varied by adjusting the duct blaster flows. For each of the air curtain supply settings (e.g. a certain supply speed and angle), the measurement was based on four wind speed settings from 0 m/s – 4 m/s. For each wind speed setting, the flow rates of the duct blaster were adjusted to achieve 18 different infiltration rates under the corresponding pressure differences through the door (i.e. 18 points of measurements for different flow rates, Q, versus the corresponding pressure differences across the door, ΔP). For this test series, 288 tests were conducted. The major parameters are shown in the Table 4 below.

Table 4. Test settings for the Air Curtain Overall Performance Tests.

Parameters	**Settings**
Air Curtain Supply Speeds	9.1 m/s and 13.75 m/s
Air Curtain Supply Angles	0° and 20°
Wind Generator Wind Speeds	Four wind speeds between 0 m/s – 4 m/s
Duct Blaster Flow Rates	18 settings
Total Measurement Points	$2 \times 2 \times 4 \times 18 = 288$

As for each of the Comparative Tests for Wind Effects, the wind generator was adjusted for different wind speeds from 0 m/s (i.e. no wind) to 4 m/s (with different winds) while other parameters were kept constant, e.g. the air curtain and the duct blaster settings. For a given air curtain supply and angle, with the increase of the wind speeds, the change of both door air infiltration and pressure difference were recorded. Therefore, the comparative tests illustrate the impact of different wind speeds on air curtain performances. 168 Comparative Tests for Wind Effects were completed.

In addition, we conducted an extra series of tests for the air curtain with a lower supply speed of 5.6 m/s, for selected cases, in order to investigate a relatively weaker air curtain jet under different wind conditions. We did not conduct a full set of different parameters for this extra series so this is listed as a separate task (a total of 168 cases). Moreover, preliminary validation tests for the single door were conducted by comparing the results to the theoretical models from the literature (Yuill, 1969).

3.2 Scaled Air Curtain Study in Wind Tunnel

3.2.1 Introduction

The experiments for the sub-scale study were conducted in the Atmospheric Boundary Layer Wind Tunnel at the Building Aerodynamics Laboratory of Concordia University (Fig. 3-6). The wind supply section has the dimension of 1.8 m × 1.8 m (width × height), and the total length of the tunnel is 12 m. The tunnel ground roughness is adjustable for different wind profile types. Observation windows made from acrylic glasses are installed at the tunnel side wall to provide the access to the visualization experimental setup such as PIV. Details about the structure and construction of the wind tunnel can be found in Stathopoulos (Stathopoulos, 1984).

The airflow in the tunnel is generated from a dual-inlet centrifugal fan with the maximum volume flow rate of 40 m^3/s. The generated wind speed ranges from 5 m/s to 12 m/s at the gradient height, above which the wind speed is not affected by the ground friction for an atmosphere boundary layer wind. At the location where the wind stagnation pressure is measured (50 mm from the ground, 1 m in front of the door chamber door), the wind speed is from 4 m/s to 10 m/s. Both speed profiles are measured from the Cobra Probe, which is fixed on a three-dimension traverse system, corresponding to the X, Y, Z directions (width, length, height, respectively).

The objectives of the current wind tunnel tests are to:

- Test sub-scale air curtain performance (1:10 of the large-scale chamber) when compared with the chamber tests, with the theoretical models of air curtains (Wang, 2014), and the single door and vestibules (Yuill, 1996).
- Verify the results of the wind effects from the large-scale wind generator tests. To compare the effects of the wind from the wind generator with those from the "actual" wind from the atmospheric boundary layer wind tunnel.

3.2.2 **Experimental Design and Setup**

3.2.2.1 Wind Speed Tests

The sub-scaled model is installed in the middle of the wind tunnel, and the round base under the model is a 360° turntable for tests of different relative wind angles. In the study, the dimension of scaled model is designed as 1:10 ratio of the large-scale model: 25 cm × 24 cm × 25 cm (L×W×H) with a fully-opened double-swing door of 6 cm × 7 cm, e.g. the door opening angle is 90° as in the large-scale chamber.

Figure 3-6. View of sub-scale model in the wind tunnel.

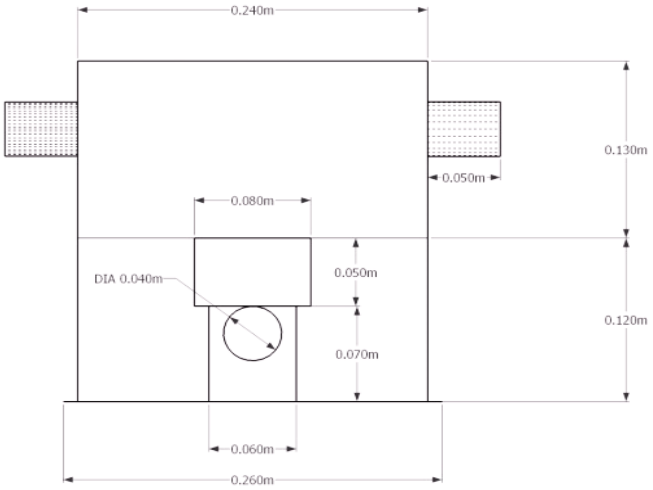

Figure 3-7. Dimensions of sub-scale model (back view of the chamber).

The top two ports of the sub-scaled building model are connected to a compressed air supply through a digital flow rate controller to generate an air curtain jet with the designed supply velocity. Meanwhile, the air curtain jet speed was also calibrated through two hot-wire anemometers.

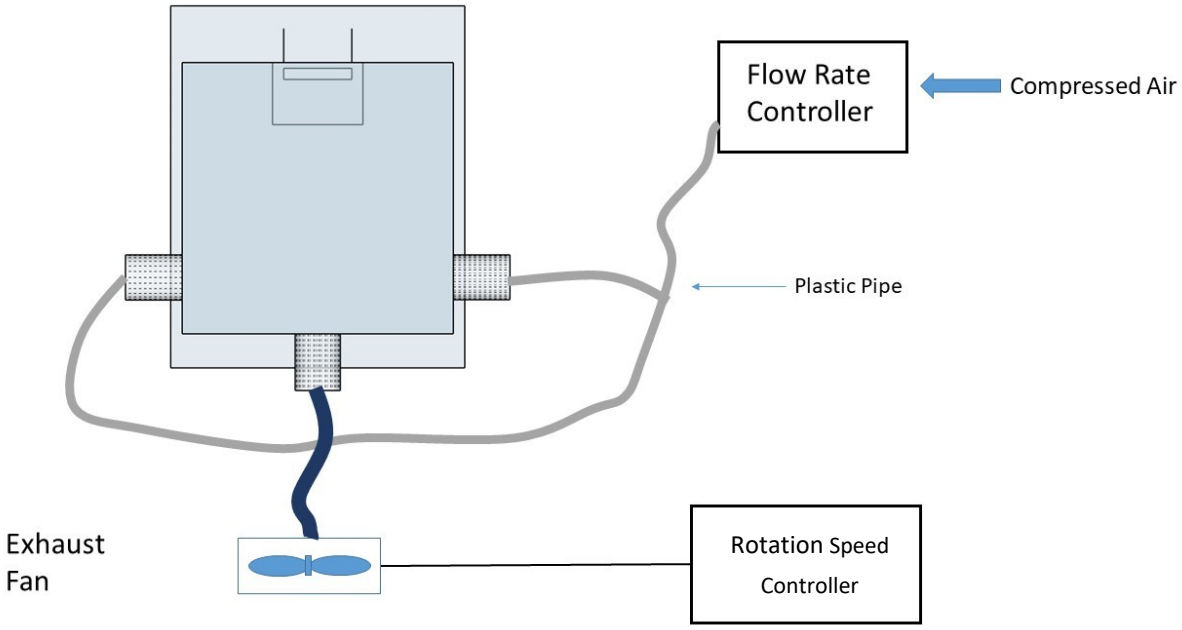

Figure 3-8. Connection of devices for experimental setup (top view of the chamber).

The terrain exposure for these tests is designed to be the open country terrain achieved by installing polypropylene carpet on the tunnel ground. The wind pressure test location is one meter away from the chamber model so that the wind field and pressure are not disturbed by the model itself: a windward recirculation zone is developed in front of the chamber and the pressure tap should be placed far enough from the model to avoid potential disturbance.

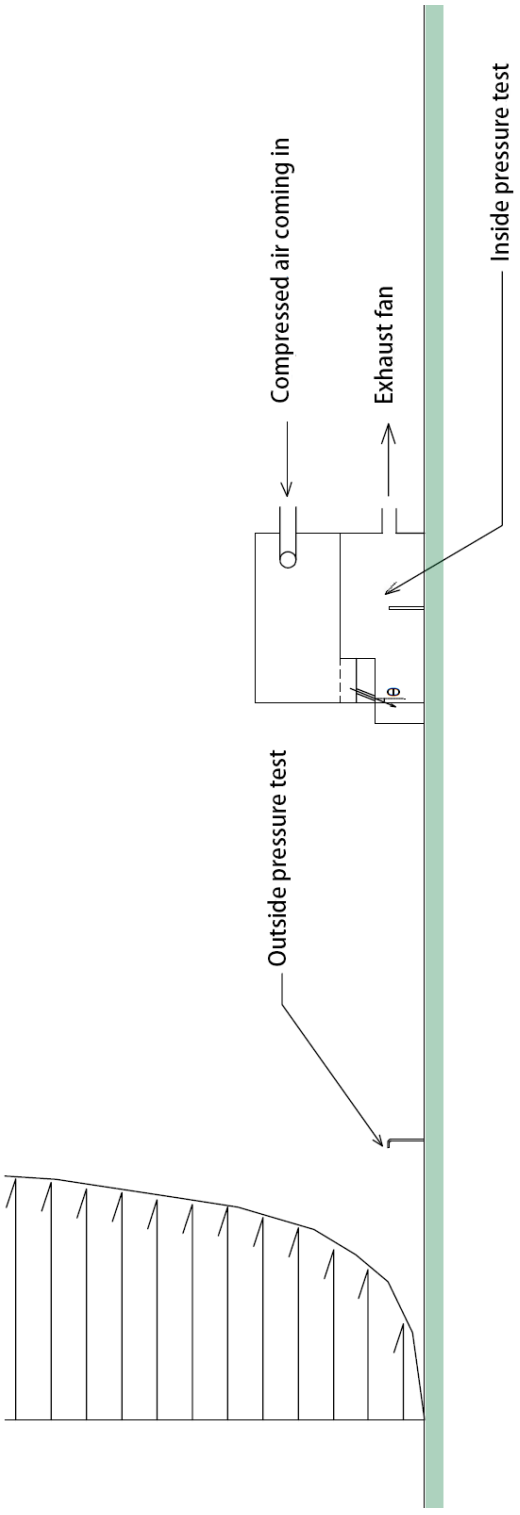

Figure 3-9. Side view of the experimental setup in the wind tunnel.

For the sub-scale chamber internal pressures, four pressure taps were installed at the same relative locations as those of the large-scale chamber, and the pressures were averaged as the chamber internal pressure. The pressure measurement system includes a sensitive pressure scanner system, the Digital Service Module (DSM 3400) from the Scanivalve, and the Electronic Pressure Scanner (ZOC33/64 Px). The DSM can be connected to the scanner with up to 64 channels. The flow rates of the chamber exhaust fans (i.e. a series of computer cooling fans, CPU fans, with digital controllers) were calculated from the digital controllers based on the rotational rates of the fans. However, to reduce uncertainties, we measured flow velocities in the duct connector section by several hot-wire anemometers and calculated the flow rate using Eq. (12).

$$Q_e = V_{ave} \cdot A_d \tag{12}$$

where,

Q_e: flow rate of the exhaust CPU fans, m^3/s

V_{ave}: average speed in the connection duct, m/s

A_d: cross-sectional area of the duct connector (12 cm × 12 cm) with a length of 20 cm.

The chamber door infiltration/exfiltration rate can then be calculated based on the mass balance of the chamber by Eq. (13).

$$Q = Q_e - Q_j \tag{13}$$

where,

Q: door infiltration/exfiltration flow rate, m^3/s

Q_j: air curtain jet flow rate measured by the digital flow controller, m^3/s.

3.2.2.2 Wind Direction Effect Tests

For the study of the wind direction effects, the building model was rotated counterclockwise at different positions (Fig. 3-10) to achieve four relative wind direction β in regard to the door: 0° (not shown), 30°, 60°, 90° and 120° (shown in Figure 3-11).

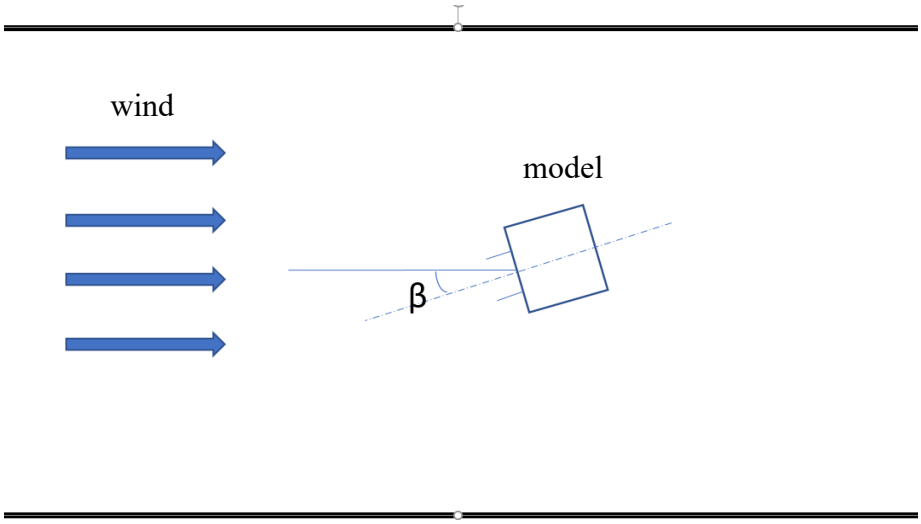

Figure 3-10. Schematic sketch of wind direction measurement (top view in wind tunnel).

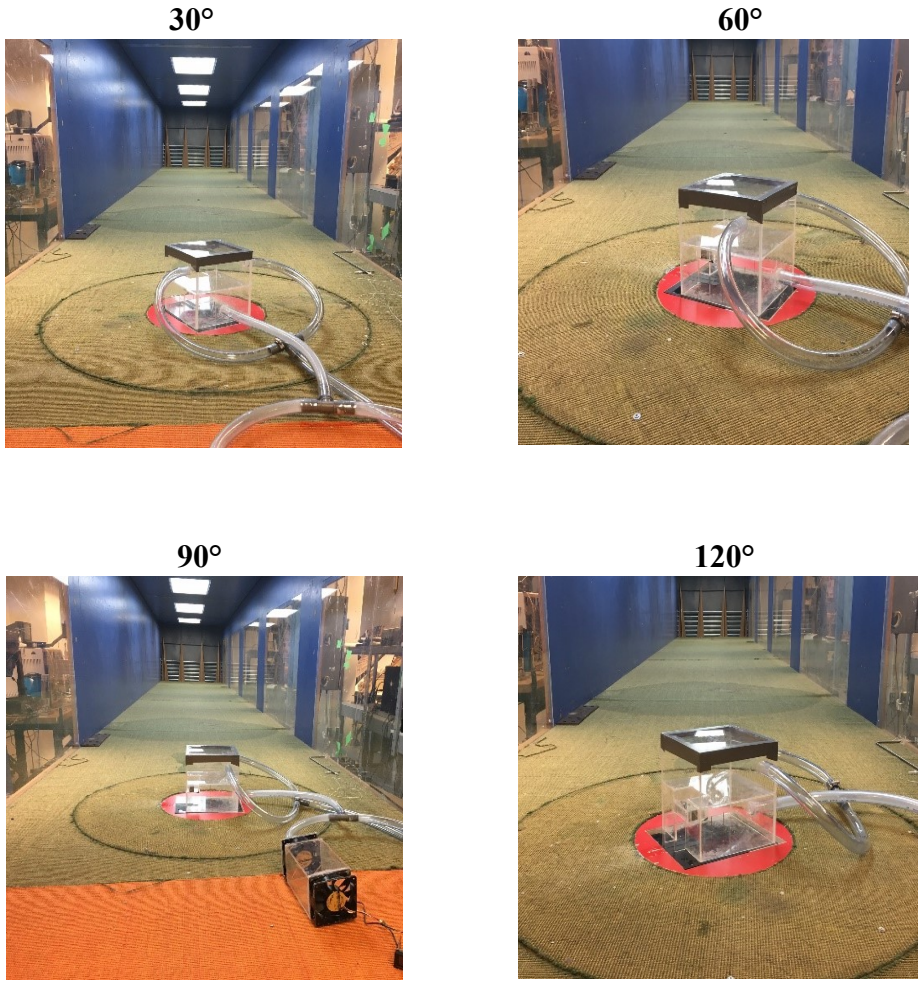

Figure 3-11. Different wind angle tests (the incoming wind pointing outwards of the page).

3.2.2.3 Particle Image Velocimetry (PIV) Test Setup

Figure 3-12 shows the PIV test setup: the laser is set outside the wind tunnel, and the chamber model and the camera are inside the tunnel. To create a vertical laser sheet, a mirror is used to reflect the horizontal laser sheet to the vertical one located in the center of the model, as well as in the center of the air curtain door.

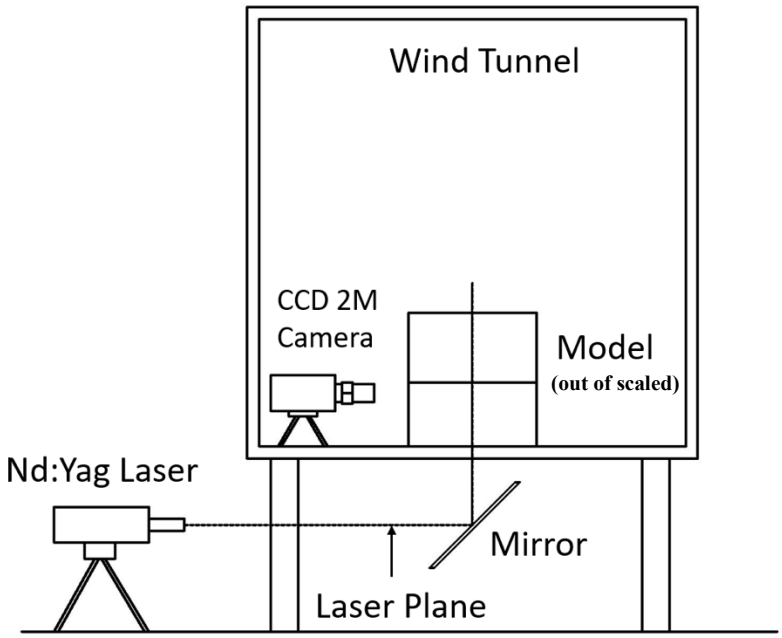

Figure 3-12. PIV setup for capturing the air curtain flow pattern.

The PIV system is a New Wave Research and Monitor model with a laser system of a NG: YAG laser head for double frame laser sheets at the pulse energy of 120 mJ and 532 nm. The camera system is from the DANTEC Dynamics ("Laser Optical CCD and CMOS Cameras | Dantec Dynamics"), capable of generating each picture of 2M (1600×1200) pixel resolution. The lens of this camera is the Nikon's 60 mm lens (60 mm F/2.8 AF NIKON). The laser illustrates the flow pattern of the air curtain supply jet in the middle cross-section. In the PIV tests, the air curtain jet is mixed with the PIV seeds of aluminum oxide (Al_2O_3) powder, of which the released amount is kept the minimal, so it can be negligible when compared to the air curtain flow. For flow outside the chamber, it is mixed with Fog

3.2.3 **Wind Speed and Wind Direction Settings**

The sub-scale air curtain jet speeds were selected as shown in the following table. The air curtain jet with 9.6 m/s is comparable to the large-scale supply of 9.1 m/s as discussed later in the section

2.3. Similarly, the results from 5.7 m/s supply in the sub-scale wind tunnel tests are comparable to those from 5.6 m/s in the large-scale chamber. The air curtain slot is 61 mm × 6 mm (Length × Width). From the table 6, there were a total of 288 measurements conducted. Here, the wind speed refers to the free stream wind velocity measured without the presence of the sub-scale model in the wind tunnel. For the study of wind angle effects, Table 7 shows that a total of 144 measurements and eight air curtain performance curves (i.e. $Q - \Delta P$) were obtained including the tests with and without the double swing door.

Table 5. Study of wind speed effects.

Test Cases		Wind Speeds	Measurements
Air Curtain Door Settings	Avg. 9.6 m/s, θ =0°	0 m/s, 4 m/s, 10m/s	108 (54 repeated)
	Avg. 9.6 m/s, θ =20°	0 m/s, 4 m/s, 10 m/s	108 (54 repeated)
	Avg. 5.7 m/s, θ=0°	0 m/s, 10 m/s	36
Single Door		0 m/s	18
Vestibule Door		0 m/s	18

Table 6. Study of wind direction effects.

Air Curtain Type	Supply Speed 9.6 m/s, Angle 0 °				
Wind Direction β (°)	0	30	60	90	120
Wind Speed (m/s)	4 m/s				
Door Swings	With/Without	With	With/Without	With	With/Without
Number of Cases	36	18	36	18	36

4. RESULTS AND DUSCUSSION

4.1 Large-scale experiment results

4.1.1 Air Curtain Overall Performance Tests

The experimental results are shown in Figs. 4-1 and 4-2 in the forms of "$Q - \Delta P$" curves. By default, a positive value of Q means infiltration and a negative value for exfiltration. ΔP is the external and internal pressure difference including the wind stagnation pressure. Fig. 4-1 shows the air curtain performance when the speed is 13.75 m/s with two supply angles, 0° and 20°, and with four types of wind machine outputs (wind speeds). Fig. 4-2 shows the performance when the supply speed is 9.1 m/s with the 0° and 20° supply angle. All the air curtain supply types are listed in the Table 5 below. The detailed test results are presented in Appendix (A)

Table 7. Air curtain supply settings.

Air Curtain Supply Types	Air Curtain Speeds	Air Curtain Angles
Supply 1	13.75 m/s	0°
Supply 2	13.75 m/s	20°
Supply 3	9.1 m/s	0°
Supply 4	9.1 m/s	20°

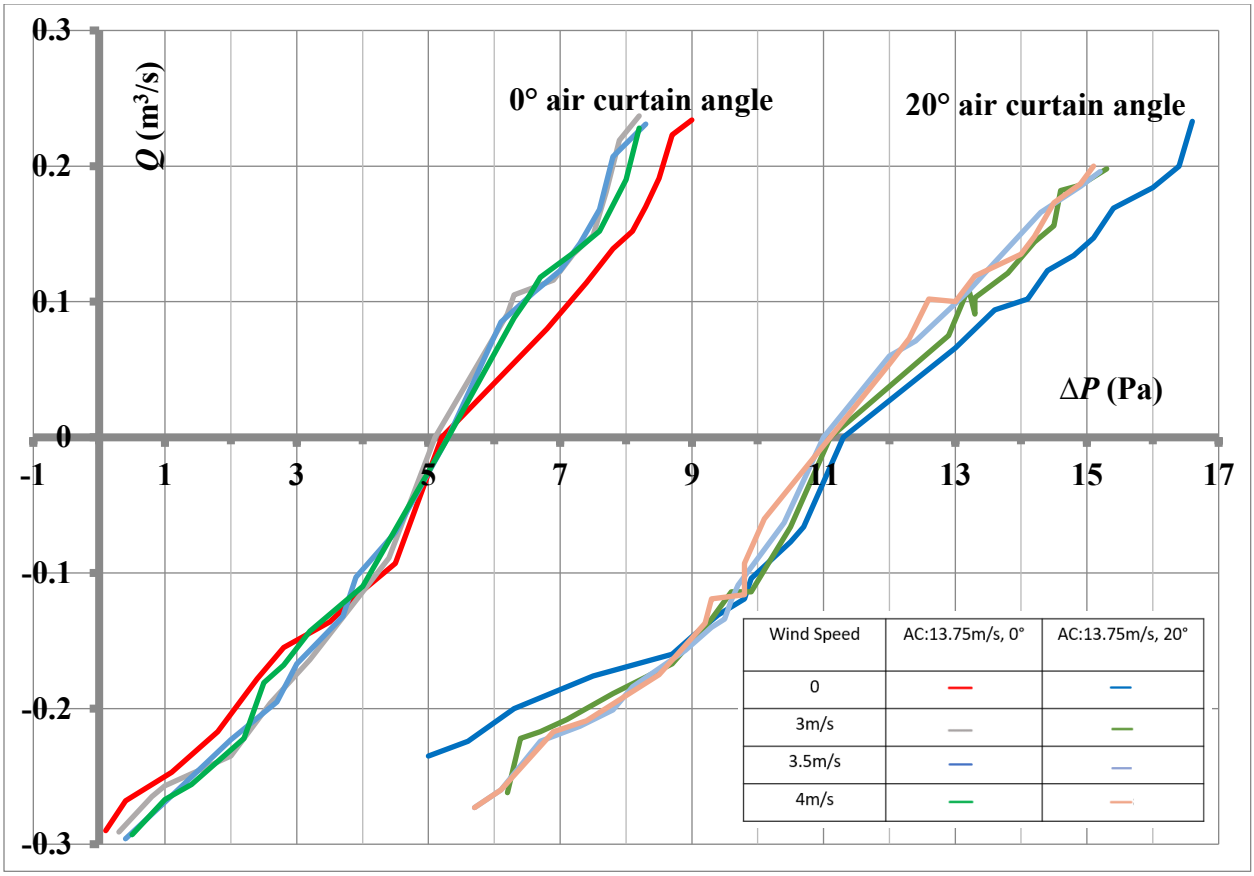

Figure 4-1. Air curtain performance for the air curtain (AC) supply speed of 13.75 m/s.

As shown in Fig. 4-1, under the condition of no wind and the air curtain supply velocity of 13.75 m/s and supply angle of 0° (i.e. air curtain jet pointing down), infiltration occurs (the infiltration breakthrough) when the pressure difference is higher than 5.3 Pa. With the increase of the wind speed from 0 to 4 m/s, the infiltration breakthrough still occurs near the pressure difference of 5.3 Pa. When the pressure difference across the air curtain door is higher than 5.3 Pa, different wind speeds show minimal impact on the air curtain, although the resultant infiltration from wind conditions is a bit more than that without the wind (0 m/s) under the same pressure differences. When the air curtain supply angle changes to 20°, the infiltration starts at the pressure difference of 11.1 Pa, indicating that the air curtain becomes “harder” to be penetrated by infiltration. The

effect of different wind speeds is similar to the 0° supply angle under the 13.75 m/s supply, showing that both air curtain supply angles provide the protection against different winds while 20° performs much better than 0°.

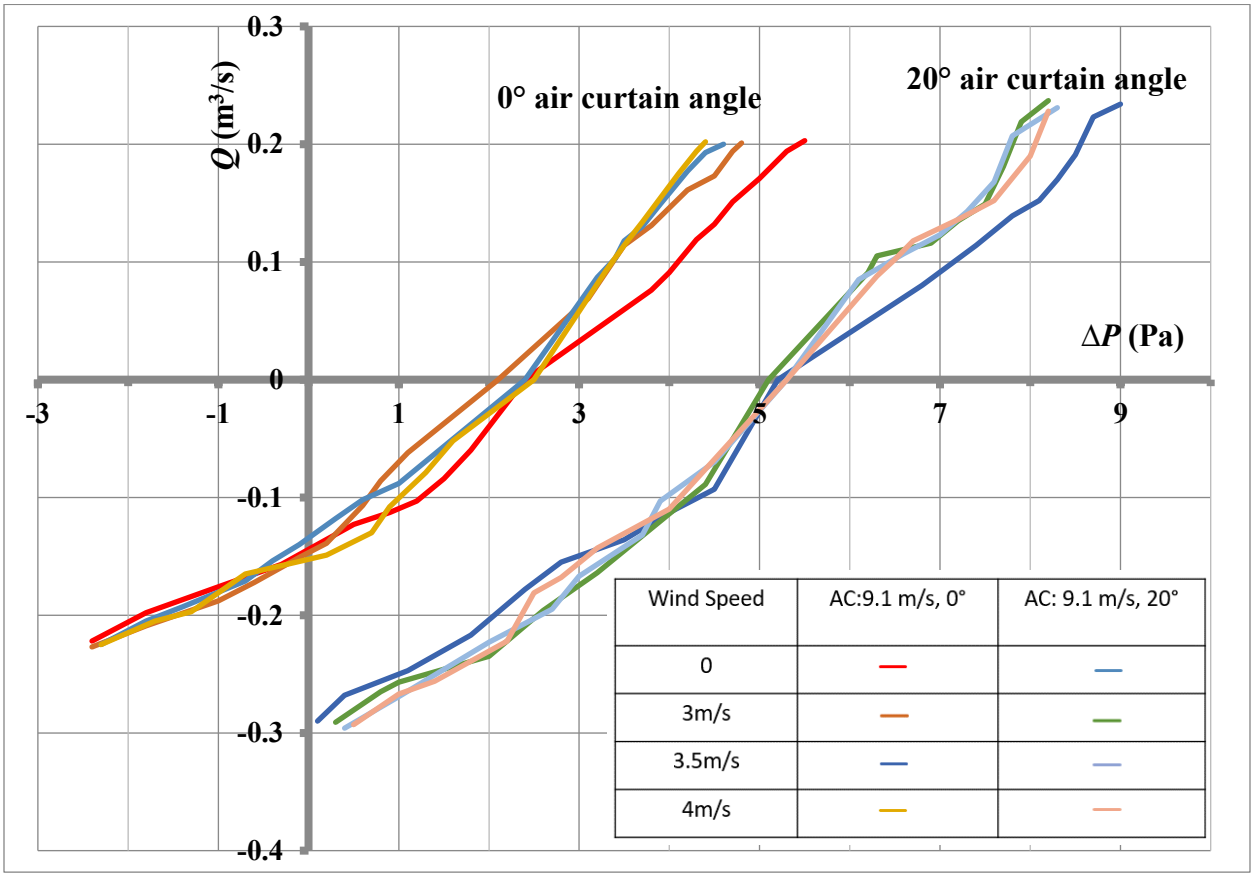

Figure 4-2. Air curtain performance for the air curtain supply speed of 9.1 m/s.

In comparison, Fig. 4-2 shows that for the air curtain supply of 9.1 m/s with these two angles of 0° and 20°, the infiltration appears at about 2.4 Pa and 5.3 Pa respectively. The trends and effects of different wind speeds are similar to those under the supply speed of 13.75 m/s. Interestingly, the infiltration breakthrough occurs at the same 5.3 Pa pressure difference for the "13.75 m/s, 0°" air curtain supply and the "9.1 m/s, 20°" supply. Therefore, by simply adjusting air curtain angle more outwards from 0° to 20°, it can achieve the similar protection against different winds when

compared to increasing the air curtain speed. For the exfiltration region ($Q < 0$), the air curtain door with both supply settings illustrate the same trends of protection against different winds. In summary, based on the air curtain Q-ΔP performance curves, the air curtain supply of 9.1 m/s and 13.75 m/s at both 0° and 20° supply angles provide good protection against the winds (up to 4 m/s) for the large-scale chamber.

4.1.2 **Comparative Tests for Wind Effects**

In the tests of the Comparative Tests for Wind Effects as shown in Fig. 4-3, the test points are grouped as a single working condition, in which the duct blaster and the air curtain were kept at the same settings while the wind from the wind generator was varied among 0 m/s, 3 m/s, 3.5 m/s and 4 m/s. In total, seven group of the working conditions have been measured for each air curtain setting.

It shows that in the condition near the zero infiltration and the duct blaster was turned off (the red circles), the change of the wind speed from 0 m/s to 4 m/s results in slight increases of both infiltration and pressure differences. However, all points still tend to follow the same Q-ΔP performance curve. When the duct blaster is on, the increase of winds again is shown to affect minimally on the infiltration through the air curtain door: for the same working condition, the infiltration rates maintain the same for all wind speeds. Therefore, Fig. 4-3 indicates that the variable wind has almost no effect on the air curtain supply of 13.75 m/s for both supply angles of 0° and 20°. In comparison, the single-door test results under 0 m/s wind are also shown in the figure, which illustrates that the single door is not protected at all: a slight increase of pressure results in a significant infiltration almost instantly. With the air curtain supply is 9.1 m/s (Fig. 4-4), the test data show the similar trends as that of 13.75 m/s air curtain, when the wind speed

increases. The difference is that the lower air curtain supply allows the infiltration breakthrough to occur at lower pressure differences, showing a weaker protecting/sealing against different winds when compared to higher air curtain supple speeds.

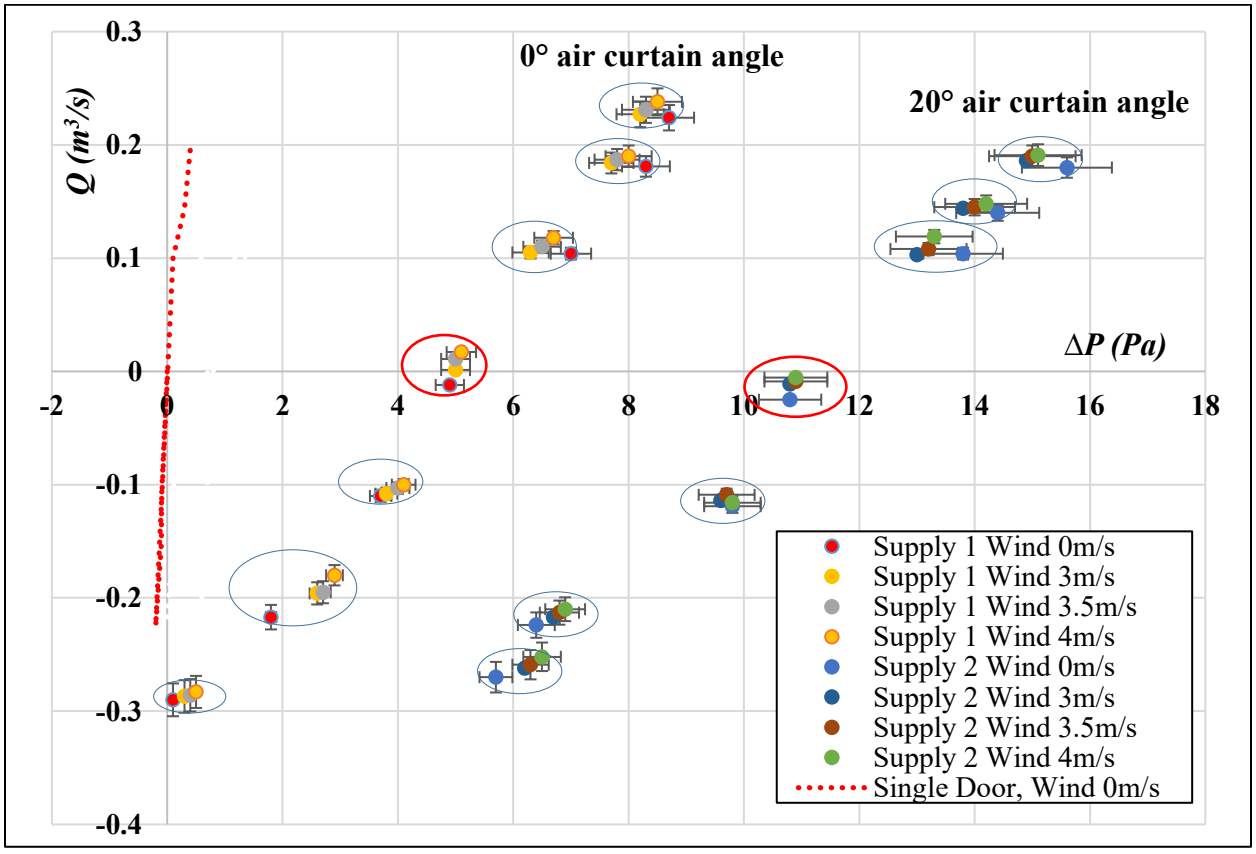

Figure 4-3. Comparative tests for wind effects for air curtains supply 1 and 2 (13.75 m/s), and the single door.

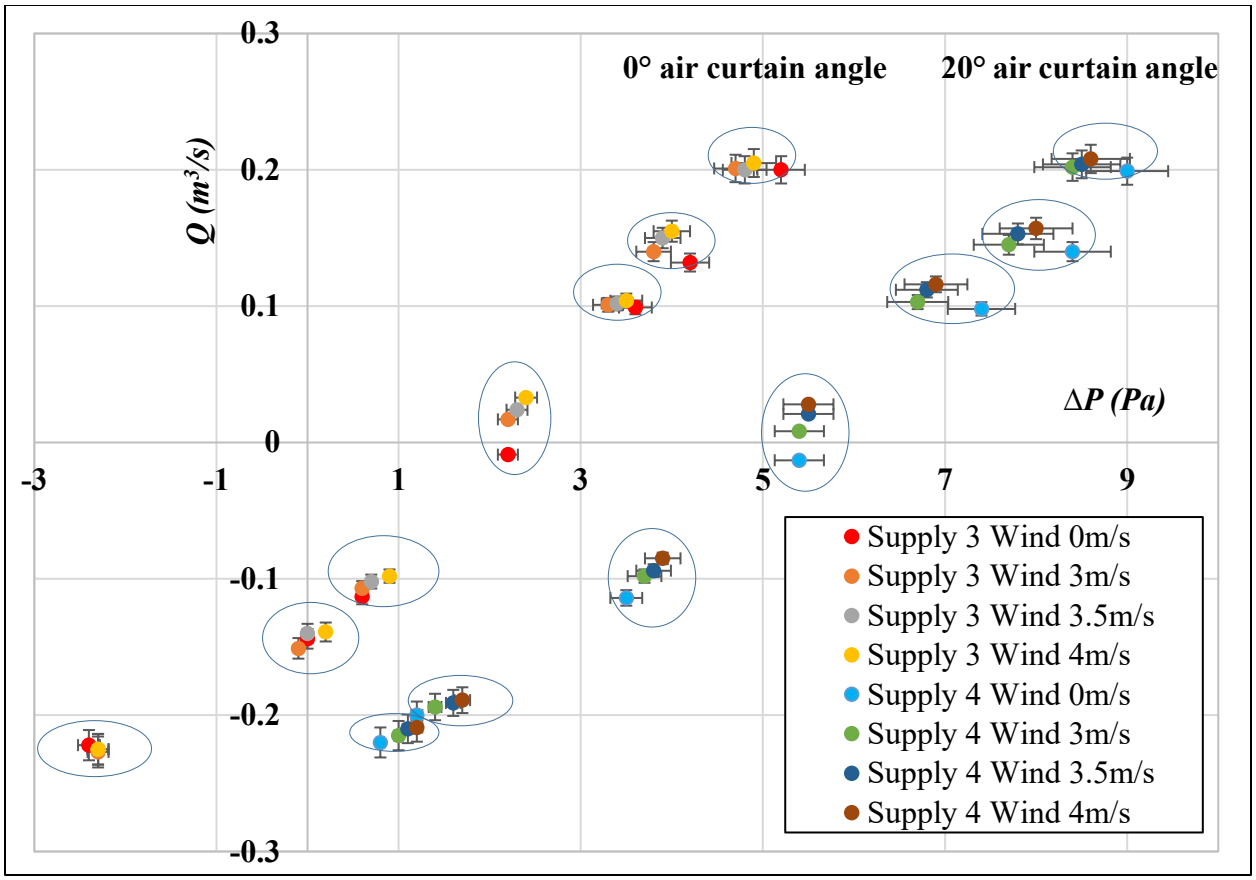

Figure 4-4. Comparative tests for wind effects for air curtain supply 3 and 4 (9.1 m/s).

The measurements in Fig. 4-5 for the case with the air curtain supply speed of 5.6 m/s and 0° supply angle, the worst case among all air curtain supplies, is designed to investigate how wind can affect weak air curtain performance. When the duct blaster was turned off and the infiltration was close to zero (the red circle in Fig. 4-5), the increased wind speed resulted in the increases of both pressure differences and the resultant infiltration rates across the air curtain door with 5.6 m/s. It reflects an important distinction of this research: the wind can affect the air curtain performance much when the air curtain supply speed is low, and the wind speed is high. While when the duct blaster turned on, the weak air curtain may not interact with wind, because the duct blaster is so strong that it already controls the inside pressure and flow rate. When the wind speed increases,

the wind pressure increases, and the pressure difference is increased, which shows the opposite trend to our previous results for strong supply like 9.1m/s. Those results (in blue circles) are the cause of the wind interacting with the chamber mechanical system (duct blaster). It still reveals that a lower air curtain supply may not maintain the air curtain performance under a strong external wind as a strong air curtain supply can do. The current large-scale chamber tests only investigate the wind up to 4 m/s, so the research team recommends more studies of higher wind speeds, for which a series of sub-scaled tests were conducted in the wind tunnel in the next section.

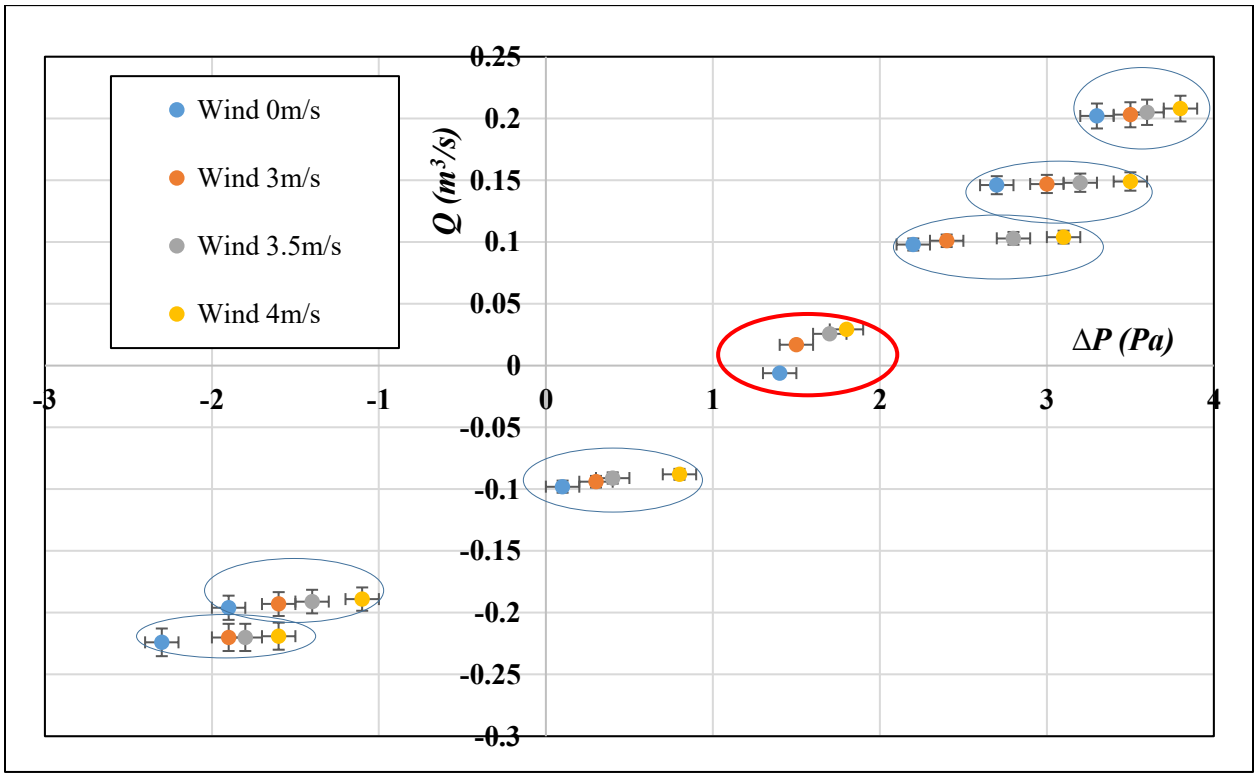

Figure 4-5. Comparative tests for wind effects for air curtain supply 5.6 m/s and 0° angle.

4.2 Sub-scale Experiment Results

4.2.1 Wind Speed Effects

The performance of the air curtain jets is evaluated by the relation of the infiltration rates versus the pressure differences across the door for the infiltration rates ranging from -0.003 m^3/s to 0.003 m^3/s (negative for exfiltration). Nine measurement cases (A1-A3, B1-B3 and C1-C3 in Fig. 4-6) under different infiltration conditions were selected for the PIV tests. The detailed tests results are included in Appendix (B).

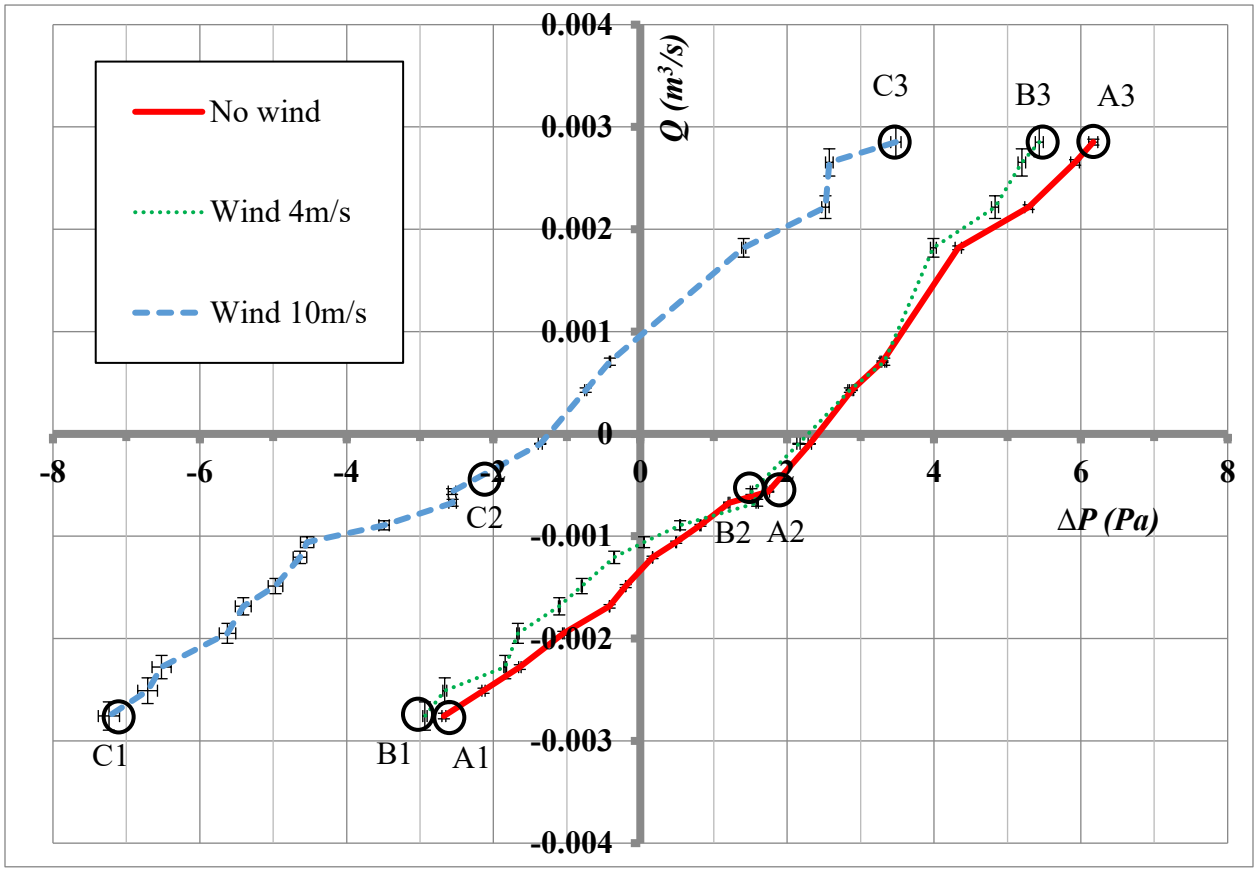

Figure 4-6. Air curtain: supply speed 9.6 m/s and supply angle 0° (Note: the measured pressure differences here include the wind stagnation pressure).

Figure 4-6 shows that for the air curtain supply speed of 9.6 m/s and the supply angle of 0°, the performance curve under 4 m/s wind is close to that of the no-wind case, indicating the air curtain is able to "protect" the door against the wind speed of 4 m/s. When the wind increases to 10 m/s, for a given pressure difference across the door, the infiltration is much greater than that of the no-wind or 4 m/s wind cases: a clear indication that the air curtain is much easier to be broken through even at a low pressure difference level, when the wind speed is 10 m/s. Specifically, for the wind speed of 0 or 4 m/s, the infiltration breakthrough point is at about 2.15 Pa, whereas it is -1.35 Pa for the 10 m/s wind. In other words, the infiltration will occur even when the chamber internal pressure is 1.35 Pa higher than that of the external pressure. It showed that the 10 m/s wind reduced the air curtain performance significantly.

(A1) ΔP_{oi} = -2.67 Pa

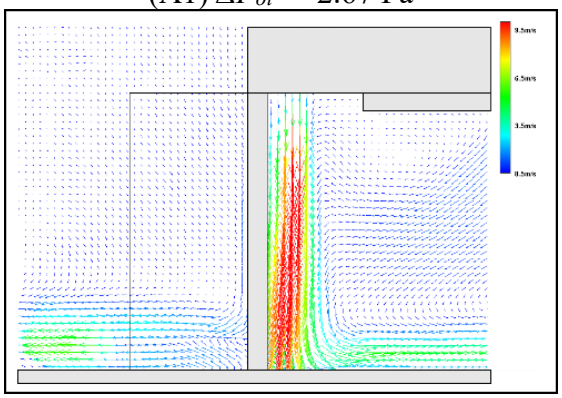

(A2) ΔP_{oi} = 1.74 Pa

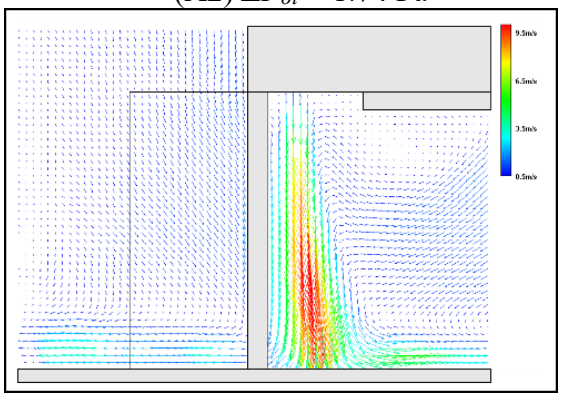

(A3) ΔP_{oi} = 6.17 Pa

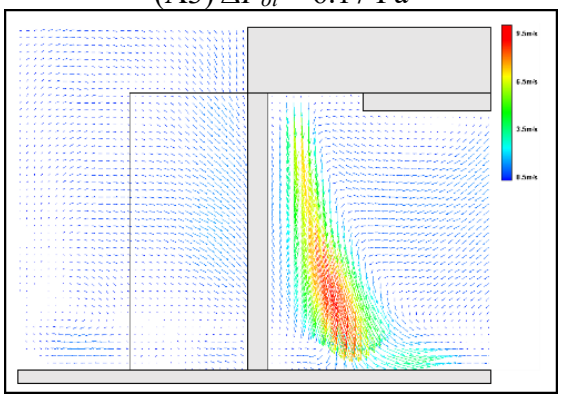

Figure 4-7. (A1-A2-A3) PIV results without wind for the 0°, 9.6 m/s air curtain.

(B1) ΔP_{oi} = -2.93 Pa

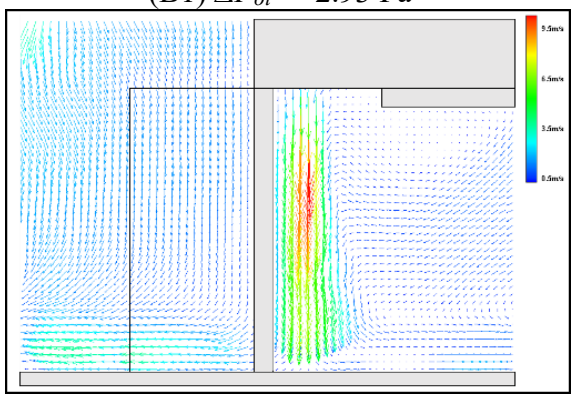

(B2) ΔP_{oi} = 1.51 Pa

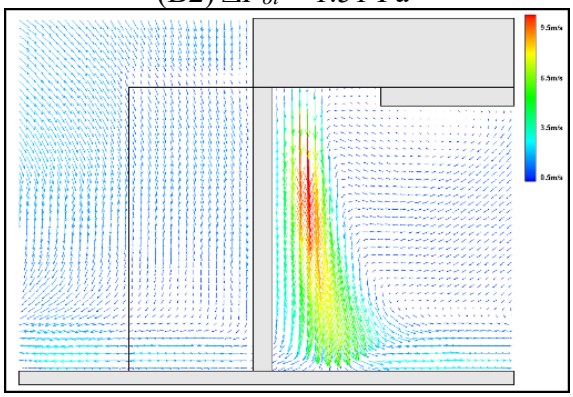

(B3) ΔP_{oi} = 5.43 Pa

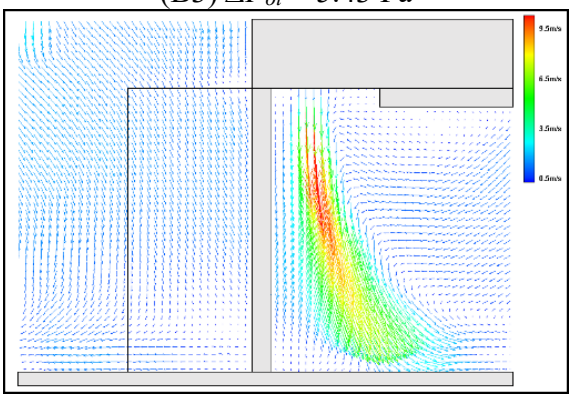

Figure 4-8. PIV results with 4 m/s outside wind for the 0°, 9.6 m/s air curtain.

(C1) ΔP_{oi} = -7.24 Pa

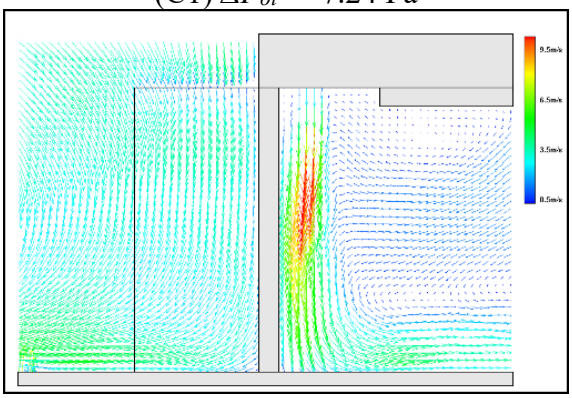

(C2) ΔP_{oi} = -2.56 PA

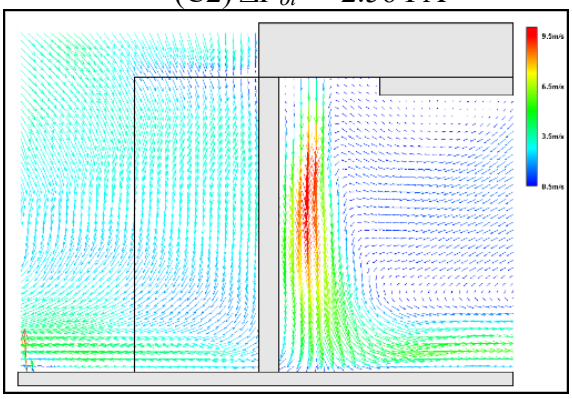

(C3) ΔP_{oi} = 3.48 Pa

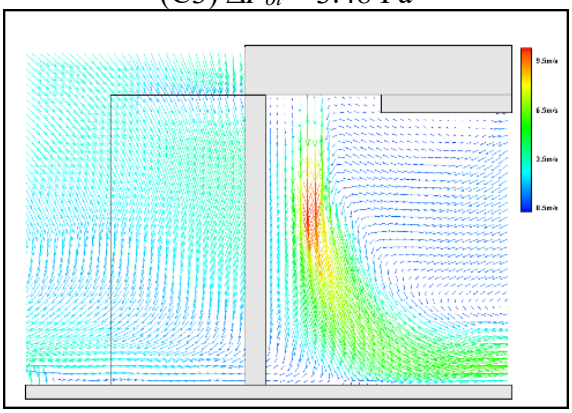

Figure 4-9. PIV results with 10 m/s wind for the 0°, 9.6 m/s air curtain.

The PIV measurements of the flow fields near the opening are shown for the air curtain of 0° supply angle and 9.6 m/s speed at the selected cases in Fig. 4-7 to Fig. 4-9. In A1, A2, B1, B2, C1,

and C2, there were no infiltration from the outside (i.e. all exfiltration cases). The PIV measurements show that the air curtain jet flows in these cases all reached the floor achieving the optimum condition. The jet streams also divided with two parts curved inwards and outwards, respectively, sealing the door from both directions. When comparing the no-wind PIV results (A1-A3) with that of the 4 m/s wind (B1-B3), the measured airflow patterns are very similar, which is consistent with the conclusions from the performance curves of these two cases: the effect of the external 4 m/s wind can be neglected. Although the PIV results for the 10 m/s wind case do not differ much from the other two cases, the air curtain flow tends to bend a bit towards the outside after leaving the air curtain, which is understandable because the cases of C1-C3 all occurred at a lower total pressure difference. For C1 and C2, the indoor pressure had to be higher than that of the outside. For example, as we can compare the flow patterns and performance curves of case B1 and C2, the internal pressure is even higher than the outside for the case C2, while the pressure difference between outside and inside is about 1.5 Pa for the case B2. Figures A3, B3, C3 show the airflow patterns of inflow breakthroughs, where the jet streams were bended inwards under the increased pressure difference across the door. Although the major portions of the jet streams were able to protect the majorities of the door, the external air infiltrates through the door near the ends of the jets and close to the floor. Therefore, for an air curtain door, the observation of the inflow breakthroughs here shows that the infiltration across the air curtain jet often occurs near the lower portion of the jet stream and could become quite significant, even though the area allowing for the infiltration may not be quite large. For future research on air curtain effectiveness and efficiency ratios, efforts should focus on the lower portion of the air curtain jet rather than the upper portion of the curtain, which is close to the air curtain supply outlet.

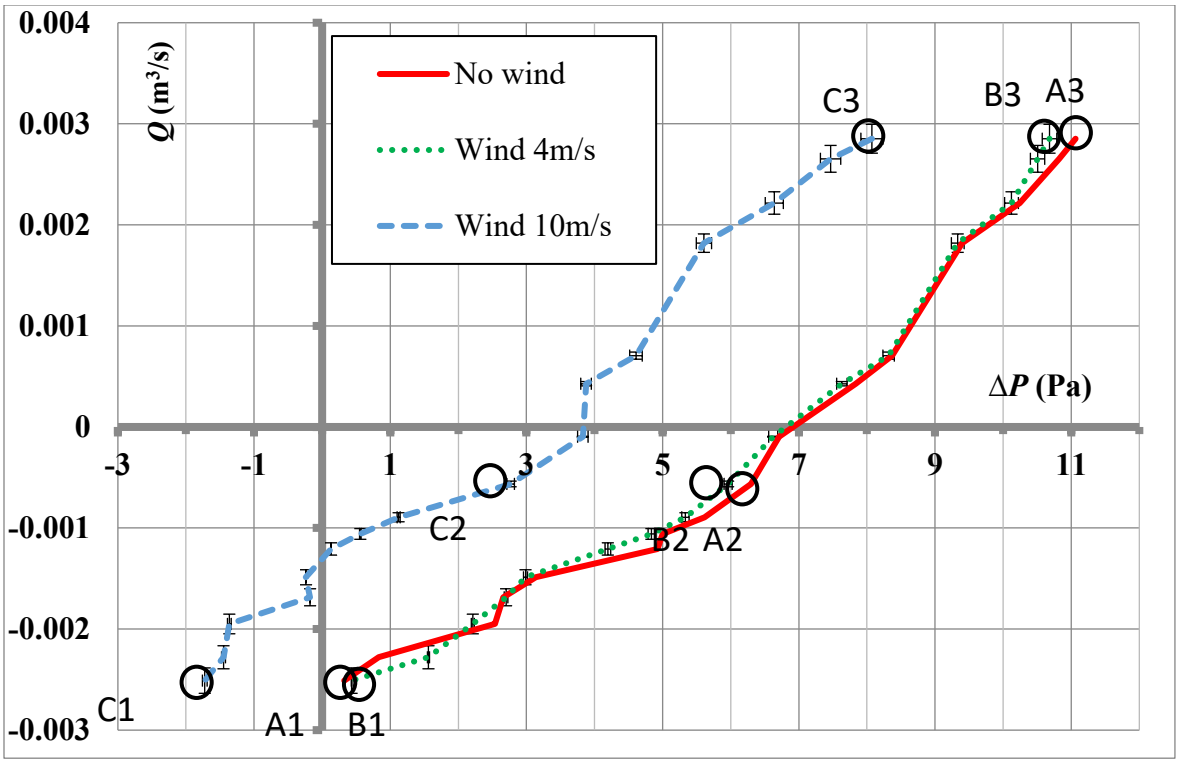

Figure 4-10. Air curtain: supply speed 9.6 m/s and supply angle 20°.

Figure 4-10 shows the performance curves for the air curtain speed of 9.6 m/s and supply angle of 20°. Similarly, the wind of 4 m/s has the minimum impact when compared to the no-wind case, and the infiltration breakthroughs occur at about 6.6 Pa for both cases. With the 10 m/s wind, the infiltration breakthrough occurs much earlier at about 3.8 Pa. Comparing to the case with 9.6 m/s and 0° (Fig. 4-6), the 20° supply angle improves the performance significantly even under the same wind situation: the 10 m/s wind creates the inflow breakthrough at -1.35 Pa for the 0° supply whereas at 3.8 Pa for the 20° supply: an increase of 5.2 Pa for resisting the 10 m/s wind. Therefore, for a given air curtain supply velocity, a small adjustment of supply angle could achieve a huge enhancement of air curtain performance at a zero cost of extra fan power.

(A1) ΔP_{oi} = 0.36 Pa

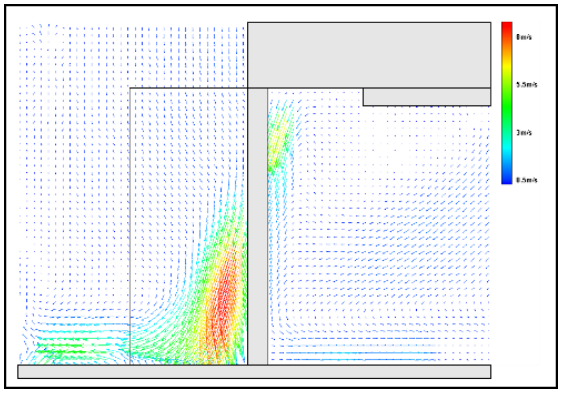

(A2) ΔP_{oi} = 6.29 Pa

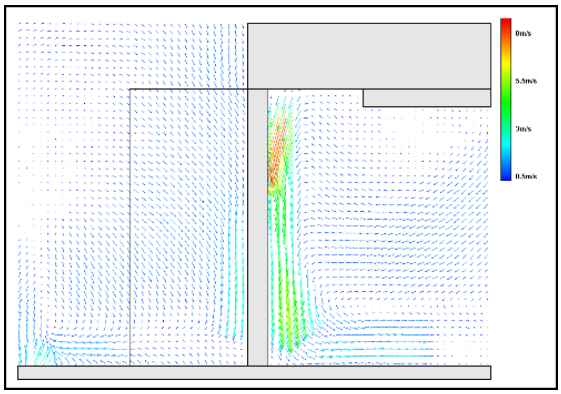

(A3) ΔP_{oi} = 11.06 Pa

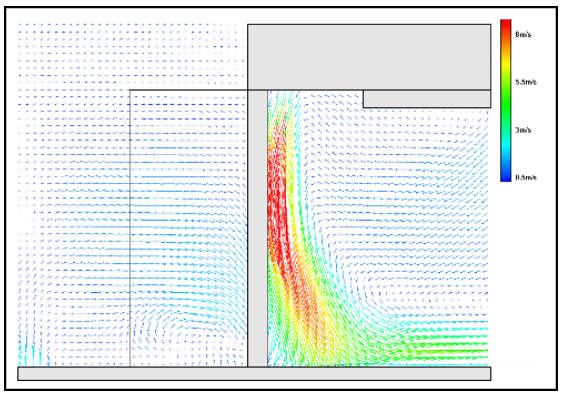

Figure 4-11. (A1-A3) PIV results without wind for the 20°, 9.6 m/s air curtain.

(B1) ΔP_{oi} = 0.48 Pa

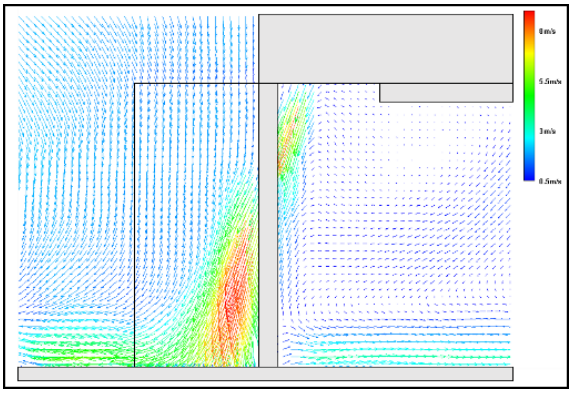

(B2) ΔP_{oi} = 5.96 Pa

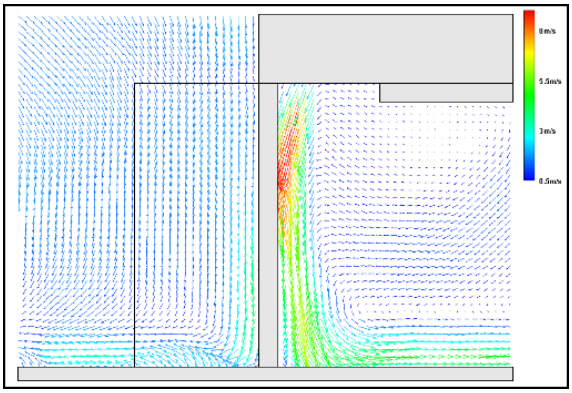

(B3) ΔP_{oi} = 10.68 Pa

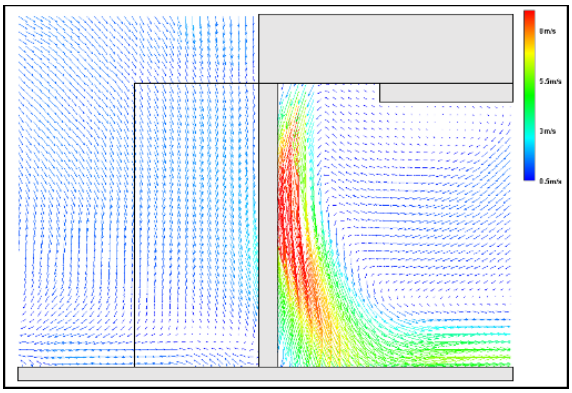

Figure 4-12. (B1-B3) PIV results with 4 m/s wind for the 20°, 9.6 m/s air curtain.

(C1) ΔP_{oi} = -1.89 Pa

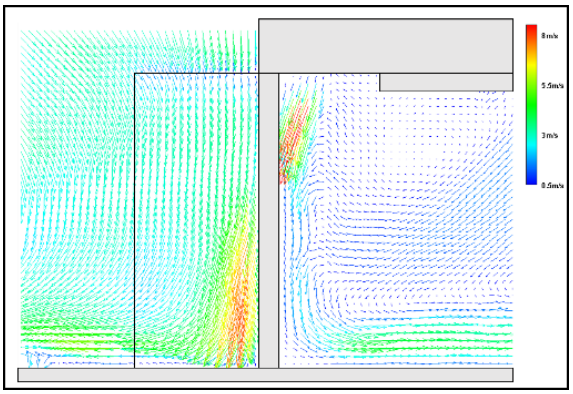

(C2) ΔP_{oi} = 2.77 Pa

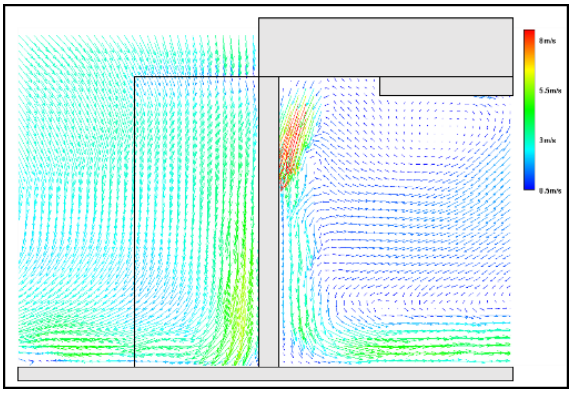

(C3) ΔP_{oi} = 8.07 Pa

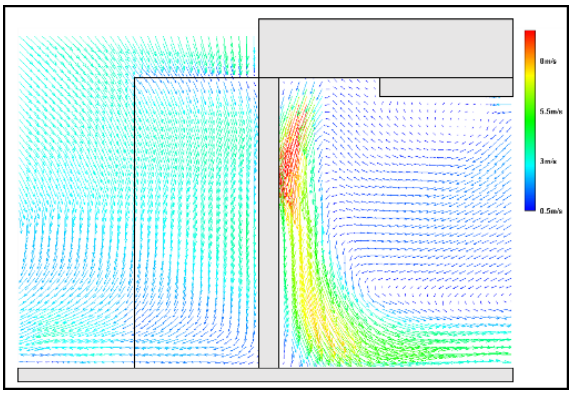

Figure 4-13. (C1-C3) PIV results with 10 m/s wind for the 20°, 9.6 m/s air curtain.

Figures 4-11 through 4-13 show the PIV results for the air curtain of 20° and 9.6 m/s without wind and with winds (4 m/s and 10 m/s). The cases of A1, B1 and C1 show the outflow breakthrough conditions, where the majorities of the air curtain jet flows exhaust to the outside of the chamber. With the increase of wind speed from 0 m/s (A1) to 10 m/s (C1), the jet stream tends to become thinner as a result of increasing incoming wind speed. The existence of the wind also creates significant mixing and turbulence near the lower corner of the chamber. Similar observations and conclusions were observed for the cases of A2, B2 and C2. In both no-wind and 4 m/s cases, the PIV results also show that the air curtain jets reach the floor and separate into two streams, so the door is protected successfully from potential infiltration/exfiltration for both sides of the door.

In the cases of A3, B3 and C3, where the inflow breakthrough occurs, the door cannot be protected effectively so significant infiltration is observed near the floor. A stronger wind, e.g. 10 m/s in C3, tends to weaken the air curtain jet so a smaller portion of the door is protected: about half of the door height was protected in the case of A3 and B3 when compared to about 1/3 of the door height in the case of C3 as visualized by the jet velocity vectors.

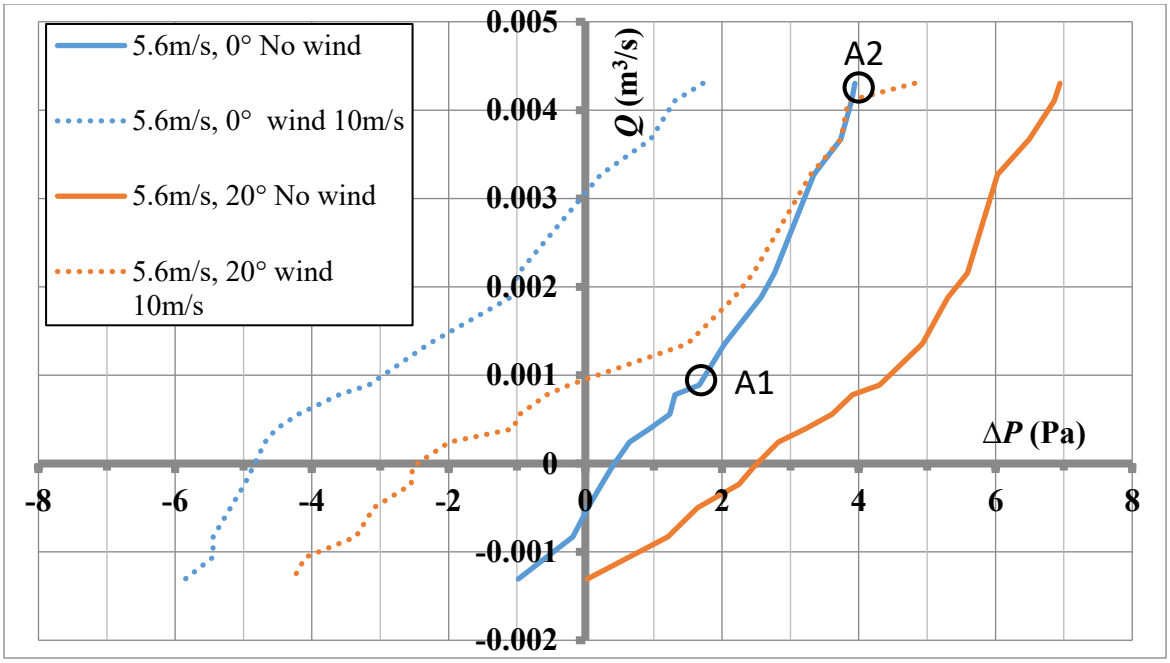

Figure 4-14. Air curtain: supply speed 5.6 m/s and supply angle 0° and 20° without wind and with 10 m/s wind.

To test the air curtain performance under a weaker jet, an additional series of tests were conducted for the 5.6 m/s air curtain supply. Fig. 4-14 shows that for the supply angle of 0° and under the no-wind condition, the infiltration starts at 0.4 Pa, and with the wind speed of 10 m/s, the infiltration appears at -4.9 Pa. For the supply angle of 20°, the infiltration starts at 2.5 Pa for without the wind, and -2.5 Pa with the wind speed of 10 m/s. The PIV results in Fig. 4-15 show that for the case of A1, although the air curtain jet seems to reach the floor, there still exists infiltration passing through the plane of the door. In comparison, the worst case in the case A2, the maximum infiltration occurs when the air curtain jet bends inwards under the high-pressure difference, so a significant amount of infiltration combines with the jet stream and then enters the chamber. When comparing the case of A2 in Fig. 4-15 for the 5.6 m/s supply with the case of C3 in Fig. 4-13 for the 9.6 m/s supply, it is apparent that the weaker air curtain jet allows more infiltration penetration and the

stronger air jet is able to protect the door under a higher-pressure difference: almost at a double pressure difference.

(A1) ΔP_{oi} =1.67 Pa (A2) ΔP_{oi} = 3.94 Pa

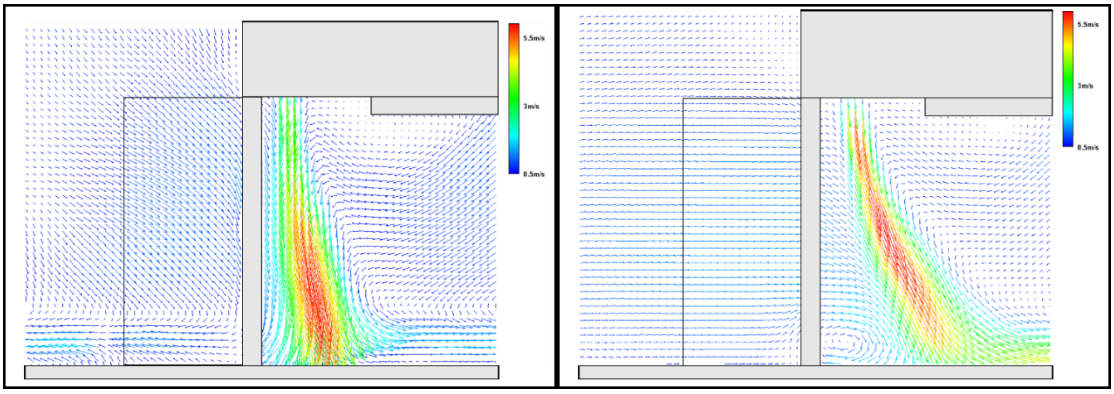

Figure 4-15. PIV results for the 0° and 5.6 m/s air curtain in no-wind condition.

4.2.2 **Wind Angle Effects**

The study of wind angle effects includes two series of tests: with the double swing door and without the door (e.g. in the cases of sliding door), because door types may play a major role for the wind effects. The detailed experimental data for wind angle effects study are included in the Appendix (C).

- **Tests with the Double Swing Door**

As shown in Fig. 4-16, when the wind attack angle increased from 0° to 90°, under the same pressure difference across the door, there will be a significant decrease of infiltration: the air curtain performs better with the increase of the wind angle. As the wind angle changes to 120°, the performance is close to that of 90° wind (i.e. parallel wind to the door plane), which is reasonable because the downwind door is subject to a minimum impact from the wind. Therefore,

the strongest wind effect on the air curtain performance is from the 0° wind: the wind blowing perpendicularly towards the door plane.

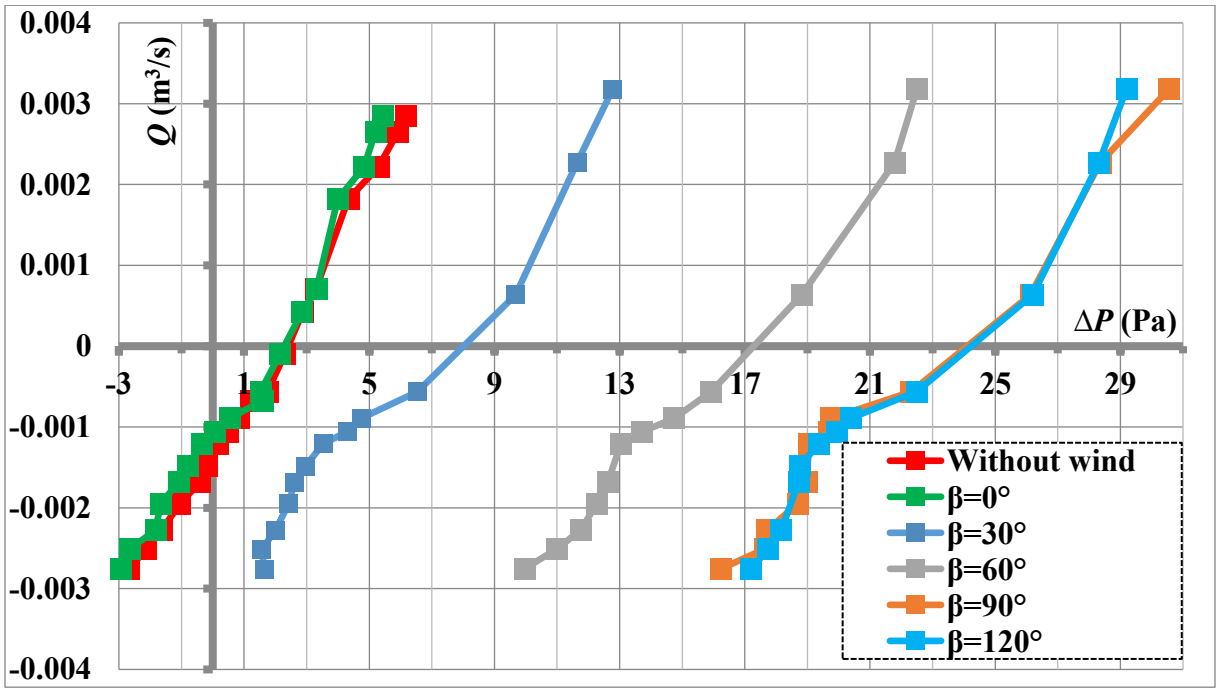

Figure 4-16. Air curtain (9.6 m/s, 0°) performance with 4 m/s wind at wind direction (β) different and with the double swing door.

- **PIV Measurement under 10 m/s, 60° Angle Wind with Double Swing Door**

The PIV tests have been conducted for two cases for the vertical and horizontal planes in order to compare the flow fields with and without the door. Figs. 4-17, 4-18 and 4-19 show the PIV results for the 10 m/s and 60° wind and the 9.6 m/s and 0° air curtain supply with the double swing door, when the infiltration is 0.00064m^3/s. Fig. 4-17 is the time-averaged PIV results of the velocity contours and the corresponding streamlines around the building model with the door. With the existence of the door, the incoming wind was confined between the double doors forming a clear downward flow, which meets with the air curtain jet near the vertical plane of the door. The air

curtain jet then spreads across the chamber floor bringing in significant amount of infiltration. Fig. 4-18 and Fig. 4-19 show a better view of the air curtain jet and the floor infiltration flow. Fig. 4-18 shows that the upper portion of the jet entrains much airflow from the outside and brings it down and then into the chamber. Fig. 4-19 shows that the existence of double doors seems to protect the entrance from the 60° wind well: the majority flow direction between the two doors is towards the outside of the chamber; due to the inwards bent air curtain from the wind effect, the jet hits the floor at a location far from the door plane, bringing in significant amount of entrained infiltration from the outside.

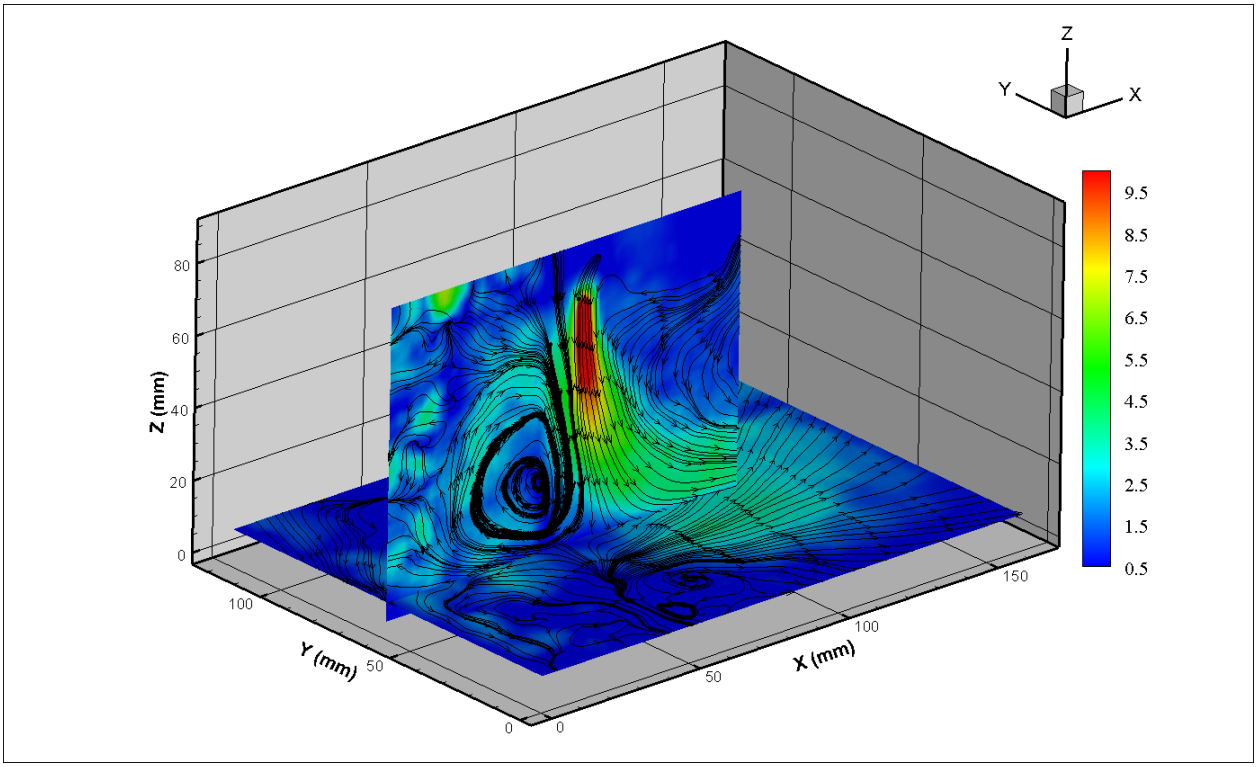

Figure 4-17. PIV results of the 3D flow streamlines of 10 m/s, 60° wind and 9.6 m/s and 0° air curtain supply.

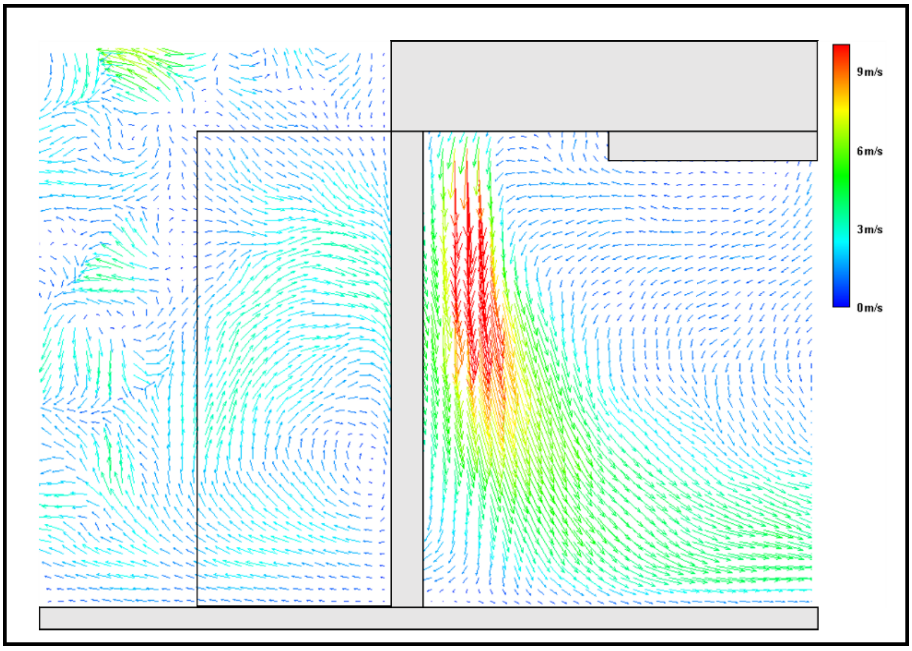

Figure 4-18. PIV results of the vertical central plane of the door with 10 m/s, 60° wind and 9.6 m/s and 0° air curtain supply.

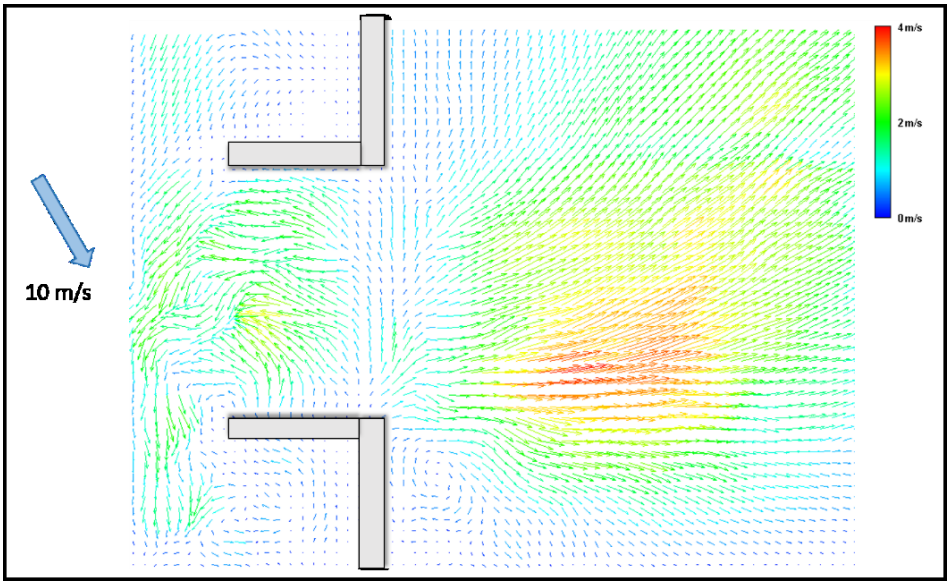

Figure 4-19. PIV results of the horizontal plane flow field at 1 cm above the floor for 10 m/s, 60° wind and 9.6 m/s and 0° air curtain supply.

- **Tests without the Double Swing Door**

After removing the double swing door, Fig. 4-20 shows that the major difference is observed for the 60° wind. It is obvious that when there is no door, the pressure difference for allowing the same infiltration rate is lower than that with the door: the infiltration breakthrough occurs at 16 Pa with the door and at 13 Pa without the door. It confirms that for the 60° wind, the double swing door indeed has the protection effect against the wind. Meanwhile, it is no surprise that the results for the cases with 0° and 120° show no major difference for the infiltration for the cases with and without the double swing door. The door under the 120° wind seems to undergo an increase of exfiltration rate, which can be explained by that the double doors may create a recirculation zone between the two doors with lower external pressure assisting more exfiltration through the door opening.

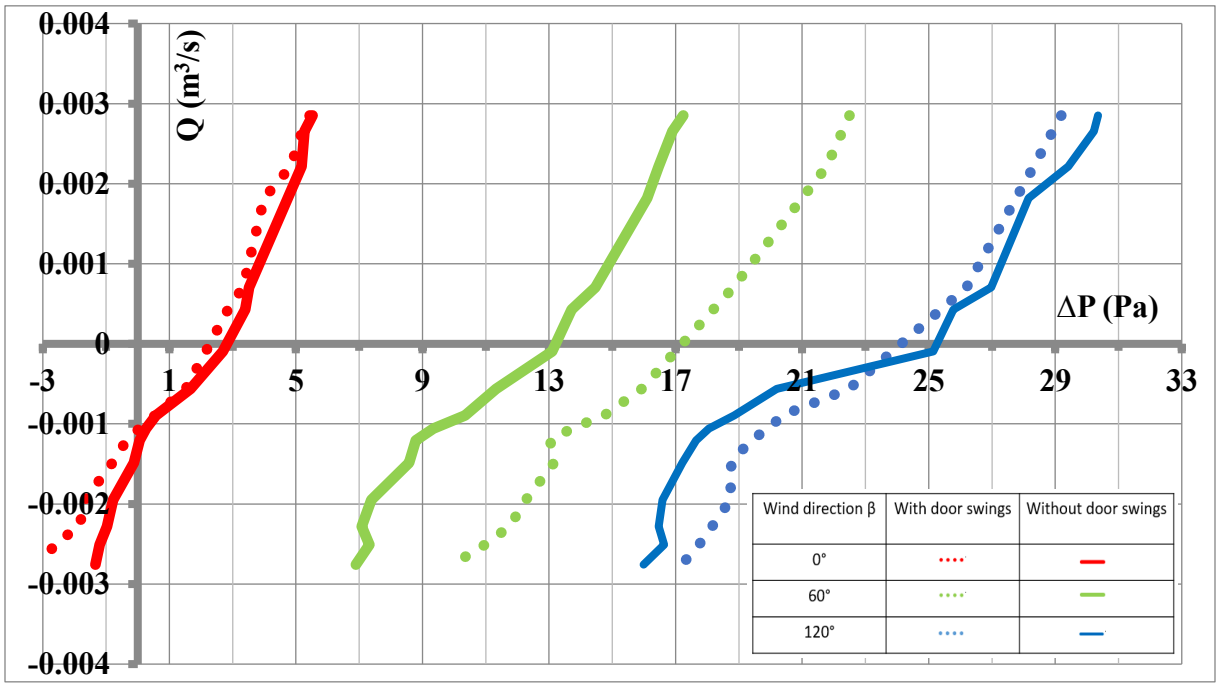

Figure 4-20. Wind angle effect comparison with and without the door with 4 m/s wind for 9.6 m/s, 0° air curtain supply.

- **PIV Measurement under 10 m/s, 60° Angle Wind without Double Swing Door**

Figure 4-21 shows the PIV measured 3D flow field around the building model with 60° wind incident angle. Without the door, the flow pattern becomes quite complicated especially in front of the door. The external wind stops down-washing along the door plane but instead moves around the upper corner of the building model forming quite a few vortexes before meeting with the air curtain jet at the lower portion. It is also clear that the air curtain provides a good protection for the top portion of the door. Meanwhile, the air curtain jet itself entrains external air and brings it down to the floor level. Fig. 4-22 and 4-23 show also how the airflow moves around the air curtain and enters the chamber at an angle near the lower corner of the door and at the floor level, where the jet flow is too weak to offer a minimum protection of the door.

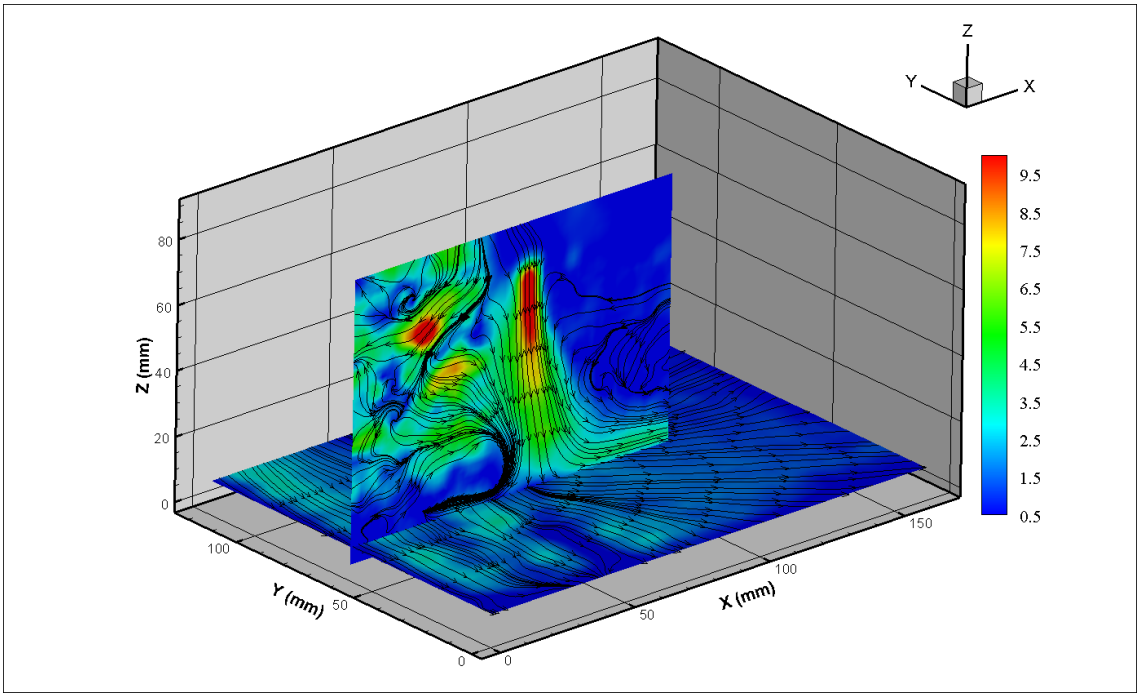

Figure 4-21. PIV results of the 3D flow streams for 10 m/s, 60° wind and 9.6 m/s, 0° air curtain without the double swing door.

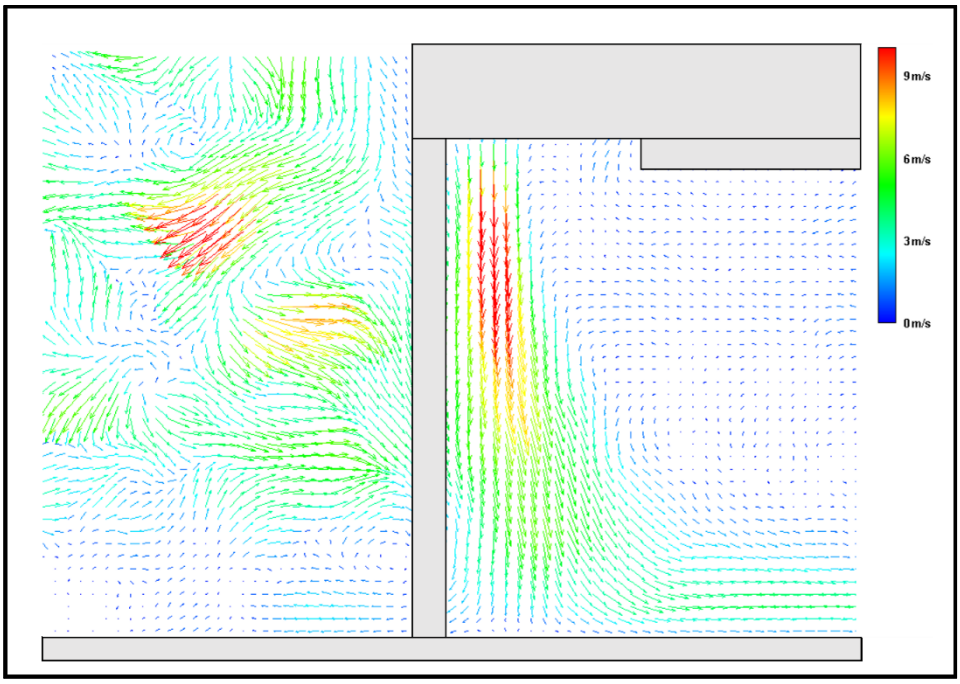

Figure 4-22. PIV results of the vertical central plane of the door for 10 m/s, 60° wind and 9.6 m/s, 0° air curtain without the double swing door.

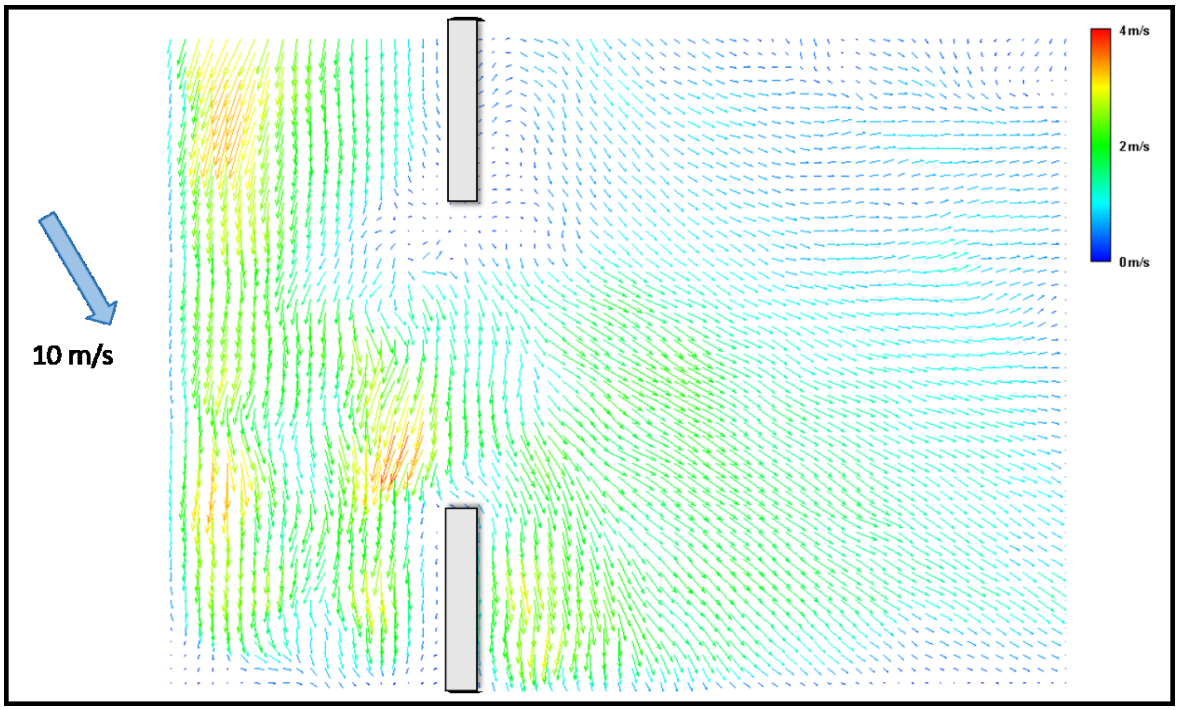

Figure 4-23. PIV results of the horizontal flow field at 1 cm above the floor for 10 m/s, 60° wind and 9.6 m/s, 0° air curtain without the double swing door.

4.2.3 **Effects of Person in the Doorway**

4.2.3.1 Air Curtain Supply of 9.6 m/s and 0°

For the cases without the wind, Fig. 4-24 compares the results the effects with and without a person standing in the doorway and two different person locations, i.e. one is that the person stands right under the air curtain and the other is the person stands three cm in front of the door. It shows that the maximum pressure difference at the optimum condition, in which the air curtain jet can just reach the floor and seal the door (Wang, 2014), is about 3.2 Pa with the person whereas it is around 2.3 Pa without the person. So, either the person in front of the door or standing right in the doorway helps to "block" infiltration through the door better than without the person, which was also confirmed by the previous studies (Wang, 2014; Goubran, 2016). The detailed test result data and person location are included in Appendix (D).

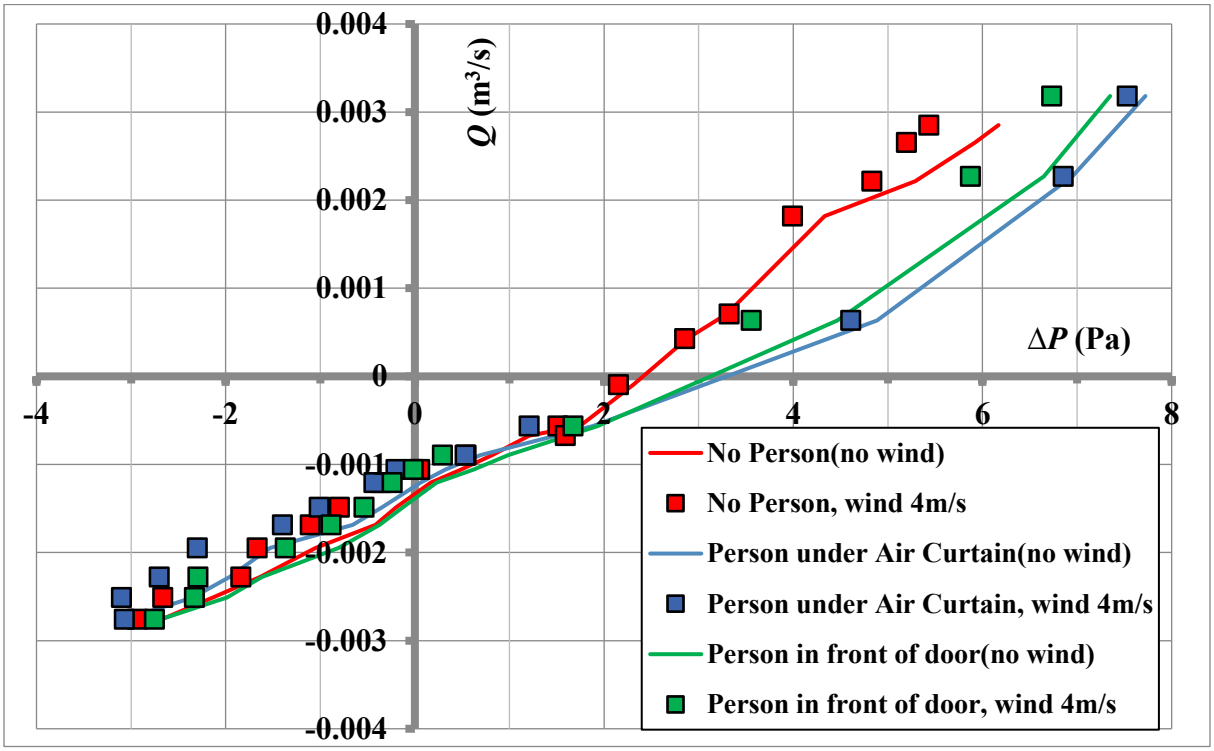

Figure 4-24. Air curtain supply 9.6 m/ and angle 0° with and without person in the doorway.

Moreover, comparing the no-wind and 4 m/s wind cases for the case of person standing right under the air curtain, the performance curves remain the same showing that the air curtain performance seems not affected by the person even under a windy condition. When comparing all the cases with the 4 m/s wind and without the wind, it is obvious that the air curtain door performance with the wind is slightly (but not quite significantly) worse than those without the wind.

Figure 4-25 illustrates the PIV results at three different operating conditions, A1, A2 and A3 when the wind is 4 m/s and 0° and the air curtain is with 9.6 m/s at the 0° supply angle. Apparently, the existence of the person under the air curtain definitely creates a complex and 3D flow pattern. In all cases, the air curtain jet reaches the head of the person and splits in halves moving around the body of the person. Depending on the pressure difference across the door, either exfiltration (A1 and A2) or infiltration (A3) occurs, while the incoming wind seems not quite to affect the door significantly.

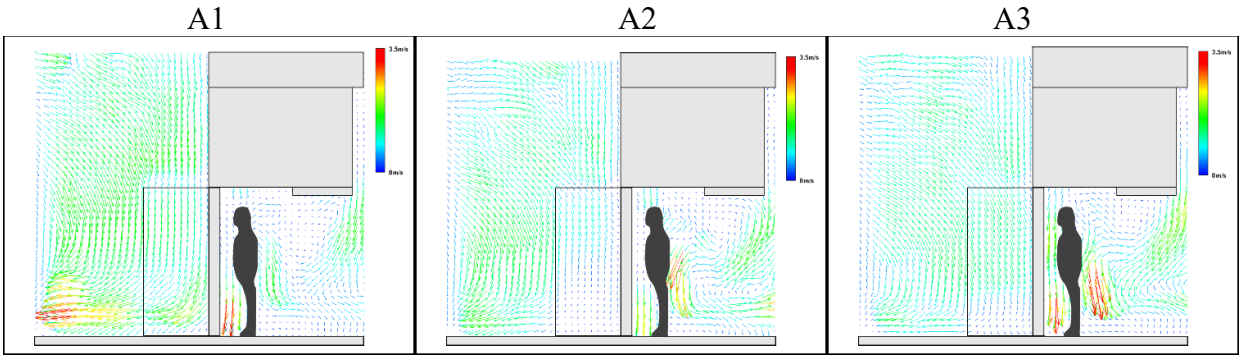

Figure 4-25. PIV results of the 4 m/s and 0° wind and the 9.6 m/s and 0° air curtain with a person under the air curtain.

4.2.3.2 Air Curtain Supply: 9.6 m/s and 20°

When the air curtain supply angle changes to 20° (i.e. air curtain blowing towards the person's head), Fig. 4-26 shows that again the person under the air curtain improves the air curtain performance as it did for the 0° air curtain supply. For the case without the person, the infiltration breakthrough starts at 6.6 Pa while with the person under the air curtain, it occurs at about 8.3 Pa. When under the 4 m/s wind, the existence of a person has the minimum effect on the air curtain, which is similar to the results for the air curtain supply of 9.6 m/s and 0° angle.

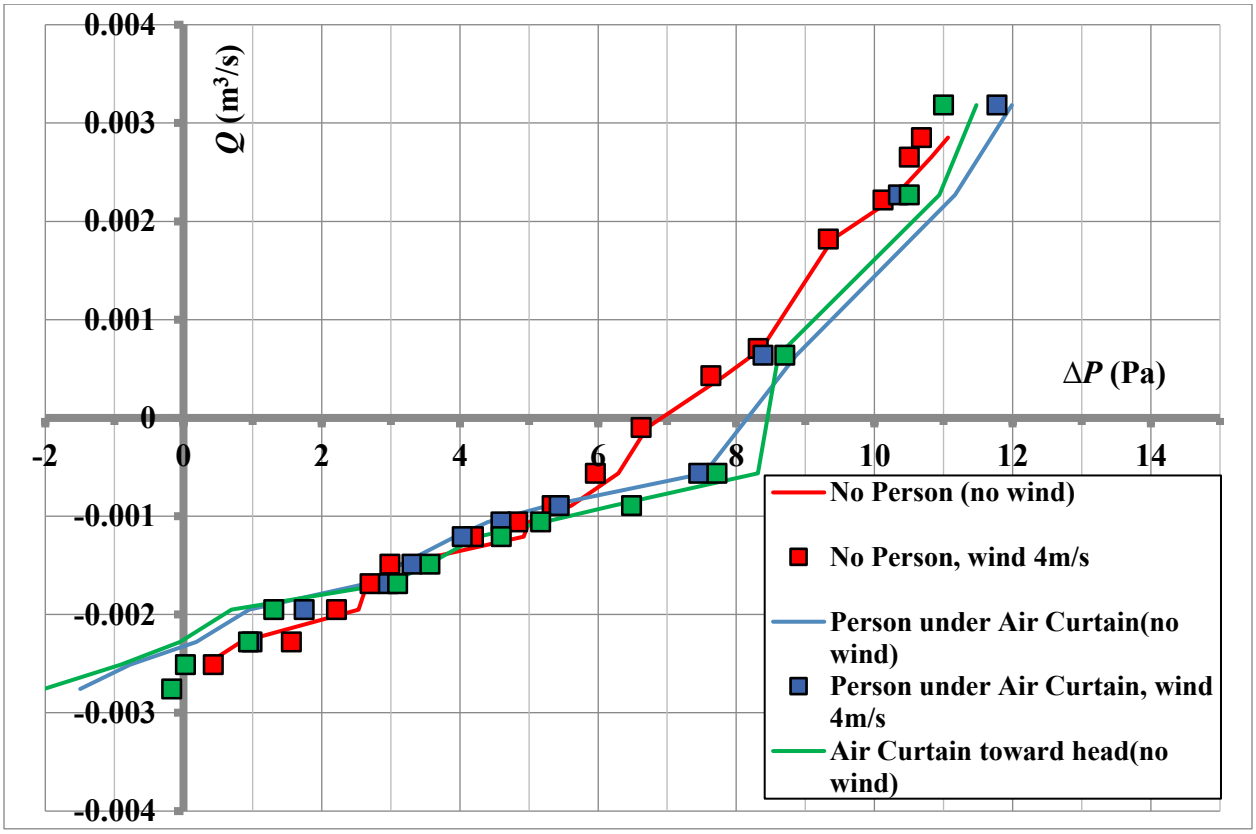

Figure 4-26. Air curtain supply 9.6 m/s and supply angle 20° with and without the person.

4.3 Large-scale tests and Sub-scale tests: Result Comparison

4.3.1 Result Comparison between Different Scales

To confirm the scaled wind tunnel tests are comparable to the large-scale tests (or vice versa), a series of extra tests for the single door and vestibule door have been conducted for no-wind conditions. Fig. 4-27 shows the scaled building model with a vestibule. The tests result data related to single door and vestibule door are included in Appendix (E)

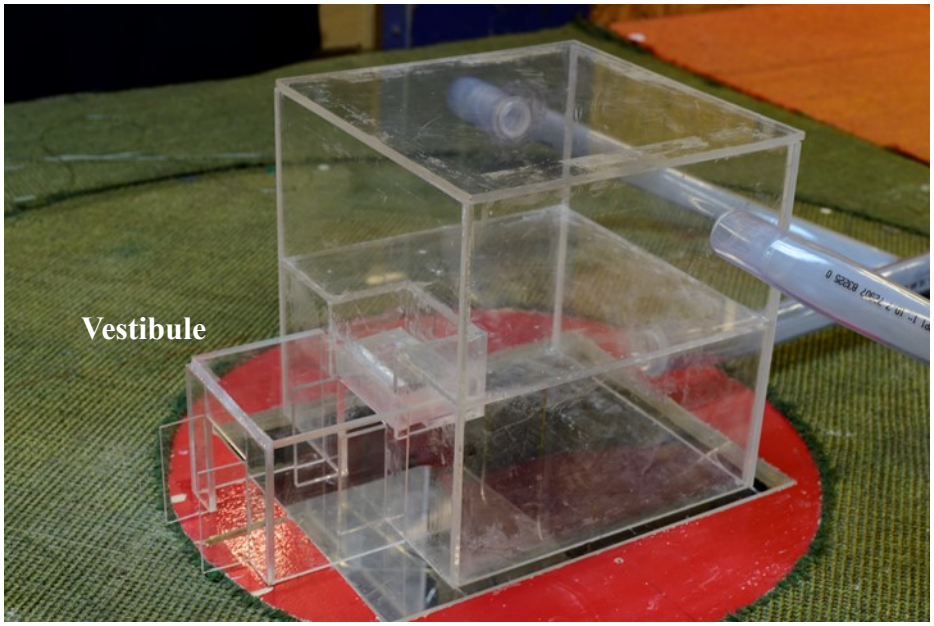

Figure 4-27. Sub-scale building model with a vestibule.

- Comparison for no-wind cases

Figure 4-28 compares the results of the scaled wind tunnel chamber tests and the large-scale chamber tests. From the single door and vestibule Q-ΔP measurements, the scaled model results are pretty close to those of the large-scale chamber, indicating the single door and the vestibule door can be properly scaled in the current study.

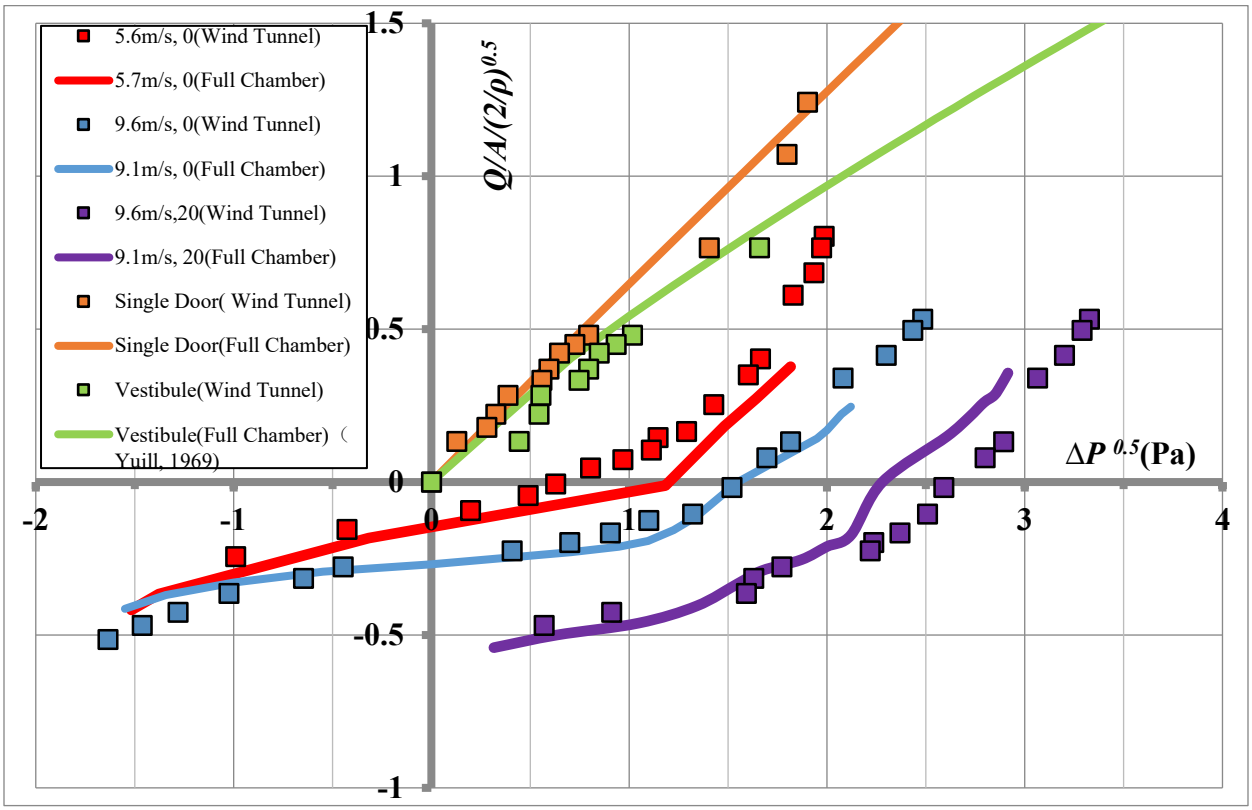

Figure 4-28. Results of comparison among difference scales without the wind.

From the air curtain results of the scaled chamber and the large-scale chamber (marked as the Full Chamber), Fig. 4-28 shows that the dimensionless performance curves are similar under different scales of air curtain and settings. This confirms the similarity for large-scale tests and sub-scale wind tunnel test, which implies that results in these two tests are comparable. Tests at other scales will be considered in the future studies to confirm the scale effect.

- Comparison for the 4 m/s wind cases

Figure 4-29 shows that under the 4 m/s wind, the dimensionless performance curves are very similar for both the large-scale chamber and the sub-scaled chamber, confirming that the study of the wind effects in the large-scale chamber and the wind tunnel are similar, comparable and valid.

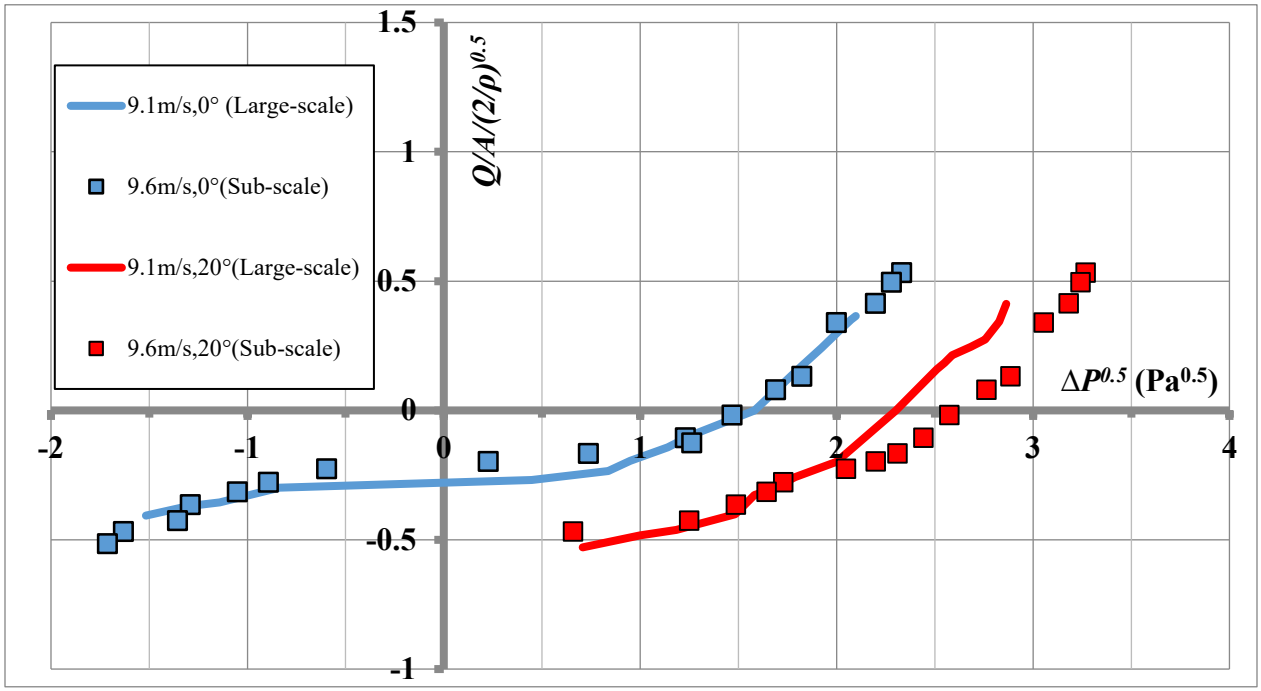

Figure 4-29. Results of comparison among different scales with the 4 m/s wind.

5. CONCLUSION AND FUTURE STUDY

5.1 Conclusions

Under the low wind speed at 4 m/s, the air curtain under tests show a good protection of the chamber and the performance under most conditions, e.g. exfiltration and small infiltration cases, remain the same as the condition without wind. For all types of air curtain studied in this research, for the strong air curtain jet (like 9.1m/s, 0°), the breakthrough pressure reduction caused by the wind is no more than 0.2 Pa under the weak wind speed of 4m/s.

For high wind speed as much as 10 m/s, the air curtain supply with 9.6 m/s no longer provides the required protection so the air curtain performance is weakened. For all the conditions, from exfiltration, optimum condition and infiltration conditions, the stronger wind causes the performance curves moving to the left so infiltration occurs at lower pressure differences and as a result more infiltration occurs at the same pressure difference when compared to the lower wind speed.

In addition, the wind direction also has impact on the air curtains performance. Results with wind incident angles shows the wind direction increase can improve the air curtain performance, when the wind incident angle ranges from 0° to 90°. Wind direction effect no longer changes the air curtain while the wind incident angle is above 120°. The door wings can also affect air curtain performance, and it can better the performance compared to that without door wings.

The results comparison between large-scale and sub-scale confirms the similarity of scaled air curtain models. It also validates the method of evaluating the performance of different openings including single doors, air curtain doors, and vestibules.

5.2 Limitations of the Study

- Limited wind speeds were tested during the tests. For the large-scale chamber, a wind speed of 3-4 m/s was tested while for the wind tunnel tests, only 4 m/s and 10 m/s wind speed were evaluated.
- The 5.6 m/s tests as the low air curtain supply show quite different performances under high wind speeds from the higher supply velocities of the air curtain. More tests for even lower supply speeds can be conducted to further confirm the impact from the high winds on low speed air curtain supplies.
- Limitation of the scaling ratio. For the most previous tests conducted in the wind tunnel, a typical scaling ratio is 1:300 to 1:500. In the current study, the ratio is 1:30 to the real building (1:10 to the large-scale chamber). Different scaling ratios need to be tested to check the impact of scaling ratios on the results.
- The wind velocity tested in the wind tunnel was either 4 m/s or 10 m/s. Due to limited time available for the experiment, the wind speed could not increase smoothly. More wind speeds will be performed through simulation.
- Finally, the scaling method for the air curtain has not yet been proven. It is based on a previous study (Hayes, 1968), which states the conditions when the air curtain starts to break (i.e. when it is unable to reach the floor and seal the doorway.)

5.3 Recommendations for Future Work

This study presents many new findings and conclusions showing the trends of wind effects on air curtain performance. For future work, a few items can be investigated further as follows:

- Developing a theoretical model or equation to generalize the wind effects on air curtain performance curves and the associated efficiency factors or effectiveness.
- Developing a general scaling method and similarity theory for different scales of air curtains based on more tests or CFD simulations.
- Investigating the wind effects on air curtains with different scales in the wind tunnel.
- Comparing the wind effect results with previous studies without wind plus wind dynamic pressure, and investigating the relation based on static pressure difference and total pressure difference.
- Investigating the impact of ambient temperatures on air curtain performance.
- Investigating the wind effect on air curtain performance for other terrain types, e.g. suburban and urban etc.

REFERENCES

Adrian, R.J. (2005). Twenty years of particle image velocimetry. *Experiments in Fluids*, *39*(2), 159–169.

Anderson, D.J., Greated, C.A., Jones, J.D.C, Nimmo, G. and Wiseall, S., 1996, Fibre optic PIV studies in an industrial combustor Proc. 8th Int. Symp. on Applications of Laser Techniques to Fluid Mechanics, Lisbon paper 18.4

ASHRAE (2007), ASHRAE Handbook-HVAC Applications, American Society of Heating, Refrigerating and Air Conditioning Engineers, Atlanta.

Belleghem, M. Van, Verhaeghe, G., T'Joen, C., Huisseune, H., De Jaeger, P., & De Paepe, M. (2012). Heat Transfer Through Vertically Downward-Blowing Single-Jet Air Curtains for Cold Rooms. *Heat Transfer Engineering*, *33*(June 2013), 1196–1206.

Cao, G., Sivukari, M., Kurnitski, J., Ruponen, M., & Seppänen, O., 2010. Particle Image Velocimetry (PIV) application in the measurement of indoor air distribution by an active chilled beam. *Building and Environment*, *45*(9), 1932–1940.

Cao, X., Liu, J., Jiang, N., & Chen, Q. (2014). Particle image velocimetry measurement of indoor airflow field: A review of the technologies and applications. *Energy and Buildings*, *69*, 367–380.

Cook, N.J., 1990. The Designer's Guide to Wind Loading of Buildings Structures, Part 2: Static Structures, BRE, Gariston.

Cook, N.J., 1975, A Boundary Layer Wind Tunnel for Building Aerodynamics, *Journal of Wind Engineering and Industrial Aerodynamics*, Vol. i, pp. 3-12.

Dantec Dynamics, & Nova Instruments. (2012). *DynamicStudio imaging platform*.

Davenport, A.G., 1960, A Rationale for the Determination of Design Wind Velocities, Proc. Amer.

Soc. Civil Eng., J. Struct. Div., 86: 3

Fischer, M., 1994, Comparison of PIV with hot-wire measurements and calculations obtained for instabilities in a flat plate boundary layer Proc. 7th Int. Symp. on Applications of Laser Techniques to Fluid Mechanics, Lisbon paper 37.4

Garret, J.R., 1994. The Atmospheric Boundary Layer, Cambridge University Press (Cambridge).

Geurts, C.P.W, Bentum, C.V., 2007. Wind Loading on Buildings: Eurocode and Experimental Approach, in T. Stathopoulos and C.C. Baniotopoulos, Wind Effects on Buildings and Design of Wind-Sensitive Structures, New York, pp. 31-65, Springer.

Goubran, S., 2016. Energy Saving Impact of Air Curtains in Commercial Buildings. Thesis, Concordia University.

Goubran, S., et al. 2016. Experimental study on the flow characteristics of air curtains at building entrances. *Building and Environment*, Volume 105, pp. 225-235

Grant, I., 1997, Particle image velocimetry: a review Proc. Inst. Mech. Eng. C 211 55–76

Hart, D.P. (2000). PIV error correction. *Experiments in Fluids*, *29*(1), 13–22.

Hayes, F.C. (1968). Heat Transfer Characteristics of the Air Curtain: A Plane Jet Subjected to Transverse Pressure and Temperature Gradients. University of Illinois.

Hayes, F.C., & Stoecker, W.F. (1969). Design Data for Air Curtains. *ASHRAE Transactions*, (2121), 168–180.

Holmes, J.D., 1977. Design and Performance of a Wind Tunnel for Modelling the Atmospheric Boundary Layer in Strong Winds, Wind Engineering Report 2/77, Department of Civil and Systems Engineering, James Cook University of North Queensland.

Höcker, R. and Kompenhans, J., 1991, Application of particle image velocimetry to transonic flows Applications of Laser Techniques to Fluid Mechanics (Proc. 5th Int. Symp., Lisbon

1990) (Berlin: Springer) pp 415–34

Melling, A. 1997. Tracer Particles and Seeding for Particle Image Velocimetry. Measurement Science and Technology 8 (12): 1406. German

Muniz, L., Martinez, R. E. and Mungal, M. G., 1996 Applications of PIV to turbulent reacting flows Proc. 8th Int. Symp. On Applications of Laser Techniques to Fluid Mechanics, Lisbon paper 3.3

Jensen, M., 1958. The model Law for Phenomena in Natural Wind. Ingenioren (international edition), 2, 4, 121-128.

Jensen, M., Franck, N., 1965. Model-Scale Tests in Turbulent Wind, Parts I and II. The Danish Technical Press, Copenhagen.

Jakobsen, M.L., McCluskey, D.R., Easson, W.J., Glass, D.H. and Greated, C.A., 1994, Pneumatic particle conveyance in pipe bend: simultaneous two-phase PIV measurements of the slip velocity between the air and the particle phases Proc.7th Int. Symp. on Applications of Laser Techniques to Fluid Mechanics, Lisbon paper 31.4

Juraeva M, et al. (2016). Influences of the train-wind and air-curtain to reduce the particle concentration inside a subway tunnel. *Tunneling and Underground Space Technology*, 52, 23-29

Krothapalli, A., Wishart, D.P. and Lourenco, L.M., 1994, Near field structure of a supersonic jet: 'on-line' PIV study Proc. 7th Int. Symp. on Applications of Laser Techniques to Fluid Mechanics, Lisbon paper 26.5

Laser Optical CCD and sCMOS Cameras | Dantec Dynamics. (n.d.). Retrieved December 1 (2015). from http://www.dantecdynamics.com/ccd-and-scmos-cameras

Li, A., Qin, E., Xin, B., Wang, G., & Wang, J. (2010). Experimental analysis on the air distribution

of powerhouse of Hohhot hydropower station with 2D-PIV. *Energy Conversion and Management*, *51*(1), 33–41.

Oliver, H.R. (1971), Wind profiles in and above a forest canopy. Q.J.R. Meteorol. Soc., 97: 548-553. doi:10.1002/qj.49709741414

Paone, N., Revel, G.M., and Nino, E., 1996 Velocity measurement in high turbulent premixed flames by a PIV measurement system Proc. 8th Int. Symp. on Applications of Laser Techniques to Fluid Mechanics, Lisbon paper 3-4

Prandtl, L., 1905. Verhandlungen des dritten internationalen Mathematiker-Kongresses in Heidel berg 1904, Krazer, A. (ed.), Leipzig: Teubner, p. 484. English trans. Ackroyd, J. A. K., Axcell, B. P., Ruban, A. I. (eds.) 2001. Early Developments of Modern Aerodynamics. Oxford: Butterworth-Heinemann, p. 77.

Qi, D., Goubran, S., Zmeureanu, R., and Wang, L. L. (2015). Effect of People on Infiltration of Building Entrance with Air Curtains. In *ISHVAC-COBEE* (p. 9). Tianjin.

Raffel, M., Höfer, H., Kost, F, Willert, C., and Kompenhans, J., 1996 Experimental aspects of PIV measurements of transonic flow fields at a trailing edge model of a turbine blade Proc. 8th Int. Symp. on Applications of Laser Techniques to Fluid Mechanics, Lisbon paper 28.1

Reuss, D.L., Adrian, R.J., Landreth, C.C., French, D.T. and Fansler, T.D., 1989, Instantaneous planar measurements of velocity and large-scale vorticity and strain rate in an engine using particle-image velocimetry, SAE paper 90092, International Congress and Exposition; Detroit, United States.

Schhchting, H., 1968, Boundary Layer Theory McGraw-Hill Book Company, Inc, New York

Schmidt, M. and Löffler, F., 1993, Experimental investigations on two-phase flow past a sphere using digital particle-image-velocimetry Exp. Fluids 14 296–304

Simiu, E., Scanlan, R.H., 1996. Wind Effects on Structures: Fundamentals and Applications to Design, third edition Wiley and Sons, New York.

Sun, Y., & Zhang, Y. (2007). An Overview of Room Air Motion Measurement: Technology and Application. *HVAC&R Research*, *13*(6), 929–950.

Stathopoulos, T., (1984). Design and Fabrication of a Wind Tunnel for Building Aerodynamics. *Journal of Wind Engineering and Industrial Aerodynamics*, 16, 361-376.

Stewart, J. N., Wang, Q., Moseley, R. P., Bearman, P. W. and Harvey, J. K., 1996. Measurement of vortical flows in a low speed wind tunnel using particle image velocimetry. Proc. 8th Int. Symp. on Applications of Laser Techniques to Fluid Mechanics, Lisbon paper 18.5

Van der Mass, J. (1992). Annex 20: Air Flow Patterns within Buildings Airflow through Large Openings. *International Energy Agency*. Lausanne. Retrieved from http://scholar.google.com/scholar?hl=en&btnG=Search&q=intitle:Air+Flow+Through+Large+Openings+in+Buildings#2

Vickery, B.J., The Design and Performance of a Low-Cost Boundary Layer Wind Tunnel, Proceed. of the Second USA - Japan Research Seminar on Wind Effects on Structures, September 1974, pp. 99-104.

Wang, L. (Leon), & Zhong, Z. (2014). An approach to determine infiltration characteristics of building entrance equipped with air curtains. *Energy and Buildings*, *75*, 312–320.

Wang, L. (Leon). (2013). *Investigation of the Impact of Building Entrance Air Curtain on Whole Building Energy Use*. *Air Movement and Control Association*. Retrieved from http://www.amca.org/UserFiles/file/Energy Initiative Web Pages/Air Curtain Study.pdf

Westerweel, J., Adrian, R. J., Eggels, J. G. M. and Nieuwstadt, F. T. M., 1993 Measurements with particle image velocimetry on fully developed turbulent pipe flow at low Reynolds number

Laser Techniques and Applications in Fluid Mechanics (Proc. 6th Int. Symp., Lisbon 1992) (Berlin: Springer) pp 285–310.

Yuill, G. (1996). *Impact of High Use Automatic Doors on Infiltration*. *ASHRAE Research Project 763-TRP*. Atlanta, USA.

Yuill, G. K., Upham, R., & Hui, C. (2000). Air leakage through automatic doors. *ASHRAE Transactions*, *106*(2), 145–160.

APPENDIX (A)

Detailed Results in the Large-scale Chamber

Overall performance tests results

1. Test results for 9.1 m/s air curtain supply speed and 0° supply angle

Wind Speed	0m/s			3m/s			3.5m/s			4m/s		
Parameters	Q (m^3/s)	ΔP (Pa)	Error (%)	Q (m^3/s)	ΔP (Pa)	Error (%)	Q (m^3/s)	ΔP (Pa)	Error (%)	Q (m^3/s)	ΔP (Pa)	Error (%)
Results	-0.198	-1.8	10.56	-0.227	-2.4	9.17	-0.225	-2.3	9.35	-0.227	-2.4	9.17
	-0.176	-1	15.00	-0.209	-1.8	10.56	-0.205	-1.8	10.56	-0.225	-2.3	9.35
	-0.157	-0.3	38.33	-0.188	-1	15.00	-0.193	-1.4	12.14	-0.205	-1.7	10.88
	-0.144	0	100.00	-0.172	-0.6	21.67	-0.171	-0.7	19.29	-0.197	-1.3	12.69
	-0.123	0.5	25.00	-0.151	-0.1	105.00	-0.154	-0.4	30.00	-0.165	-0.7	19.29
	-0.113	0.9	16.11	-0.139	0.2	55.00	-0.14	-0.1	105.00	-0.149	0.2	55.00
	-0.103	1.2	13.33	-0.107	0.6	21.67	-0.118	0.3	-28.33	-0.13	0.7	19.29
	-0.084	1.5	11.67	-0.086	0.8	17.50	-0.102	0.6	21.67	-0.108	0.9	16.11
	-0.06	1.8	10.56	-0.062	1.1	14.09	-0.088	1	15.00	-0.079	1.3	12.69
	0	2.4	9.17	0	2.1	9.76	0	2.4	9.17	-0.052	1.6	11.25
	0.076	3.8	7.63	0.069	3.1	8.23	0.087	3.2	8.13	0	2.5	9.00
	0.091	4	7.50	0.114	3.5	7.86	0.103	3.4	7.94	0.093	3.3	8.03
	0.119	4.3	7.33	0.131	3.8	7.63	0.118	3.5	7.86	0.114	3.5	7.86
	0.132	4.5	7.22	0.161	4.2	7.38	0.13	3.7	7.70	0.134	3.7	7.70
	0.151	4.7	7.13	0.173	4.5	7.22	0.149	3.9	7.56	0.175	4.1	7.44
	0.171	5	7.00	0.194	4.7	7.13	0.177	4.2	7.38	0.194	4.3	7.33
	0.194	5.3	6.89	0.201	4.8	7.08	0.193	4.4	7.27	0.202	4.4	7.27
	0.203	5.5					0.2	4.6				

2. Test results for 9.1 m/s air curtain supply speed and 20° supply angle

Wind Speed	0m/s			3m/s			3.5m/s			4m/s		
Parameters	Q (m3/s)	ΔP (Pa)	Error (%)	Q (m3/s)	ΔP (Pa)	Error (%)	Q (m^3/s)	ΔP (Pa)	Error (%)	Q (m^3/s)	ΔP (P)	Error (%)
Results	-0.29	0.1	105.00	-0.291	0.3	38.33	-0.296	0.4	30.00	-0.293	0.5	25.00
	-0.268	0.4	30.00	-0.265	0.8	17.50	-0.269	1	15.00	-0.267	1	15.00
	-0.247	1.1	14.09	-0.257	1	15.00	-0.223	2	10.00	-0.256	1.4	12.14
	-0.217	1.8	10.56	-0.235	2	10.00	-0.195	2.7	8.70	-0.222	2.2	9.55
	-0.178	2.4	9.17	0.196	2.6	8.85	-0.167	3	8.33	-0.181	2.5	9.00
	-0.155	2.8	8.57	0.164	3.2	8.13	-0.132	3.7	7.70	-0.168	2.8	8.5
	-0.136	3.5	7.86	0.114	4	7.50	-0.103	3.9	7.56	-0.143	3.2	8.13

	-0.113	4	7.50	0.089	4.4	7.27	-0.07	4.5	7.22	-0.11	4	7.50
	-0.093	4.5	7.22	0	5.1	6.96	-0.07	4.5	7.22	0	5.3	6.89
	0	5.2	6.92	0.091	6.2	6.61	0	5.3	6.89	0.088	6.3	6.59
	0.08	6.8	6.47	0.091	6.2	6.61	0.085	6.1	6.64	0.102	6.5	6.54
	0.114	7.4	6.35	0.105	6.3	6.59	0.107	6.6	6.52	0.102	6.5	6.54
	0.139	7.8	6.28	0.116	6.9	6.45	0.107	6.6	6.52	0.118	6.7	6.49
	0.152	8.1	6.23	0.135	7.2	6.39	0.123	7	6.43	0.136	7.2	6.39
	0.17	8.3	6.20	0.149	7.5	6.33	0.143	7.3	6.37	0.152	7.6	6.32
	0.191	8.5	6.18	0.181	7.7	6.30	0.168	7.6	6.32	0.19	8	6.25
	0.223	8.7	6.15	0.219	7.9	6.27	0.207	7.8	6.28	0.228	8.2	6.22
	0.234	9	6.11	0.237	8.2	6.22	0.231	8.3	6.20	0.228	8.2	6.22

3. Test results for 13.75 m/s air curtain supply speed and 0° supply angle

Wind Speed	0m/s			3m/s			3.5m/s			4m/s		
Parameters	Q (m^3/s)	ΔP (Pa)	Error (%)	Q (m^3/s)	ΔP (Pa)	Error (%)	Q (m^3/s)	ΔP (Pa)	Error (%)	Q (m^3/s)	ΔP (Pa)	Error (%)
Results	-0.22	0.8	17.50	-0.225	1	15.00	-0.225	1.1	14.09	-0.22	0.8	17.50
	-0.2	1.2	13.33	-0.214	1.4	12.14	-0.214	1.6	11.25	-0.209	1.1	14.09
	-0.185	1.9	10.26	-0.184	1.9	10.26	-0.178	2	10.00	-0.174	1.7	10.88
	-0.166	2.2	9.55	-0.14	2.7	8.70	-0.14	2.7	8.70	-0.152	2.1	9.76
	-0.148	2.5	9.00	-0.118	3.3	8.03	-0.14	2.7	8.70	-0.123	2.5	9.00
	-0.127	3.2	8.13	-0.089	3.5	7.86	-0.14	2.4	9.17	-0.105	2.9	8.45
	-0.114	3.6	7.78	-0.048	4.6	7.17	-0.114	3.1	8.23	-0.08	3.4	7.94
	-0.081	4.1	7.44	0	5.5	6.82	-0.084	3.6	7.78	-0.08	3.4	7.94
	-0.052	4.8	7.08	0.086	6.2	6.61	-0.064	4.7	7.13	-0.062	4	7.50
	0	5.6	6.79	0.103	6.7	6.49	0	5.5	6.82	-0.05	4.3	7.33
	0.078	7.4	6.35	0.103	6.7	6.49	0.088	6.2	6.61	-0.05	4.3	7.33
	0.108	8	6.25	0.121	7.2	6.39	0.112	6.8	6.47	0	5.3	6.89
	0.108	8	6.25	0.133	7.5	6.33	0.127	7	6.43	0.09	6.5	6.54
	0.126	8.4	6.19	0.151	7.9	6.27	0.144	7.3	6.37	0.114	6.8	6.47
	0.14	8.6	6.16	0.151	7.9	6.27	0.157	7.6	6.32	0.136	7.1	6.41
	0.16	8.9	6.12	0.178	8.2	6.22	0.173	7.9	6.27	0.157	7.4	6.35
	0.173	9.1	6.10	0.194	8.5	6.18	0.187	8.1	6.23	0.18	7.8	6.28
	0.199	9.4	6.06	0.202	8.8	6.14	0.204	8.5	6.18	0.204	8.2	6.22

4. Test results for 13.75 m/s air curtain supply speed and 20° supply angle

Wind Speed	0m/s			3m/s			3.5m/s			4m/s		
Parameters	Q (m^3/s)	ΔP (Pa)	Error (%)	Q (m^3/s)	ΔP (Pa)	Error (%)	Q (m^3/s)	ΔP (Pa)	Error (%)	Q (m^3/s)	ΔP (Pa)	Error (%)
Results	-0.235	5	7.00	-0.262	6.2	6.75	-0.273	5.7	6.75	-0.273	5.7	6.75

	-0.224	5.6	6.79	-0.222	6.4	6.64	-0.26	6.1	6.64	-0.26	6.1	6.64
	-0.2	6.3	6.59	-0.217	6.7	6.49	-0.224	6.7	6.49	-0.217	6.9	6.45
	-0.16	8.7	6.15	-0.189	7.8	6.28	-0.201	7.8	6.28	-0.175	8.5	6.18
	-0.147	9	6.11	-0.167	8.7	6.23	-0.184	8.1	6.23	-0.159	8.8	6.14
	-0.131	9.4	6.06	-0.134	9.3	6.12	-0.157	8.9	6.12	-0.137	9.2	6.09
	-0.119	9.8	6.02	-0.114	9.6	6.08	-0.14	9.3	6.08	-0.119	9.3	6.08
	-0.104	9.9	6.01	-0.114	9.9	6.05	-0.134	9.5	6.05	-0.116	9.8	6.02
	-0.077	10.5	5.95	-0.09	10.2	6.04	-0.12	9.6	6.04	-0.093	9.8	6.02
	-0.066	10.7	5.93	-0.066	10.5	6.03	-0.109	9.7	6.03	-0.06	10.1	5.99
	0	11.3	5.88	0	11.1	5.96	-0.063	10.4	5.96	0	11.1	5.90
	0.066	13	5.77	0.075	12.9	5.91	0	11	5.91	0.054	12	5.83
	0.094	13.6	5.74	0.091	13.3	5.83	0.06	12	5.83	0.073	12.3	5.81
	0.102	14.1	5.71	0.103	13.3	5.81	0.071	12.4	5.81	0.1	13	5.77
	0.134	14.8	5.68	0.121	13.8	5.76	0.108	13.2	5.76	0.119	13.3	5.75
	0.147	15.1	5.66	0.144	14.2	5.74	0.124	13.5	5.74	0.135	14	5.71
	0.184	16	5.63	0.182	14.6	5.70	0.166	14.3	5.70	0.173	14.5	5.69
	0.2	16.4	5.61	0.186	14.9	5.67	0.185	14.9	5.67	0.187	14.9	5.67
	0.233	16.6	5.60	0.198	15.3	5.66	0.196	15.2	5.66	0.2	15.1	5.66

Comparative Tests Results

1. Test results for 9.1 m/s air curtain supply speed and 0° supply angle

Wind Speed	0m/s			3m/s			3.5m/s			4m/s		
Parameters	Q (m^3/s)	ΔP (Pa)	Error (%)	Q (m^3/s)	ΔP (Pa)	Error (%)	Q (m^3/s)	ΔP (Pa)	Error (%)	Q (m^3/s)	ΔP (Pa)	Error (%)
Results	-0.222	-2.4	9.17	-0.227	-2.3	9.35	-0.225	-2.3	9.35	-0.225	-2.3	9.35
	-0.144	0	100.00	-0.151	-0.1	105.00	-0.14	0	100	-0.139	0.2	100
	-0.113	0.6	21.67	-0.107	0.6	21.67	-0.102	0.7	19.29	-0.098	0.9	16.11
	-0.0089	2.2	9.55	0.017	2.2	9.55	0.024	2.3	9.35	0.033	2.4	9.17
	0	2.4	9.17	0	2.2	9.55	0	2.4	9.17	0	2.4	9.17
	0.099	3.6	7.78	0.101	3.3	8.03	0.102	3.4	7.94	0.104	3.5	7.86
	0.132	4.2	7.38	0.14	3.8	7.63	0.15	3.9	7.56	0.155	4	7.50
	0.2	5.2	6.92	0.201	4.7	7.13	0.2	4.8	7.08	0.205	4.9	7.04

2. Test results for 9.1 m/s air curtain supply speed and 20° supply angle

Wind Speed	0m/s			3m/s			3.5m/s			4m/s		
Parameters	Q (m^3/s)	ΔP (Pa)	Error (%)	Q (m^3/s)	ΔP (Pa)	Error (%)	Q (m^3/s)	ΔP (Pa)	Error (%)	Q (m^3/s)	ΔP (Pa)	Error (%)
Results	-0.29	0.1	105.00	-0.287	0.3	38.33	-0.286	0.4	30.00	-0.283	0.5	25.00
	-0.217	1.8	10.56	-0	2.6	8.85	-0.195	2.7	8.70	-0.18	2.9	8.45

				.196								
	-0.11	3.7	7.70	-0.108	3.8	7.63	-0.103	4	7.50	-0.1	4.1	7.44
	-0.012	4.9	7.04	0.0012	5	7.00	0.011	5	7.00	0.017	5.1	6.96
	0	5.2	6.92	0	5.1	6.96	0	5.3	6.89	0	5.3	6.89
	0.104	7	6.43	0.105	6.3	6.59	0.11	6.5	6.54	0.118	6.7	6.49
	0.181	8.3	6.20	0.184	7.7	6.30	0.187	7.8	6.28	0.19	8	6.25
	0.224	8.7	6.15	0.227	8.2	6.22	0.231	8.3	6.20	0.238	8.5	6.18

3. Test results for 13.75 m/s air curtain supply speed and 0° supply angle

Wind Speed	0m/s			3m/s			3.5m/s			4m/s		
Parameters	Q (m^3/s)	ΔP (Pa)	Error (%)	Q (m^3/s)	ΔP (Pa)	Error (%)	Q (m^3/s)	ΔP (Pa)	Error (%)	Q (m^3/s)	ΔP (Pa)	Error (%)
Results	-0.22	0.8	17.50	-0.215	1	15.00	-0.21	1.1	14.09	-0.209	1.2	13.33
	-0.2	1.2	13.33	-0.194	1.4	12.14	-0.191	1.6	11.25	-0.189	1.7	10.88
	-0.114	3.5	7.86	-0.098	3.7	7.70	-0.094	3.8	7.63	-0.085	3.9	7.56
	-0.013	5.4	6.85	0.0083	5.4	6.85	0.021	5.5	6.82	0.028	5.5	6.82
	0	5.4	6.85	0	5.5	6.82	0	5.5	6.82	0	5.3	6.89
	0.098	7.4	6.35	0.103	6.7	6.49	0.112	6.8	6.47	0.116	6.9	6.45
	0.14	8.4	6.19	0.145	7.7	6.30	0.153	7.8	6.28	0.157	8	6.25
	0.199	9	6.11	0.202	8.4	6.19	0.204	8.5	6.18	0.208	8.6	6.16

4. Test results for 13.75 m/s air curtain supply speed and 20° supply angle

Wind Speed	0m/s			3m/s			3.5m/s			4m/s		
Parameters	Q (m^3/s)	ΔP (Pa)	Error (%)	Q (m^3/s)	ΔP (Pa)	Error (%)	Q (m^3/s)	ΔP (Pa)	Error (%)	Q (m^3/s)	ΔP (Pa)	Error (%)
Results	-0.27	5.7	6.75	-0.262	6.2	6.75	-0.259	6.3	6.75	-0.252	6.5	6.75
	-0.224	6.4	6.56	-0.217	6.7	6.56	-0.213	6.8	6.56	-0.21	6.9	6.56
	-0.119	9.8	6.02	-0.114	9.6	6.02	-0.109	9.7	6.02	-0.116	9.8	6.02
	-0.025	10.8	5.93	-0.011	10.8	5.93	-0.0089	10.9	5.93	-0.0055	10.9	5.93
	0	11.3	5.88	0	11.1	5.88	0	11	5.88	0	11.1	5.88
	0.104	13.8	5.72	0.103	13	5.72	0.108	13.2	5.72	0.119	13.3	5.72
	0.14	14.4	5.69	0.144	13.8	5.69	0.145	14	5.69	0.148	14.2	5.69
	0.18	15.6	5.64	0.186	14.9	5.64	0.19	15	5.64	0.191	15.1	5.64

APPENDIX (B)

Detailed Results from Wind Speed Effect Sub-Scale Tests in Wind Tunnel

1. Test results for 9.6 m/s air curtain supply speed and 0° supply angle

Wind Speed		0m/s	4m/s	10m/s
Parameters	Q(m^3/s)	ΔP(Pa)	ΔP(Pa)	ΔP(Pa)
Results	0.002852	6.169727	5.434514	3.481043
	0.002653	5.921468	5.196229	2.574255
	0.002216	5.289687	4.831291	2.521614
	0.001819	4.33088	3.992026	1.408243
	0.000706	3.298031	3.322343	-0.41382
	0.000428	2.87798	2.854979	-0.74377
	-9.7E-05	2.308709	2.15427	-1.3624
	-0.00056	1.742341	1.513329	-2.56478
	-0.00067	1.208549	1.591639	-2.55633
	-0.00089	0.818532	0.541376	-3.48998
	-0.00106	0.488448	0.050858	-4.53762
	-0.00121	0.167023	-0.35535	-4.63567
	-0.00149	-0.19928	-0.79684	-4.96891
	-0.00169	-0.41867	-1.10378	-5.40811
	-0.00195	-1.04882	-1.66657	-5.62256
	-0.00228	-1.64047	-1.8402	-6.52067
	-0.00251	-2.13586	-2.66273	-6.71084
	-0.00276	-2.675	-2.93317	-7.23817

2. Test results for 9.6 m/s air curtain supply speed and 20° supply angle

Wind Speed		0m/s	4m/s	10m/s
Parameters	Q(m^3/s)	ΔP(Pa)	ΔP(Pa)	ΔP(Pa)
Results	0.002852	11.0636	10.68087	8.073043
	0.002653	10.82265	10.50532	7.465908
	0.002216	10.24351	10.12287	6.639436
	0.001819	9.39808	9.333244	5.606148
	0.000706	8.366836	8.31849	4.607895
	0.000428	7.832931	7.631552	3.874996
	-9.7E-05	6.708668	6.623455	3.827343
	-0.00056	6.294703	5.960588	2.767716
	-0.00067	5.954671	5.647469	1.9450868
	-0.00089	5.614638	5.33435	1.122458
	-0.00106	5.001386	4.834224	0.559865

	-0.00121	4.923615	4.195364	0.129767
	-0.00149	3.139477	2.986174	-0.237644
	-0.00169	2.658548	2.700161	-0.177847
	-0.00195	2.535022	2.212217	-1.363608
	-0.00228	0.829844	1.560956	-1.448829
	-0.00251	0.324011	0.432221	-1.724051
	-0.00276	0.356412	0.475443	-1.8964565

3. Test results for 5.7 m/s air curtain supply speed and 0° supply angle

Wind Speed		0m/s	10m/s
Parameters	Q(m^3/s)	ΔP(Pa)	ΔP(Pa)
Results	0.004303	3.943477	1.719959
	0.004104	3.892935	1.306074
	0.003667	3.737877	0.954195
	0.00327	3.341741	0.225631
	0.002157	2.768806	-0.976385
	0.001879	2.568665	-1.096713
	0.001354	2.036189	-2.287891
	0.000887	1.665544	-3.166889
	0.000778	1.312333	-3.59871
	0.000557	1.236812	-4.199845
	0.000392	0.935716	-4.519590
	0.000244	0.648144	-4.684504
	-3.7E-05	0.395477	-4.857681
	-0.00023	0.238547	-4.987408
	-0.0005	0.039081	-5.216502
	-0.00083	-0.1824	-5.445597
	-0.00106	-0.58143	-5.448477
	-0.00131	-0.98045	-5.85241

4. Test results for 5.7 m/s air curtain supply speed and 20° supply angle

Wind Speed		0m/s	10m/s
Parameters	Q(m^3/s)	ΔP(Pa)	ΔP(Pa)
Results	0.004303	6.94294	4.816441
	0.004104	6.856414	3.848834
	0.003667	6.490871	3.736
	0.00327	6.030091	3.294438
	0.002157	5.588335	2.456987
	0.001879	5.303055	2.176398
	0.001354	4.927881	1.494857
	0.000887	4.300206	-0.23868
	0.000778	3.909797	-0.56021
	0.000557	3.609237	-0.95846

	0.000392	3.217168	-1.06142
	0.000244	2.823657	-1.98909
	-3.7E-05	2.46622	-2.52565
	-0.00023	2.24781	-2.54487
	-0.0005	1.645424	-3.09508
	-0.00083	1.206283	-3.35473
	-0.00106	0.617548	-4.09675
	-0.00131	0.028813	-4.27391

APPENDIX (C)

Detailed Results from Wind Direction Effect Sub-Scale Tests in Wind Tunnel

1. Test results for 9.6 m/s air curtain supply speed and 0° supply angle (with doors)

Wind Direction β		0°	30°	60°	90°	120°
Parameters	Q(m^3/s)	ΔP(Pa)	ΔP(Pa)	ΔP(Pa)	ΔP(Pa)	ΔP(Pa)
Results	-0.00276	-2.93317	1.641204	9.948469	16.2161	17.19706
	-0.00251	-2.66273	1.572494	10.97345	17.62006	17.74046
	-0.00228	-1.8402	1.997858	11.75496	17.71279	18.15851
	-0.00195	-1.66657	2.432042	12.26843	18.68803	18.73404
	-0.00169	-1.10378	2.615291	12.61703	18.97463	18.71461
	-0.00149	-0.79684	2.955032	13.16167	19.40054	18.75712
	-0.00121	-0.35535	3.529512	13.03971	19.0538	19.37155
	-0.00106	0.050858	4.296034	13.71324	19.68498	19.94653
	-0.00089	0.541376	4.733829	14.74099	19.75767	20.37079
	-0.00056	1.513329	6.53869	15.92507	22.31913	22.48752
	0.000637	4.042742	9.678861	18.82192	26.12866	26.19636
	0.00227	6.192135	11.63982	21.78064	28.36013	28.32093
	0.003182	7.40784	12.78157	22.49795	30.55691	29.19169

2 Test results for 9.6 m/s air curtain supply speed and 0° supply angle (without doors)

Wind Angle		No wind	0°	60°	120°
Parameters	Q(m^3/s)	ΔP(Pa)	ΔP(Pa)	ΔP(Pa)	ΔP(Pa)
Results	-0.00276	-1.57018	-1.33893	6.895102	15.98947
	-0.00251	-1.23087	-1.20673	7.324483	16.63471
	-0.00228	-0.99666	-0.97712	7.080277	16.46417
	-0.00195	-0.78069	-0.78069	7.384692	16.5896
	-0.00149	-0.36601	-0.1179	8.580661	17.21435
	-0.00121	-0.20951	0.06327	8.79296	17.64609
	-0.00106	0.126407	0.260009	9.346086	18.04899
	-0.00089	0.337134	0.578727	10.342	18.85021
	-0.00056	1.278538	1.662932	11.32463	20.1989
	-9.7E-05	2.110347	2.693382	13.09863	25.14424
	0.000428	2.674872	3.395092	13.71169	25.78589
	0.000706	3.151583	3.515331	14.46138	26.97089

	0.001819	4.254923	4.740003	16.10429	28.15986
	0.002216	5.016613	5.176828	16.46366	29.41727
	0.002653	5.448806	5.272317	16.89554	30.22037
	0.002852	5.702815	5.526535	17.24326	30.35285

APPENDIX (D)

Detailed Results from Person Effect Sub-Scale Tests in Wind Tunnel

1. Test results for 9.6 m/s air curtain supply speed and 0° supply angle

Person Location		Under air curtain		In front of door	
Wind Speed		0m/s	4m/s	0m/s	4m/s
Parameters	Q(m^3/s)	ΔP(Pa)	ΔP(Pa)	ΔP(Pa)	ΔP(Pa)
Results	-0.00276	-3.0635	-3.07126	-2.68679	-2.75054
	-0.00251	-2.34875	-3.10143	-1.98843	-2.32758
	-0.00228	-1.96069	-2.70035	-1.61816	-2.29177
	-0.00195	-1.53068	-2.29693	-0.80794	-1.36684
	-0.00169	-0.65653	-1.39943	-0.37418	-0.88564
	-0.00149	-0.34554	-1.0087	-0.12545	-0.53502
	-0.00121	0.060227	-0.43267	0.228893	-0.23731
	-0.00106	0.323094	-0.19856	0.620769	-0.01358
	-0.00089	0.691953	0.531831	0.985186	0.292653
	-0.00056	1.882711	1.210477	1.93219	1.673516
	0.000637	4.885484	4.609537	4.468086	3.558312
	0.00227	6.948971	6.856533	6.64955	5.874337
	0.003182	7.722578	7.530337	7.350202	6.731787

2. Test results for 9.6 m/s air curtain supply speed and 20° supply angle

Person Location		Under air curtain		In front of door	
Wind Speed		0m/s	4m/s	0m/s	4m/s
Parameters	Q(m^3/s)	ΔP(Pa)	ΔP(Pa)	ΔP(Pa)	ΔP(Pa)
Results	-0.00276	-1.49452	-0.89671	-2.01909	-0.17311
	-0.00251	-0.77523	-0.46514	-0.90614	0.028089
	-0.00228	0.187481	0.993058	-0.0519	0.93892
	-0.00195	0.949068	1.746796	0.696744	1.304926
	-0.00169	2.646123	2.966273	2.97132	3.09782
	-0.00149	3.158019	3.307192	3.549604	3.564267
	-0.00121	3.931043	4.032071	4.260268	4.599475
	-0.00106	4.40838	4.594958	5.225142	5.1669
	-0.00089	5.277404	5.439127	6.219166	6.482061
	-0.00056	7.54113	7.454594	8.312885	7.720682
	0.000637	8.870418	8.389249	8.607545	8.703849

	0.00227	11.16785	10.34689	10.93932	10.50252
	0.003182	11.98752	11.77202	11.47498	10.99846

3. Location of the person model.

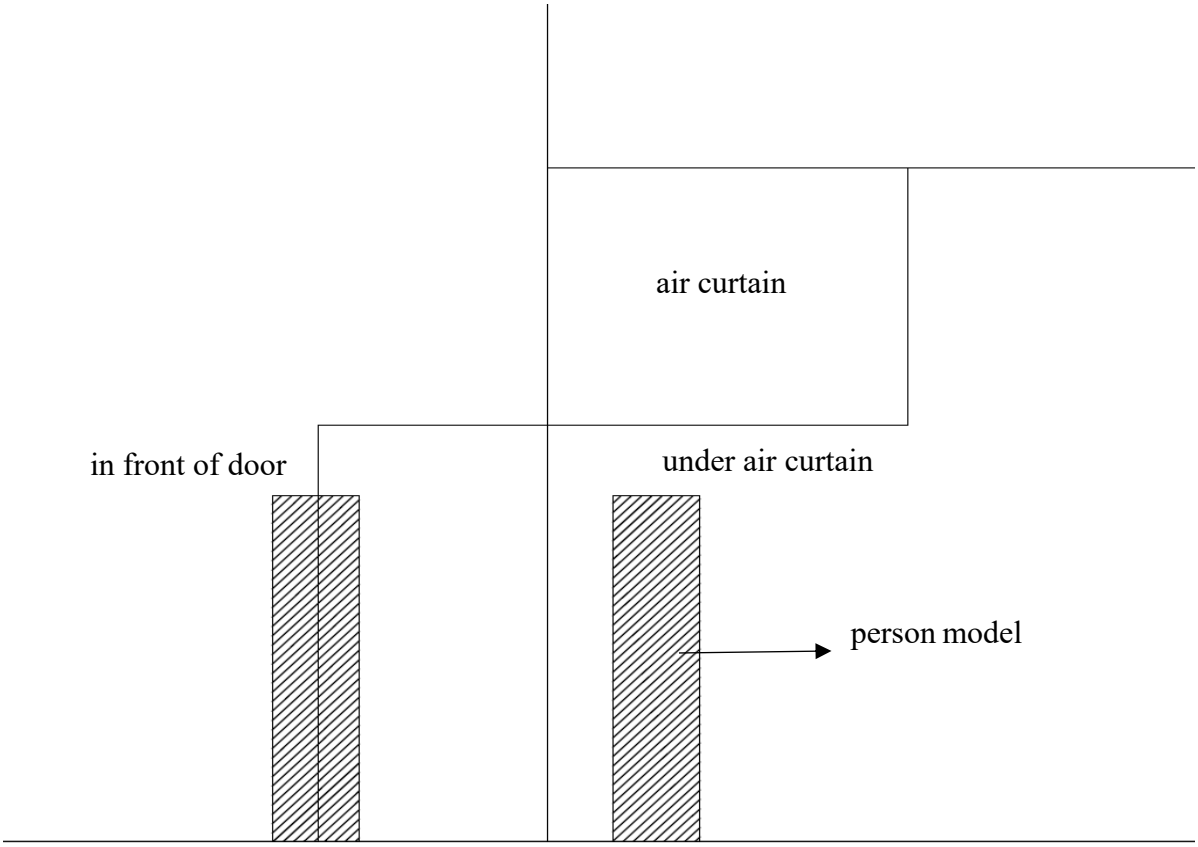

APPENDIX (E)

Detailed Results of Single Door and Vestibule Sub-Scale Tests in Wind Tunnel

Opening Type		Single Door	Vestibule
Parameters	Q(m^3/s)	ΔP(Pa)	ΔP(Pa)
Results	0.000709	0.016578	0.196771
	0.000957	0.078666	0.284724
	0.001188	0.10579	0.296781
	0.001518	0.150183	0.306641
	0.001781	0.311984	0.557904
	0.001979	0.35313	0.632122
	0.00226	0.419705	0.718297
	0.002408	0.52498	0.871919
	0.002573	0.63224	1.032691
	0.004103	1.974315	2.74973
	0.005737	3.232097	
	0.006649	3.616889	